

# Theoretical Studies of Properties of Clusters

## Dissertation

zur Erlangung des Grades des Doktors der Naturwissenschaften  
der Naturwissenschaftlich-Technischen Fakultät III  
Chemie, Pharmazie und Werkstoffwissenschaften  
der Universität des Saarlandes

vorgelegt von

Habib ur Rehman

Saarbrücken, 2008



## Dedication

This thesis is dedicated to all of my family members, especially to my  
father *Shams ur Rehman*



# Acknowledgment

In the name of Allah, the Most Merciful, the Most Beneficial. First of all, I would like to express my deep and sincere gratitude to my supervisor, Prof. Dr. Michael Springborg, Physical and Theoretical Chemistry Department, University of Saarland. His wide knowledge and his logical way of thinking have been of great value for me. His understanding, encouraging and personal guidance have provided a good basis for the completion of present thesis.

I am deeply grateful to my colleague, Dr. Yi Dong, for her valuable advice, friendly help and for her important support throughout this work and my stay in Saarbrücken.

I want to thank all members of the " AK Springborg " for providing an excellent and inspiring working atmosphere, especially Dr. Valeri G. Grigoryan, Michael Bauer, Violina Tevekeliyska and Elisaveta Kasabova.

My warm thanks are due to former group members of " AK Springborg " , especially to my friends Dr. Abu Md. Asaduzzaman and Dr. Sudip Roy for their kind support and guidance through out my study.

I wish to thank Dr. Ranjit Nanda, University of Missouri, for his friendly help in studies during his stay in our group.

I also wish to thank Ingelore Weidenfeld for her sympathetic help in secretarial work.

I wish to extend my warmest thanks to all of my friends who prayed for my success and have given moral support during my stay in Saarbrücken. I would like to thank Awais Anwar, Mohammed Usman Anwar, Dr. Mohammed Abbas, Chand Tufail, Amir Wasim, Javed Iqbal, Ameer Fawad Zahoor and Hameed Wazir.

I owe my loving thanks to my wife Qurat-ul-Ann and to all of my family members. Without their encouragement and understanding it would have been impossible for me to finish this work. I am thankful to you ' ANN ' for your strong trust and endless patience during my stay in Saarbrücken.



---

# Contents

---

<b>Contents</b>	<b>i</b>
<b>Abstract</b>	<b>1</b>
<b>Zusammenfassung</b>	<b>3</b>
<b>1 Introduction</b>	<b>5</b>
1.1 Nanoscience and Cluster Studies . . . . .	5
1.2 Organization of work . . . . .	9
<b>2 Theory and Method For Calculations</b>	<b>11</b>
2.1 Density-Functional Theory . . . . .	11
2.2 Density-Functional Tight-Binding Method . . . . .	15
2.3 Method for Global Optimization . . . . .	19
<b>3 Results of Semiconductor Cluster Studies</b>	<b>21</b>
3.1 Introduction . . . . .	21
3.2 Structures of $\text{Si}_n, \text{Ge}_n$ , and $\text{Si}_n\text{Ge}_n$ Clusters . . . . .	24
<b>4 Tools For Structural Analysis</b>	<b>37</b>
4.1 Structural Similarity . . . . .	37
4.2 Common Neighbor Analysis . . . . .	49
4.3 Stability Function . . . . .	58
4.4 Radial Distribution Function . . . . .	65
4.5 Shape Analysis . . . . .	70
<b>5 Properties of <math>\text{Cu}_n</math> Clusters</b>	<b>81</b>
5.1 Introduction . . . . .	81
5.2 Structures of Cu clusters: $\text{Cu}_2$ to $\text{Cu}_{36}$ . . . . .	83

5.3 Tools for Structural Analysis . . . . .	87
<b>6 Summary and Conclusions</b>	<b>101</b>
<b>Bibliography</b>	<b>105</b>
<b>Eidesstattliche Versicherung</b>	<b>113</b>

---

# Abstract

---

This work is based on calculation of total-energy minimum structures for various cluster systems using Density-Functional Tight Binding method combined with genetic algorithm method. Cluster systems which we have investigated include both semiconductor clusters and metallic clusters. Results of theoretical studies of binary homogeneous  $\text{Si}_n\text{Ge}_n$  clusters, indicates the formation of mixed alloy structures for these clusters. We observe mostly hetero-atomic Si-Ge bonds in  $\text{Si}_n\text{Ge}_n$  clusters, which shows that both Si and Ge have strong tendency to form bonds with each other. We also observe that there are very few Si-Si bonds compared to Ge-Ge bonds in binary  $\text{Si}_n\text{Ge}_n$  clusters. We have calculated the bond energies for  $E_{\text{Si-Ge}}$ ,  $E_{\text{Ge-Ge}}$  and  $E_{\text{Si-Si}}$  which also favors the formation of more hetero Si-Ge, and Ge-Ge bonds as compared to Si-Si bonds. In these alloy structures, Si shows very poor tendency to be coordinated to another Si atom. In general, % age coordination of Si decreases from 5 or 4, as in pure  $\text{Si}_n$  clusters to 3 in binary  $\text{Si}_n\text{Ge}_n$  clusters whereas, for Ge atoms % age coordination number increases from 3 to 4 as compared to pure  $\text{Ge}_n$  clusters. Further more, for binary homogeneous  $\text{Si}_n\text{Ge}_n$  clusters, we have found that these binary clusters have different growth pattern as compared to their elemental counterparts. This gives rise to different structures for  $\text{Si}_n\text{Ge}_n$  clusters when comparing to pure elemental clusters in the same size range. Our observation is clearly depicted in similarity function analysis of these cluster structures in which we observe that binary clusters show very poor similarity with elemental clusters. Our stability function analysis predicts stable cluster structures for all the clusters systems.

In the second part of our work, we have studied the geometries and structural and electronic properties of the  $\text{Cu}_n$  clusters in the size range  $2 \leq n \leq 36$  atoms. An intensive search for low-energy minima of  $\text{Cu}_n$  clusters was carried out using DFTB method combined with genetic algorithm meth-

ods for an unbiased global structure optimization. We have used various descriptors for analyzing the  $\text{Cu}_n$  clusters including stability, shape, and similarity analysis as well as radial distances of atoms and HOMO-LUMO gap studies. We have obtained the global minimum-total energy structure of  $\text{Cu}_n$  clusters in the size range  $n \leq 10$  which are reported in earlier studies.

---

# Zusammenfassung

---

In dieser Arbeit wurden mit Hilfe der Dichtefunktional-*tight-binding*-Methode (DFTB) die energetisch niedrigsten Strukturen verschiedener Clustersysteme untersucht. Die dabei betrachteten Systeme umfassen Halbleiter und Metall Cluster. Das Ziel dieser Arbeit ist es, die strukturellen und elektronischen Eigenschaften dieser Systeme zu klären. In Kapitel 1 erfolgt eine kurze Darstellung von früheren Untersuchungen von Halbleitern und metallischen Clustern. Anschliessend wird ein Überblick über den Aufbau dieser Arbeit gegeben. Die Dichtefunktional-Theorie (DFT) und die Dichtefunktional-*tight-binding*-Methode (DFTB) werden in Kapitel 2 besprochen. Der genetische Algorithmus, den wir zur Berechnung des globalen Energieminimums verwendet haben, wird an dem Ende dieses Kapitels dargestellt.

Kapitel 3 und 4 enthalten die theoretische Ergebnisse von der Untersuchung der Halbleiter und Kapitel 5 diese von der Untersuchung der metallischen Clustern.

Cluster sind Systeme, die zwischen kleinen Molekülen und makroskopischen Festkörpern liegen. Die Bestimmung der exakten Struktur ist der wichtigste Schritt bei der Clusteruntersuchung, dennoch erweist sich globale Struktur-optimierung als sehr schwieriger Prozess.

In dem ersten Teil dieser Arbeit werden die Ergebnisse von der Untersuchung der Halbleiter  $\text{Si}_n$ ,  $\text{Ge}_n$  und  $\text{Si}_n\text{Ge}_n$  Cluster gezeigt, wobei für Si and Ge  $n$  zwischen 2 und 44 Atome und für die bimetallische Cluster zwischen 2 und 22 Si-Ge Einheiten liegt. Um die strukturellen and energetischen Eigenschaften von den optimierten Clustern in Abhängigkeit von der Clustergrösse darzustellen und zu diskutieren, wurden die Stabilitäts- und Ähnlichkeits-funktionen, die radiale Verteilung, die gesamte Clusterform, die Symmetrie, der HOMO-LUMO Abstand untersucht. Die Ergebnisse zeigen für die bimetallische Cluster die Bildung von Mischlegierungen,

hauptsächlich Bindungen zwischen den Heteroatomen Si und Ge und sehr wenig Si-Si Bindungen im Vergleich zu Ge-Ge. Die gleiche Ergebnisse zeigen auch die ausgerechneten Bindungsenergien  $E_{Si-Ge}$ ,  $E_{Ge-Ge}$  und  $E_{Si-Si}$ . Die Koordinationszahl von Si wird reduziert-von 5 oder 4 in  $Si_n$  auf 3 in den bimetallischen Cluster. Die umgekehrte Tendenz wird bei Ge beobachtet-von 3 in  $Ge_n$  auf 4 in den  $Si_nGe_n$  Clustern. Des weiteren wurde festgestellt, daß die bimetallische homogene Cluster unterschiedlich im Vergleich zu den reinen Elementen wachsen, was auch zu verschiedenen Strukturen führt. Dieser Strukturunterschied zwischen  $Si_nGe_n$  und  $Si_n$ ,  $Ge_n$  mit gleicher Anzahl von Atomen kann durch die Ähnlichkeitsfunktion dargestellt werden. Die Ergebnisse der Stabilitätsfunktion-untersuchungen zeigen stabile Strukturen für die drie Systeme.

Der zweite Teil der Arbeit enthält die Ergebnisse von den theoretischen Untersuchungen der strukturellen und energetischen Eigenschaften von  $Cu_n$  mit  $2 \leq n \leq 36$  Atomen. Die gleiche theoretische Methode wurde auch hier verwendet und die Eigenschaften von den optimierten Clustern wurden in Abhängigkeit von der Cluster- grÖße untersucht und diskutiert. Für  $n \leq 10$  wurden globale Strukturen erhalten, die im Einklang mit früheren theoretischen Untersuchungen sind.

Eine kurze Schlussfolgerung mit einem Überblick über die Beobachtungen bei den einzelnen Systemen stellt den letzten Teil der Arbeit dar (Kapitel 6).

# Chapter 1

---

## Introduction

---

### 1.1 Nanoscience and Cluster Studies

Nanoscience, a branch of material science where materials at nanometer size range are investigated, has found most central place in the field of research over the last decades. Both experimentalists and theoreticians have contributed for this field but contributions from theoreticians are growing rapidly. Nanoscience has started in early 1980's and its major development was birth of cluster science and since then clusters and nanoparticles in the size range of some 10s to some 10 000s of atoms are studied extensively. These systems are of special interest because they have sizes in a range where quantum confinement or quantum-size effects (QSE) play important role for the unique, size dependent properties of these materials. Thus, the determination of the size dependent properties of these nano-particles and to find relation between size and properties is not easy for these systems. In experimental studies the clusters are rarely isolated, but instead they often interact with some other medium while theoretical studies deal with isolated clusters of a well defined size for which it is overwhelmingly complicated to determine the structure. The identification of the structure of the lowest total energy for a cluster of  $N$  atoms requires searching in a geometry space of  $3N-6$  dimensions, which for any but the smallest values of  $N$  hardly is possible.

In our present work, we will try to identify the structures of lowest total energy for different cluster systems by carefully searching through the geometric space and then will try to look at the structural and electronic properties associated with these cluster systems. We have used Density-Functional

Tight Binding method (DFTB) for our calculations. The optimization is carried out by so-called genetic algorithm that has been developed in our own group. The DFTB method and the algorithm are both explained in chapter two of this thesis. The cluster systems which we have studied include both semiconductors and metallic clusters.

Semiconductor clusters are a special class of matter with sizes in between single atoms and semiconductor quantum dots [1]. A tremendous effort has been invested in the structural characterization of clusters of the group 4 semiconductor elements, Silicon and Germanium. These are two most important microelectronics materials, so understanding the growth habit of their clusters is of substantial practical relevance. In the bulk, both Si and Ge pack in a tetrahedral 'diamond' lattice. Over the past two decades or so, free Silicon clusters have been extensively studied both experimentally [2]-[9] and theoretically [10]-[30],[52] compared to Germanium clusters [31]-[51]. A central issue concerning the  $Si_n$  and  $Ge_n$  clusters is their lowest energy geometric structures, namely, their global minima as a function of size  $n$ . Major efforts have been undertaken towards finding the global minimum structures in different size ranges and at different levels of theory. Looking at the structural developments of both  $Si_n$  and  $Ge_n$  clusters, it is reasonable to ask what happens for hetero-clusters like  $Si_nGe_n$ . One should anticipate that there should be interesting properties existing for binary  $Si_nGe_n$  micro clusters. Si-Ge technology has been studied extensively in the past ten years and the binary hetero structures  $Si/Si_{1-x}Ge_x$  have produced a new generation of high performance heterojunction bipolar transistors (HBT), field effect transistors and infrared detectors [53, 54]. Moreover atomic scale analysis of Si-Ge materials is becoming more and more important as semiconductor devices are constantly being scaled down. The concepts obtained from Si-Ge in the bulk form may not be directly applicable to Si-Ge at the nanoscale level due to lattice strains and surface energy effects. Therefore, fundamental understanding of the structural and electronic properties of Si-Ge nanoclusters is going to play an important role in the advancement in the nanoscale devices. Studies on binary semiconductor clusters may provide us insight into the bulk alloy structures. Considering the importance of these semiconductor alloy systems, we have selected to study binary homogeneous Si-Ge clusters. In order to make a comparison between pure and binary Si-Ge clusters, we have also investigated the total-energy minimum structures of pure  $Si_n$  and  $Ge_n$  clusters using DFTB method.

Up to now, mixed  $Si_nGe_n$  clusters remain unexplored compared to their elemental counterparts. S.D.Li *et.al*, [55] investigated the low-energy struc-

tures of  $Si_mGe_n$  (for  $m + n \leq 10$ ) clusters using tight-binding methods with out frequency analysis. Later on, they performed a more extensive study on binary  $A_mB_n$  (A,B= Si,Ge,C and  $m + n \leq 10$ ) [56] clusters using the B3LYP-DFT method but only on selected initial geometries with high symmetries. They have found that geometries of  $A_mB_n$  binary clusters follow similar structural patters with lower symmetries when compared with corresponding elemental  $Si_s$  and  $Ge_s$  in this size range. J.Tarus *et.al* [57] have studied the 'segregation in SiGe clusters' using classical molecular dyanamics (MD) method. Their main finding in this article is that Ge has strong tendency to segregate onto the surface of clusters. Jer-Lai Kuo *et.al* [58] has recently studied  $Si_mGe_n$  clusters with  $(m+n) \leq 7$  using B3LYP-DFT and CCSD(T) methods. They have found that  $Si_mGe_n$  clusters have similar structural patterns as those of corresponding elemental clusters of  $Si_s$  and  $Ge_s$ . Abu *et.al* [59] has studied the structural and electronic properties of core-shell Si-Ge nanoparticles using LDA-DFTB method. Very recently Jerzy Leszczynski *et.al*, [105] have also studied  $Ge_nSi_m$  in the size range  $n+m = 2-5$  using advanced *ab initio* approaches. From these studies we observe that globally optimized total energy minimum structures for  $Si_mGe_n$  clusters have only been studied for very small size range *i.e.*, ( $m + n \leq 10$ ) and these binary clusters largely remain unstudied in the medium size range. Keeping this in mind, we have investigated the structural growth pattern and variation in properties with increasing  $n$ , for medium sized binary homogeneous  $Si_nGe_n$  (size range = 22 Si-Ge units) clusters. Furthermore, in order to compare the structural growth pattern and properties of binary  $Si_nGe_n$  clusters with their elemental counter parts, we have studied the globally optimized structures and properties of both  $Si_n$  and  $Ge_n$  clusters in the same size range with DFTB method.

Metal clusters, like semiconductor clusters have been object of extensive theoretical and experimental investigations, due to their unique physical and chemical properties determined by their restricted size. Among the metal clusters, Copper clusters constitute one of the more studied metals in the field of cluster science. During the last decade many parameter-free studies on small Copper clusters have been published. These include the density-functional study on small neutral and charged Copper clusters by Massobrio *et.al*, [60] and the similar work by Calaminici *et.al*, [61] on neutral and charged clusters, as well as others studies based on either *ab initio* [62] or density-functional [63] approaches. It has been observed that except for the absolutely smallest Copper clusters, there are different assumptions on the structure of clusters based on different potentials. For this reason

we have studied copper clusters in the medium size range upto  $n=36$  atoms and their structural and electronic properties are investigated in detail.

In our present work all the calculations are performed using Density Functional Tight Binding Method combined with genetic algorithm method (method for global optimization) for the determination of total energy minimum structures for all cluster systems. Search for the global total-energy minimum structures for different cluster systems and extracting information about their structural and electronic properties have been an important topic of our work.

## 1.2 Organization of work

This work is organized as follows. After the introductory initial chapter, we have discussed briefly Density Functional Theory and then our method (DFTB) used for calculations in chapter two. Density Functional Tight Binding method (DFTB) has been used through out this work for the calculations of total energy minimum structures of pure Silicon ( $Si_n$ ), pure Germanium ( $Ge_n$ ) and homogeneous binary ( $Si_nGe_n$ ) clusters. Copper clusters ( $Cu_n$ ) have also been studied using the same method. We have presented the genetic algorithm method in detail afterwards which is used to obtain the globally optimized structures for our systems. In chapter three we have discussed the geometric structures obtained from global optimization of semiconductor clusters including both elemental and binary clusters, Silicon and Germanium. In chapter 4, we have given various tools for analysing our semiconductor cluster structures, which include similarity functions, common neighbours analysis, radial distribution functions, stability functions, HOMO-LUMO Gap analysis and shape analysis. All these tools enable us to study the structural and electronic properties of investigated clusters in detail. In chapter five we have presented the results of theoretical studies of  $Cu_n$  clusters and their structural and electronic properties are discussed in detail. In chapter 6 we will conclude our results and work.



## Chapter 2

---

# Theory and Method For Calculations

---

In this chapter we will give a short overview of Density Functional Theory and, afterwards, introduce the Density Functional Tight Binding Method (DFTB) that has been applied through out this work to calculate the electronic and structural properties of nanoparticles and finally talk about the optimization method with which we have obtained globally optimized total-energy minimum structures for our systems.

### 2.1 Density-Functional Theory

The most central problem of quantum chemistry is to solve Schrodinger-wave equation [67]

$$\hat{h}\psi = E\psi \quad (2.1)$$

Applying the Born-Oppenheimer approximation is a first step towards an approximate solution of the Schrodinger-wave equation. The resulting equation is the time-independent Schrodinger wave equation for the electrons

$$\hat{h}_e\psi_e = E_e\psi_e \quad (2.2)$$

where  $\psi_e = \psi_e(x_1, x_2, x_3, \dots, x_N)$  is the electronic wavefunction depending on position  $r_i = (x_i, y_i, z_i)$  and spin  $\sigma_i$  of each electron  $i$  [ $x_i = (r_i; \sigma_i) = (x_i, y_i, z_i, \sigma_i)$ ]. Knowing the complete N-electron wavefunction  $\psi_e$  is more than actually required for the calculations of experimental observable, because these only depend on the coordinates of one or two electrons. Thomas

and Fermi [68] proposed that one can determine the electron density in three-dimensional position-space instead of electronic wavefunction and from that obtain all information of interest. The resulting equation that directly determines electronic density  $\rho(r)$  is much easier to solve than Schrodinger wave equation itself. This so-called Thomas-Fermi method has been one of the most important steps in the development of Density-Functional Theory (DFT). However the results obtained from Thomas-Fermi approach are very inaccurate, because the approach is constructed as an approximation instead of an exact alternative to solve the Schrodinger wave equation *e.g.*, the Thomas-Fermi method does not give an electronic shell structure. Density-functional theory itself is based on the two theorems [69] by Pierre Hohenberg and Walter Kohn that have been published in 1964. Walter Kohn has been honored with the Nobel-prize in chemistry (together with John Pople) for this fundamental work.

### The Hohenberg-Kohn Theorems

The first Hohenberg-Kohn theorem states that it is possible to calculate any ground state property of a given system by the knowledge of electron-density  $\rho(r)$  only. Therefore, the total(electronic)energy of the system  $E_e$  is a well-defined functional of the electron density:

$$E_e[\rho(r)] = F[\rho(r)] + \int \rho(r)V_{ext}(r)dr \quad (2.3)$$

Here,  $F[\rho(r)]$  is a universal potential that is independent of the external potential  $V_{ext}(r)$  and, therefore, also of the geometry of the nuclei of the system. The external potential is determined first of all by the Coulomb Potentials of the atomic nuclei but may, moreover, contain additional (*e.g.*, electrostatic or gravitational) potentials. Through the potential, the electron density  $\rho(r)$  determines the Hamilton operator and thereby, all ground-state properties. The total number of electrons for the system of the interest is also defined by  $\rho(r)$ :

$$N = \int \rho(r)dr \quad (2.4)$$

The second Hohenberg-Kohn theorem states that a variation of the ground-state electron density [starting from the exact electron density  $\rho(r)$ ],

$$\tilde{\rho}(r) = \rho(r) + \delta\rho(r) \quad (2.5)$$

results in a positive change of the total ground-state energy:

$$E_e[\tilde{\rho}(r)] > E_e[\rho(r)] \quad (2.6)$$

By changing the electron density to  $\tilde{\rho}(r)$ , the number of electrons in the system are unchanged:

$$\int \tilde{\rho}(r)dr = \int \rho(r)dr \quad (2.7)$$

Thus, the variational principle holds for the energy as a density functional.

## The Kohn-Sham Equations

The last mentioned problem, *i.e.*, the Hohenberg-Kohn theorems do not explicitly give any functionals, is still unsolved. In 1965 Walter Kohn and Lu Jeu Sham published a method for the calculation of the electron density with the so-called Kohn-Sham equations [70]. The Kohn-Sham Equations are a set of single-particle equations similar to the Hartree-Fock equations. The problem, how to calculate the total energy as a density functional, has been transformed to the solution of this set single-particle equations. We will now have a closer look at an N-particle system: the total (electronic) energy  $E_e[\rho(r)]$  of the system to interest can be described as,

$$E_e[\rho(r)] = T[\rho(r)] + \int \rho(r)[V_{ext}(r) + \frac{1}{2}V_C(r)]dr + \acute{E}_{XC}[\rho(r)] \quad (2.8)$$

Here, T is the kinetic energy of the system,  $\int \rho(r)V_{ext}(r)dr$  is the energy resulting from the external potential, and  $\frac{1}{2} \int \rho(r)V_C(r)dr$  the Coulomb energy which is resulting from the electron repulsion (the factor  $\frac{1}{2}$  deletes the double-counted terms).  $\acute{E}_{xc}$  is the so-called exchange correlation energy. This term contains all terms that are not included in the other three addend. After exertion of the variational principle using the Lagrange multiplier  $\mu$  (which is the chemical potential for the electrons), we get

$$\frac{\delta T}{\delta \rho} + V_{ext}(r) + V_C(r) + \frac{\delta \acute{E}_{XC}}{\delta \rho} = \mu \quad (2.9)$$

where  $\mu$  has been introduced to satisfy the condition,

$$N = \int \rho(r)dr \quad (2.10)$$

The trick of Kohn and Sham is to introduce a system similar to the original one but with  $N$  particles that are non-interacting. These  $N$  non-interacting particles shall move in an external potential  $V_{eff}(r)$  that is defined in such a

way that the electron density and the energy are equal to the electron density and the energy of the original system to interacting particles. Equations [1.8] and [1.9] therefore become much more easier for this fictive system:

$$E_e[\rho(r)] = T^{KS}[\rho(r)] + \int V_{eff}(r)\rho(r)dr \quad (2.11)$$

After applying the variational principle we obtain,

$$\frac{\delta T^{KS}}{\delta \rho} + V_{eff}(r) = \mu \quad (2.12)$$

with

$$V_{eff}(r) = \frac{\delta T}{\delta \rho} - \frac{\delta T^{KS}}{\delta \rho} + V_{ext}(r) + V_C(r) + \frac{\delta \acute{E}_{xc}}{\delta \rho(r)} \quad (2.13)$$

Here the kinetic energy  $T^{KS}$  of the fictive system is not equal to the kinetic energy of the real system. The Hamiltonian is now simplified to a great extend and can be written as the sum of N single-particle operators  $\hat{h}_{eff}$ :

$$\hat{H} = \sum_{i=1}^N \left[ -\frac{1}{2} \nabla_{r_i}^2 + V_{eff}(r_i) \right] = \sum_{i=1}^N \hat{h}_{eff}(i) \quad (2.14)$$

We can write the many-body wavefunction as a single Slater determinant

$$\psi = | \psi_1, \psi_2, \psi_3, \dots, \psi_N | \quad (2.15)$$

and the single-particle equations are,

$$\hat{h}_{eff}(i)\psi_i = \epsilon_i\psi_i \quad (2.16)$$

These determine the single-particle energies  $\epsilon_i$ . Finally, the electron density is the sum over the N orbitals with the lowest single-particle energies  $\epsilon_i$ :

$$\rho(r) = \sum_{i=1}^N n_i | \psi_i(r) |^2 \quad (2.17)$$

where  $n_i$  is the occupation number of the  $i$ -th orbital. The electron density of the system consisting of non-interacting particles has been constructed in such a way that it is equal to the electron density of the real system. However, the single-particle wavefunctions of the non-interacting particles  $\psi_i$  and energies  $\epsilon_i$  are not identical with those of the electrons but practice has shown that they provide a good approximation to them.

## The Local-Density Approximation

A problem originates from the exchange-correlation energy  $E_{xc}[\rho(r)]$  and the according potential

$$V_{xc}(r) = \frac{\delta T}{\delta \rho} - \frac{\delta T^{KS}}{\delta \rho} + \frac{\dot{E}_{xc}}{\delta \rho} \equiv \frac{\delta E_{xc}}{\delta \rho} \quad (2.18)$$

because they are unknown. However, the exchange-correlation energy can be written as

$$E_{xc}[\rho(r)] = \int \epsilon_{xc}(r)\rho(r)dr \quad (2.19)$$

where  $E_{xc}$  can be expressed approximately in terms of the electron density and its derivatives:

$$\epsilon_{xc}(r) = \epsilon_{xc}[\rho(r), |\nabla\rho(r)|, \nabla^2\rho(r), \dots] \quad (2.20)$$

The local-density approximation (LDA) approximates  $\epsilon_{XC}$  as depending only on the electron density  $\rho(r)$ .

## 2.2 Density-Functional Tight-Binding Method

The Density-Functional Tight Binding method has been used throughout this work to optimize the structures of investigated clusters and to calculate their structural and electronic properties. DFTB method has been developed by G.Seifert *et.al*, [64, 65, 66]. The DFTB method is based on the Density-Functional Theory of Hohenberg and Kohn [69] in the formulation of Kohn and Sham [70]. The single-particle eigenfunctions  $\psi_i(r)$  are expanded in a suitable set of localized atom-like basis functions  $\phi_m(r)$  :

$$\psi_i(r) = \sum_i c_{im}\phi_m(r) \quad (2.21)$$

Here,  $m$  is a compound index that describes the atom at which the function is centered, the angular dependence of the function, as well as its radial dependence. These functions are obtained from self-consistent density-functional calculations on the isolated atoms employing a large set of Slater-type basis functions. The Hamilton operator  $\hat{h}$  is defined as

$$\hat{h}_{eff} = \hat{t} + V_{eff}(r) \quad (2.22)$$

Here,  $\hat{t}$  is kinetic energy operator ( $\hat{t} = \frac{1}{2}\nabla^2$ ), and the effective Kohn-Sham potential  $V_{eff}(r)$  is approximated as a simple superposition of the potentials

of the neutral atoms,

$$V_{eff}(r) = \sum_j V_j^0(|r - R_j|), \quad (2.23)$$

where  $R_j$  is the position of  $j$ th atom.

Furthermore, we make use of a tight-binding approximation, so that

$$h_{mn} = \langle \phi_m | \hat{t} + \sum_j V_j^0 | \phi_n \rangle = \langle \phi_m | \hat{t} + V_{j_m}^0 + (1 - \delta_{j_n, j_m}) V_{j_n}^0 | \phi_n \rangle \quad (2.24)$$

where  $R_{j_m}$  and  $R_{j_n}$  are the positions of the atoms at which the  $m$ th and  $n$ th basis functions are centered, respectively. The Kronecker- $\delta$  is included in order to assure that the potential is not double counted for  $j_n = j_m$ . Through this approximation, only two center terms in the Hamiltonian matrix are considered, but all two-center terms ( $h_{mn} = \langle \phi_m | \hat{h} | \phi_n \rangle$ ,  $S_{mn} = \langle \phi_m | \phi_n \rangle$ ) are calculated exactly within the Kohn-Sham basis. These approximations lead to the secular equations

$$\sum_m c_{nm}(h_{mn} - \epsilon_i S_{mn}) = 0 \quad (2.25)$$

Using the Kohn-Sham eigenvalues  $\epsilon_i$ , the total energy  $E[\rho(r)]$  may be written as

$$E_e[\rho(r)] = \sum_i^{occ} \epsilon_i - \frac{1}{2} \left[ \int V_{eff}(r) \rho(r) dr - \int V_{ext}(r) \rho(r) dr \right] + E_{xc} - \frac{1}{2} \int V_{xc}(r) \rho(r) dr + E_N \quad (2.26)$$

Here, the external potential  $V_{ext}$  is the electrostatic potential from the nuclei,  $E_{xc}$  the exchange correlation energy,  $V_{xc}$  the corresponding potential,  $E_N$  the nuclear repulsion energy, and  $\rho(r)$  is the electron density. Since the difference between superposed atomic electron densities and the true electron density of the system of interest is only small and since by far the largest parts of the interatomic interactions are of fairly short range, the major part of the total energy is contained in the difference of the single particle energies of the system of interest,  $\epsilon_i$ , and of the isolated atoms,  $\epsilon_{jm}$  ( $\epsilon_{jm}$  is the  $j$ th eigenvalue of the  $m$ th atom), *i.e.*,

$$\epsilon_B = \sum_i^{occ} \epsilon_i - \sum_j \sum_m \epsilon_{jm} \quad (2.27)$$

The short-ranged interactions can be approximated by simple pair-potentials, so that the expression for total energy becomes,

$$E_B \approx \sum_i^{occ} \epsilon_i - \sum_j \sum_m \epsilon_{jm} + \frac{1}{2} \sum_{j \neq j'} U_{jj'}(|R_j - R_{j'}|) \quad (2.28)$$

List of Diatomic molecules		
Compound	Diatomic	Valence Electrons
SiGe	Si <sub>2</sub> , Ge <sub>2</sub> , SiGe, GeSi	Si:3s,3p; Ge: 4s,4p
Si	Si <sub>2</sub>	3s,3p
Ge	Ge <sub>2</sub>	4s,4p
Cu	Cu <sub>2</sub>	3d,4s,4p

Table 2.1: Shows list of diatomic molecules for which parameter-free DFT calculations have been performed to obtain potentials for the DFTB calculations. The right column gives those orbitals whose electrons are treated within frozen-core approximations.

$U_{jj'} | R_j - R_{j'} |$ ) is determined as the difference of  $\epsilon_B$  and  $\epsilon_B^{SCF}$  for diatomic molecules (with  $\epsilon_B^{SCF}$  being the total energy from exact density-functional calculation). Finally we will consider only valence electrons for our calculations, whereas the others will be treated as frozen core. With these approximations all relevant information on the above mentioned matrix elements can be extracted from calculations on isolated two-atomic systems, in our cases on these two-atomic systems shown in table [Table 2.1]. The local total-energy minimization is performed by using the forces. Here, the force  $F_j$  that acts on the  $j$ th atom of interest can be calculated using the Hellmann-Feynman theorem,

$$F_j = -\frac{\partial E}{\partial R_j} \quad (2.29)$$

The forces can be split up into two parts, one acting on the electrons only  $F_j^e$ , the other one acting exclusively on the nuclei  $F_j^N$ ,

$$F_j = F_j^e + F_j^N \quad (2.30)$$

The nuclear part consists of the sum of the derivatives of the repulsive energies of the nuclei,

$$F_j^N = \sum_{j \neq j'} \frac{\partial}{\partial R_j} \left( \frac{Z_j Z_{j'}}{|R_j - R_{j'}|} \right) \quad (2.31)$$

whereas, the electronic part can be written as the sum of orbital contributions,

$$F_j^e = \sum_i n_i F_{ji} = -\frac{\partial}{\partial R_j} \left( \sum_i n_i \langle \phi_i | \hat{h} | \phi_i \rangle \right) \quad (2.32)$$

Here,  $n_i$  is the occupation number of the  $i$ th orbital (either being  $n_i=0$ , or  $n_i=1$ ), and as consequence we sum only over the occupied orbitals ( $n_i=1$ ,  $i=1,\dots,\text{occ}$ ).  $F_{ji}$  can be written as

$$F_{ji} = \sum_{m,n} c_{im}c_{in} \left( -\frac{\partial H_{mn}}{\partial R_j} + \epsilon_i \frac{\partial S_{mn}}{\partial R_j} + \frac{\partial V_{mn}^{ee}}{\partial R_j} \right) \quad (2.33)$$

$V_{mn}^{ee}$  are the matrix elements of the electron-electron potential ( $V^{ee} = V_H + V_{xc}$ ). The component of the potential is compensated by the nuclear part  $F_j^N$ ,

$$F_j^N \approx \sum_{m,n} c_{im}c_{in} \frac{\partial V_{mn}^{ee}}{\partial R_j} \quad (2.34)$$

These two terms are approximated by the repulsive term  $U(R)$ ,

$$U(R) = \begin{cases} \sum_n a_n (R - R_1)^n & \text{for } R < R_1 \\ 0 & \text{for } R \geq R_1 \end{cases} \quad (2.35)$$

The forces that are acting on an atom positioned at  $R_j$ , can finally be calculated as,

$$F_j = -\nabla_j E_{tot} = \sum_i \sum_{m,n}^{occ} \left( -\frac{\partial H_{m,n}}{\partial R_j} + \epsilon_i \frac{\partial S_{m,n}}{\partial R_j} \right) + \frac{1}{2} \sum_{j \neq j'} \frac{\partial}{\partial R_j} U(|R_j - R_{j'}|) \quad (2.36)$$

## 2.3 Method for Global Optimization

In Cluster studies, the most important and that's why most difficult job is to find the globally optimized structures. Global structure optimization is difficult because of the omnipresence of local minima, and the number of which increases exponentially with the size of clusters. We can get the idea, how difficult is to find global optimized structure by this simple fact that a 13-atom Leonard-Jones cluster has at least 1506 distinct local minima and there are good reasons to expect roughly as many local minima for more realistic potentials modeling various elements. Global optimization is difficult also because of the fact that the one has to explore the entire space of potential surface so that searching will not miss the lowest total energy minimum, and also take care that enough individual relaxation has been done. Numerous approaches have been suggested for solving the global optimization problem, among them, Simulated Annealing (SA), Basin-Hopping (BH), Genetic algorithms (GA) are most often used methods. In our present work we have applied a new global optimization method that has been developed by our group. Initial structures are generated using random-number generators and then combined with genetic algorithms to get optimized structures.

### Random Number Generator

A random number generator is a computational device designed to generate a sequence of numbers that lack any pattern *i.e.*, appear random. The many applications of randomness has lead to many different methods for generating random data. In dealing with structure optimization problem, we want to have very many different initial structures that we hope could cover the entire space and later leading to relaxed structures, so we need random number generator that generates as many divities possible. One of the system-supplied random numbers generators is called a 'random number generator' named like 'ran' and a calling sequence like `x=ran(iseed)`. You initialize `iseed` to a arbitrary value before the first call to run. Each initializing value will typically return a different subsequent random sequence, or at least a different subsequence of some one enormously long sequence. The same initializing value of `iseed` will always return to the same random sequence. The system-supplied random number generator (`iseed`) can supply random number from 0 to 1, and since the same initializing value of `iseed` can always give the same random sequence, there is one advantage that we

can trace back to the structures that were generated. In the present work we shall use random number generator to generate initial structures that will be improved with genetic algorithm method.

## Genetic Algorithm

Genetic algorithms are used as a search technique in computing to find exact or approximate solutions to optimizations and search problems. When they are used in atomic cluster studies, they are named as Cluster Genetic Algorithms (CGA). The cluster genetic algorithms works by randomly selecting and mating the more fit individuals in a generation to produce the next generation of offsprings, where fitness is the measure of the energetic stability for an individual cluster structure. Global minima is than found as some off the new offsprings will have lower energy than their ancestors. Until now, different genetic operators have been used to optimize the structure of clusters. As global optimization faces two different requirements, one, the search has to explore the entire space in order to not miss the global minimum and secondly, local relaxation should be sufficient in order to provide an accurate total energy for that initial structure. Because of these tough requirements, one has to remember that there is no guarantee that any method will identify the structure of the global total-energy minimum accurately.

The genetic algorithm method, which we used for our calculations is described as follows : Suppose that we have optimized the structure of the cluster with  $n$  units. From this structure we construct a first generation consisting of  $M$  independent clusters for the  $(n+1)$  unit system by randomly adding one atom (In case of homogeneous bimetallic SiGe clusters, we added one atom each of Si and Ge) and letting these structures to relax to their nearest total-energy minima. Subsequently, a new set of clusters is constructed by cutting each of the original ones randomly into two parts that are interchanged (under the constraints mentioned above) and, afterwards, allowed to relax. Out of the total set of  $2M$  structures, the  $M$  ones of the lowest energy are kept as the next generation. This procedure is repeated until the lowest total energy is unchanged for a large number of generations.

## Chapter 3

---

# Results of Semiconductor Cluster Studies

---

### 3.1 Introduction

Main aim of our work lies in finding and exploring the geometric structures of pure and binary semiconductor clusters, Silicon and Germanium upto 44 atoms . For investigation of structural and electronic properties, first important step is to find the global minima of cluster structures. The method for structural optimization has been described in chapter 2 and its not an easy task. The genetic algorithm that has been applied through out our work is very effective and strong tool but still it has some limitations. It requires more computational effort and time. DFTB routine takes long time as the number of atoms increases. In this chapter, we will present and discuss the geometric structures of pure  $\text{Si}_n$ , pure  $\text{Ge}_n$  and binary semiconductor  $\text{Si}_n\text{Ge}_n$  clusters obtained from DFTB calculations.

As it has been described above, free Silicon clusters have been studied more, both experimentally and theoretically, compared to Germanium clusters. Previous studies have confirmed that  $\text{Si}_n$  and  $\text{Ge}_n$  have identical structures upto  $n = 12$  [75]-[81]. Ground state structures of small Silicon clusters in the size range ( $n \leq 11$ ) have been well established using *ab initio* and Density Functional Theory (DFT) calculation [11, 12, 104]. Jackson and coworkers [15] reported systematic searches for the global minima of Silicon cation and neutral clusters in the medium size range of Si  $19 \leq n \leq 28$ , using either single-parent evolution algorithm or the big bang algorithm coupled with density functional tight binding method (DFTB) [106, 107, 108].

Recently, the size range  $25 \leq n \leq 29$  has received increasingly attention [27, 110, 109, 111, 112] largely because earlier experiments [3, 4, 5, 8, 84] have revealed a structural transition from prolate to near spherical geometry at around  $\text{Si}_{27}$  for both cation and anion Silicon clusters. A more recent experimental/theoretical photoelectron spectroscopy study [113] also confirmed the structural transitions occurring at  $\text{Si}_{27}$  for anion clusters. To date, the true global minima for many  $\text{Si}_n$  clusters in medium size range are still debatable [112, 107, 108, 114, 115, 116]. The observed mobility of silicon cation cluster  $\text{Si}_n^+$  indicates that isomers are prolate for  $n < 25$  and oblate for  $n > 33$ , while the both shaped isomers coexist in the size range of 25-33 [4, 5]. Germanium is contiguous to Silicon in the periodic table. It also shows many important characteristics similar to Silicon. For the small Ge clusters, their ground-state structures have similar geometries in comparison with Si except for their bond lengths. Previous studies have confirmed that the global minimum  $\text{Si}_n$  and  $\text{Ge}_n$  have identical structures [75]-[81] up to  $n = 12$ . The main difference is the increase in bond lengths of Ge clusters by about 4-5% compared to Si. But for the larger Ge and Si clusters, their ground state structures are different [83, 84]. Shvartsburg *et.al*, have performed a systematic ground state geometry search for  $\text{Ge}_n$  neutral and cations in the  $n < 16$  size range using density functional theory(local-density approximation) and gradient-corrected methods [45]. They also made a comparison between the Si and Ge clusters in which the structures of  $\text{Ge}_n$  and  $\text{Si}_n$  for  $n > 14$  differ in details. Since the pure elemental clusters in small size range have identical geometries, it is reasonable to ask whether binary clusters  $\text{Si}_n\text{Ge}_n$  would preserve such trend and for larger values of  $n$  if they show homogeneous or non-homogeneous growth process. Studies on binary semiconductor clusters may provide us an answer to this question. For binary  $\text{Si}_n\text{Ge}_n$ , available data about globally optimized structures is limited to small cluster size ( $m+n \leq 10$ ). For binary Si-Ge clusters, Tarus *et.al*, [57] have studied the geometrical structures and the distribution of atomic species in  $\text{Si}_m\text{Ge}_m$  clusters at 0 K utilizing different optimizing tools. They found out that there is a strong segregation of Ge to the surface. Zhi-Hao Jin *et.al*, [56] have found that  $\text{Si}_m\text{Ge}_n$  ( $m+n \leq 10$ ) have similar ground state structures to corresponding elemental  $\text{Si}_s$  and  $\text{Ge}_s$  clusters. A very recent study of binary  $\text{Si}_m\text{Ge}_n$  ( $m+n \leq 7$ ) by Jer-Lai Kuo *et.al*, [58] have found that binary clusters are found to have similar ground-state structures as the corresponding elemental clusters. After giving a short description of the available data about binary and elemental Si-Ge clusters, we will proceed to our results of DFTB calculations for global optimization of

binary homogeneous  $\text{Si}_n\text{Ge}_n$ , and pure  $\text{Si}_n$  and  $\text{Ge}_n$  clusters upto medium size range ( $n \leq 44$  atoms).

### 3.2 Structures of $\text{Si}_n, \text{Ge}_n$ , and $\text{Si}_n\text{Ge}_n$ Clusters

The globally optimized total energy minimum structures of pure and binary Si-Ge clusters obtained from DFTB are shown in figures [3.1-3.8]. Bond length comparison of our cluster systems is presented in Table [3.1]. Our results for binary  $\text{Si}_n\text{Ge}_n$  clusters are in well agreement with one of the recent studies on  $\text{Ge}_n\text{Si}_m$  ( $m+n = 5$ ) by Jerzy Leszczyński *et.al*, [105].  $\text{Si}_3$  and  $\text{Ge}_3$  both have an isosceles triangle structure with  $\text{C}_{2v}$  point group which is confirmed by most of the previous studies [75]-[81]. From geometric point of view, four-atom clusters are very important as they can show the onset of three-dimensional (3D) evolution. Here we have found that all the four-atomic cluster systems have a  $\text{D}_{2h}$  planar rhombus structure as found in previous studies [42, 50, 103, 104, 105]. In case of  $\text{Si}_4$  the bondlengths of each side is equal to 2.31 Å and that of additional bond along the shorter diagonal is 2.65 Å where as in case of  $\text{Ge}_4$ , each side is 2.55 Å, and shorter diagonal has 2.92 Å, which is in good agreement with Erm Kikuchi *et.al*, [50]. We can see that there is an increase of bondlengths in case of  $\text{Ge}_4$  as compared to  $\text{Si}_4$ . In case of  $\text{Si}_2\text{Ge}_2$  planer rhombus structure ( $\text{D}_{2h}$ ) has side bondlengths equal to 2.5 Å where as shorter diagonal has bondlength of 2.63 Å. There is no Si-Si interaction in this four-atomic cluster. Our structure for  $\text{Si}_2\text{Ge}_2$  is in very good agreement with S.D.Li *et.al*, [55] and Pawel Wielgus *et.al*, [105]. Pawel Wielgus *et.al*, [105] have found the side bondlengths in  $\text{Si}_2\text{Ge}_2$  equal to 2.415 Å which is slightly shorter than our bondlengths. A trigonal bipyramid structure with  $\text{D}_{3h}$  point group is obtained for  $\text{Si}_5$  and  $\text{Ge}_5$ .  $\text{Si}_6$  has  $\text{D}_{4h}$  tetragonal where as  $\text{Ge}_6$  has  $\text{C}_2$  symmetry.  $\text{Si}_3\text{Ge}_3$  takes an edge-capped distorted bipyramid as its ground state structure ( $\text{C}_{2v}$ ). The edge-capping Si atom is directly connected to two Ge atoms in the four membered horizontal plane to form more Si-Ge bonds. Si-Si interaction is very weak  $r_{\text{si-si}} = 3.5$  Å. This result is also in very good agreement with S.D.Li *et.al*, [55].  $\text{Si}_7$  has  $\text{D}_{5h}$  pentagonal bipyramid structure where as  $\text{Ge}_7$  has distorted pentagonal bipyramid structure with  $\text{C}_{2v}$  point group. For  $\text{Si}_8$  cluster, we have obtained a singly capped pentagonal bipyramid which is in agreement with the results based on the tight binding molecular dynamics calculation by I.H.Lee *et.al*, [121].  $\text{Si}_4\text{Ge}_4$  has also a singly capped pentagonal bipyramid structure ( $\text{C}_s$  structure) which is comparable to the  $\text{C}_s$  structure of S.D.Li *et.al*, [55].  $\text{Ge}_8$  has distorted bicapped octahedron structure with  $\text{C}_{2h}$  point group. We have found a bicapped pentagonal bipyramid with  $\text{C}_{2v}$  point group as the global energy minima for  $\text{Si}_9$  cluster. For this structure the two caps are on the same side of the pyramid.  $\text{Ge}_9$  has Bernal structure with

( $C_{2v}$ ) pointgroup.  $Si_{10}$  is a magic number cluster which has been extensively studied theoretically. Our calculation confirms that a tetra capped trigonal prism with  $C_{3v}$  point group is the global minimum structure for  $Si_{10}$ .  $Si_5Ge_5$  has structure resembling to  $Si_{10}$  cluster structure. We have found a  $C_s$  distorted tricapped tetragonal antiprism or a distorted pentacapped trigonal prism structure as global energy minima for  $Si_{11}$  cluster. This was also proposed by Sieck *et.al*, [114]. Our results differ from the global energy minima of Ho and co workers [24]. They have found a tricapped trigonal prism with two additional caps on side trigonal faces  $C_{2v}$  structure. Our results also differ from Rohlfing and Raghavachari [11] calculations who predicted a ( $C_s$ ) bicapped tetragonal antiprism with additional caps on side trigonal faces structure. For  $Si_{12}$  cluster we have found a  $C_s$  structure which can be described as hexacapped trigonal prism. This structure has been a selected isomer for detailed study of  $Si_{12}$  cluster with combined tight-binding and density functional molecular dynamics investigation of  $Si_{12}$  cluster by Bahel and Ramakrishna [18]. Much more theoretical studies have been devoted to the  $Si_{13}$  cluster because of the possibility of finding a high symmetry ( $I_h$ ) core based icosahedral structure. However, existence of such icosahedral structure for  $Si_{13}$  has been subject of much more debate [19, 85, 117, 118, 119, 120]. We have found a  $C_s$  symmetry structure for  $Si_{13}$  cluster, which can be viewed as a slightly distorted  $C_{2v}$  structure. Our result is in good agreement with Ho *et.al*, [24]. Our result differs from DF-TB calculation by I.Rata *et.al*, [106] and work of X.C.Zeng *et.al*, [86] who have found a  $C_{2v}$  structure which can be described as a distorted tricapped trigonal prism with an additional rhombus capped on one edge of the prism. For  $Si_{14}$  cluster, a number of low lying isomers have been reported in the literature [21, 85, 106]. We have found a  $C_s$  structure as a global minimum structure for  $Si_{14}$  which was also found by Sieck *et.al*, [21]. This structure has two stacked rhombi with distortion and one fivefold ring capped with an atom. For  $Si_{15}$ , we have found  $C_1$  structure as global minimum structure which is in agreement with structure from global geometry optimization using basin-hopping method by Zeng *et.al*, [30]. For  $Si_{16}$  cluster, we have found a very symmetric and highly stable structure with  $C_{2v}$  point group. This structure is based on a stacking sequence of fourfold and fivefold rings with capping atoms. Our result differs from Ho *et.al*, [24] and Zeng *et.al*, [30], who predicted  $C_{2h}$  symmetry for  $Si_{16}$  cluster. We have found a  $C_1$  symmetry structure for  $Si_{17}$ ,  $Si_{18}$  and  $Si_{19}$  which are in agreement with results of Zeng *et.al*, [30]. For  $Si_{20}$  we have found a prolate structure with two distinct  $Si_{10}$  rings, this structure has  $C_1$  symmetry. From the

Bond length Comparison ( $\text{\AA}$ )				
Type	This work	[122]	experimental	[105]
Si <sub>2</sub>	2.25	2.27	2.36	2.25
Ge <sub>2</sub>	2.39	2.38	2.46	2.399
SiGe	2.32	2.33	2.41	2.32

Table 3.1: Bond Length Comparison

global minimum structures we can say that Si<sub>*n*</sub> clusters clearly have prolate structures till Si<sub>24</sub> and from Si<sub>25</sub> to Si<sub>37</sub> there is a gradual change from prolate to nearly spherical structures. The point groups of Si<sub>*n*</sub> cluster from Si<sub>3</sub> to Si<sub>20</sub> and for Ge<sub>*n*</sub> clusters from Ge<sub>3</sub> to Ge<sub>15</sub> are given in the Table [3.2] and [3.3] respectively.

Looking at the total energy minimum structures of binary Si<sub>*n*</sub>Ge<sub>*n*</sub>, and pure Si<sub>*n*</sub>, Ge<sub>*n*</sub> clusters obtained from DFTB calculations, we can observe that binary homogeneous Si<sub>*n*</sub>Ge<sub>*n*</sub> clusters do not follow the same growth pattern as that of pure Si<sub>*n*</sub> and pure Ge<sub>*n*</sub> clusters except for very small cluster size. Our structures for hetero Si<sub>*n*</sub>Ge<sub>*n*</sub> clusters do not resemble with those of pure Si<sub>*n*</sub> and pure Ge<sub>*n*</sub> cluster structures. Same is the case for both pure Si<sub>*n*</sub> and pure Ge<sub>*n*</sub> clusters as they also follow different growth patterns except for very small cluster size. Here we would like to mention that some geometric structures of Si<sub>*n*</sub> and Ge<sub>*n*</sub> clusters do resemble with some of the previous studies, as discussed above. Similarly binary Si<sub>*n*</sub>Ge<sub>*n*</sub> clusters, with two and three Si-Ge units also have structures which are already obtained from earlier studies. In case of binary Si<sub>*n*</sub>Ge<sub>*n*</sub> clusters, as the cluster size grows, we can observe that Si-Ge interactions are strong as we see more number of Si-Ge bonds. Also Si-Si interactions are very weak as seen from small sized binary Si<sub>*n*</sub>Ge<sub>*n*</sub> clusters. These structural developments give rise to formation of mixed alloy structures for binary Si<sub>*n*</sub>Ge<sub>*n*</sub> clusters.

In order to learn about these structural developments in detail, we have used various kinds of structural analysis tools, which we will discuss in next chapter.

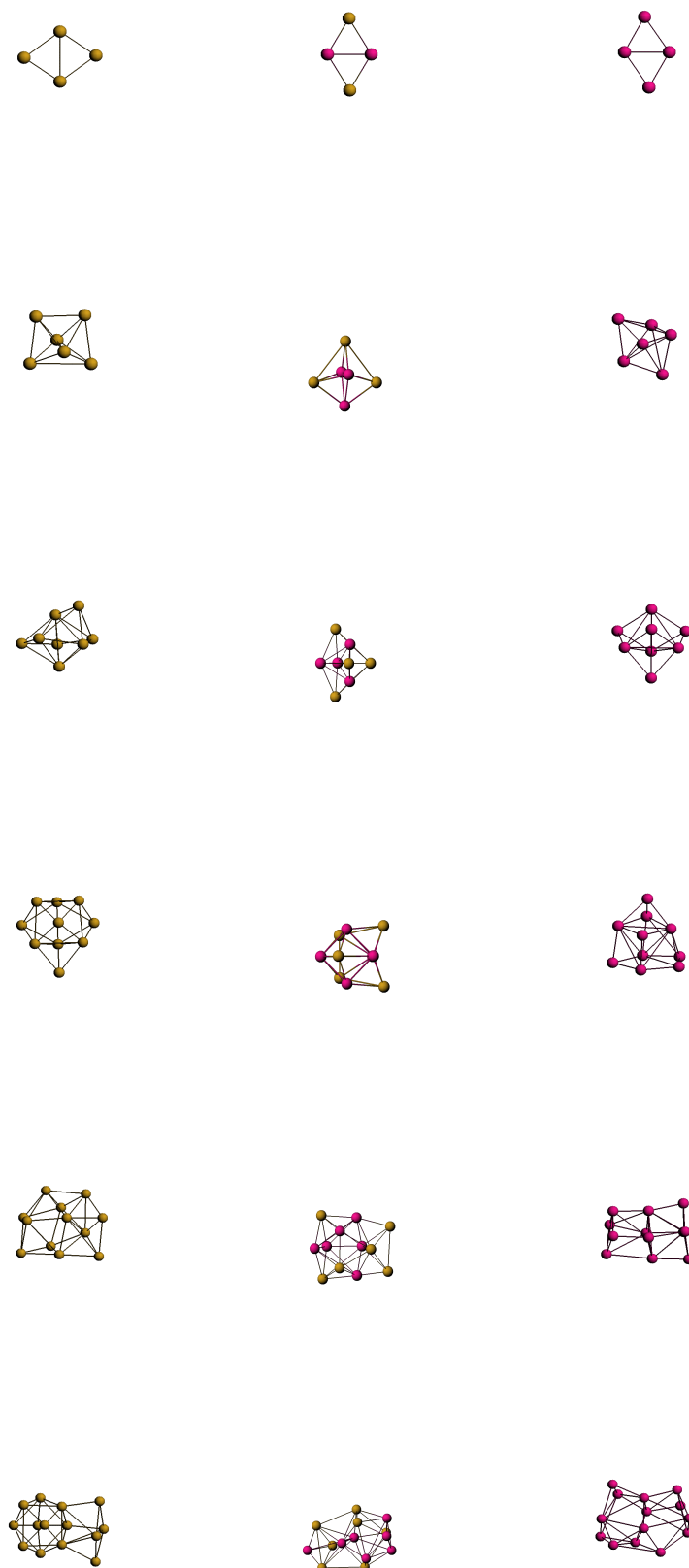


Figure 3.1: The optimized geometries of the energetically lowest isomers of  $Si_n$  (light green),  $Ge_n$  (pink) and  $Si_nGe_n$  clusters for  $2 \leq N \leq 7$  units

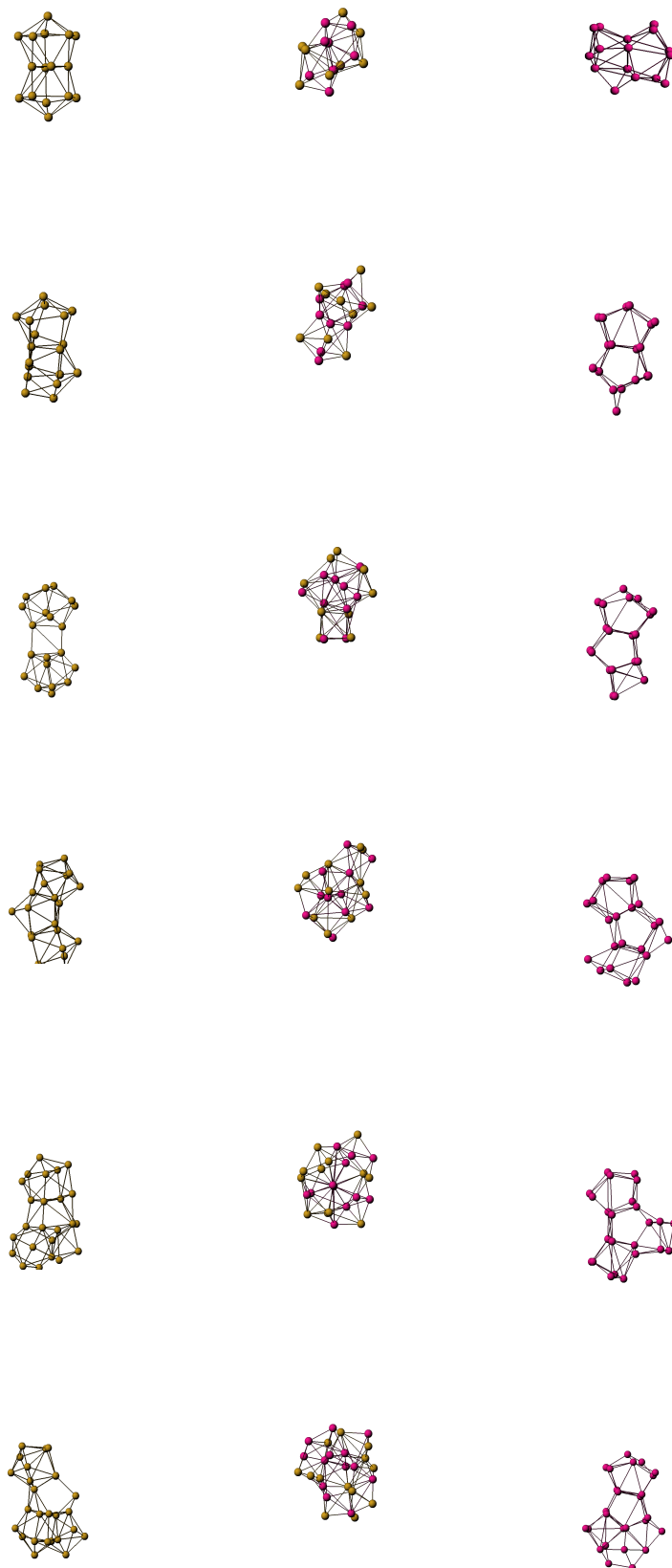


Figure 3.2: The optimized geometries of energetically lowest isomers of  $\text{Si}_n$  (light green),  $\text{Ge}_n$  (pink) and  $\text{Si}_n\text{Ge}_n$  clusters for  $8 \leq N \leq 13$  units

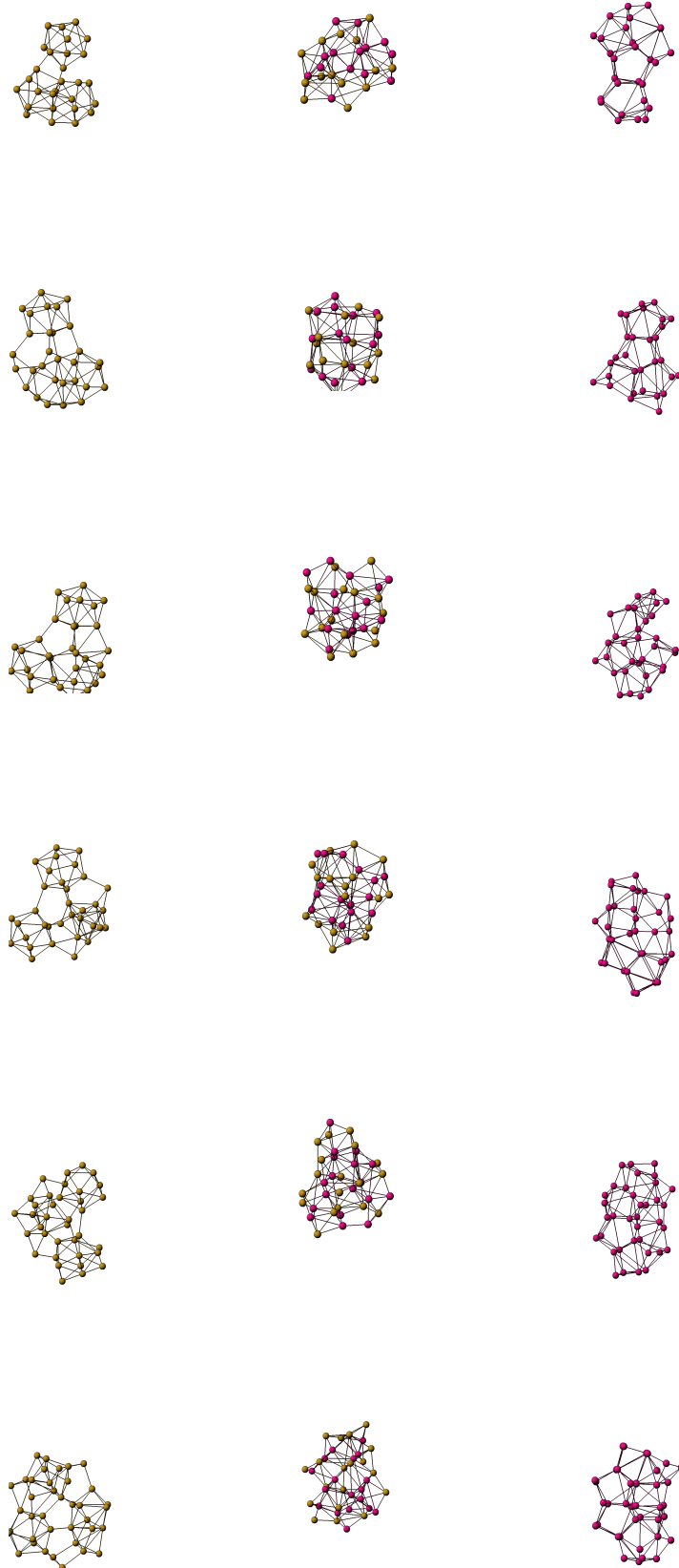


Figure 3.3: The optimized geometries of energetically lowest isomers of  $Si_n$  (light green),  $Ge_n$  (pink) and  $Si_nGe_n$  clusters for  $14 \leq N \leq 19$  units

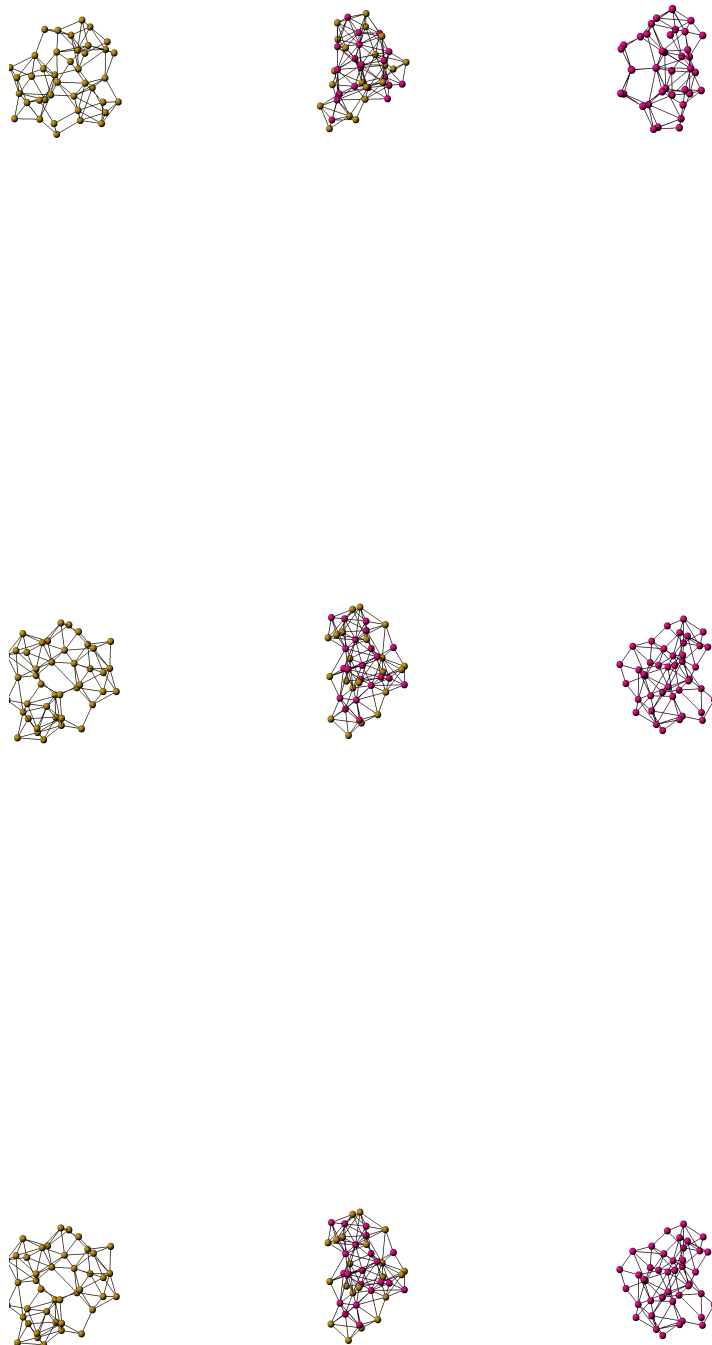


Figure 3.4: The optimized geometries of energetically lowest isomers of  $\text{Si}_n$  (light green),  $\text{Ge}_n$  (pink) and  $\text{Si}_n\text{Ge}_n$  clusters for  $20 \leq N \leq 22$  units

Point Group comparison for $Si_n$ clusters			
n	This work	[29]	[30]
3	$C_{2v}$	$C_{2v}$	$C_{2v}$
4	$D_{2h}$	$D_{2h}$	$D_{4h}$
5	$D_{3h}$	$D_{3h}$	$D_{5h}$
6	$D_{4h}$	$C_{2v}$	$C_{2v}$
7	$D_{5h}$	$D_{5h}$	$C_{3v}$
8	$C_s$	$C_1$	$O_h$
9	$C_{2v}$	$C_{2v}$	$C_{2v}$
10	$C_{3v}$	$C_{3v}$	$D_{5h}$
11	$C_s$	$C_{2v}$	$C_{2v}$
12	$C_s$	$C_{2v}$	$D_{2d}$
13	$C_s$	$C_{2v}$	$C_{2v}$
14	$C_s$	$C_s$	$D_{3h}$
15	$C_1$	$D_{6d}$	$C_1$
16	$C_{2v}$	$C_s$	$D_{4d}$
17	$C_1$	$C_2$	$C_s$
18	$C_1$	$C_s$	$C_s$
19	$C_1$	$C_s$	$C_s$
20	$C_1$	$C_2$	$C_1$

Table 3.2: Point Group comparison for  $Si_n$  clusters

Point Group comparison for Ge <sub>n</sub> clusters				
n	This work	[45]	[48]	[75]
3	C <sub>2v</sub>	C <sub>2v</sub>	C <sub>2v</sub>	C <sub>2v</sub>
4	D <sub>2h</sub>	D <sub>2h</sub>	D <sub>2h</sub>	D <sub>2h</sub>
5	D <sub>3h</sub>	D <sub>3h</sub>	D <sub>3h</sub>	D <sub>3h</sub>
6	C <sub>2</sub>	D <sub>4h</sub>	D <sub>4h</sub>	D <sub>4h</sub>
7	C <sub>2v</sub>	D <sub>5h</sub>	D <sub>5h</sub>	D <sub>5h</sub>
8	C <sub>2v</sub>	C <sub>2h</sub>	C <sub>2h</sub>	C <sub>s</sub>
9	C <sub>2v</sub>	C <sub>2v</sub>	C <sub>2v</sub>	C <sub>2v</sub>
10	C <sub>1</sub>	C <sub>3v</sub>	D <sub>3v</sub>	C <sub>3v</sub>
11	C <sub>1</sub>	C <sub>s</sub>		C <sub>2v</sub>
12	C <sub>1</sub>	C <sub>2v</sub>		C <sub>2v</sub>
13	C <sub>1</sub>	C <sub>2v</sub>		C <sub>s</sub>
14	C <sub>1</sub>	C <sub>s</sub>		
15	C <sub>1</sub>	C <sub>s</sub>		

Table 3.3: Point Group comparison for Ge<sub>n</sub> clusters

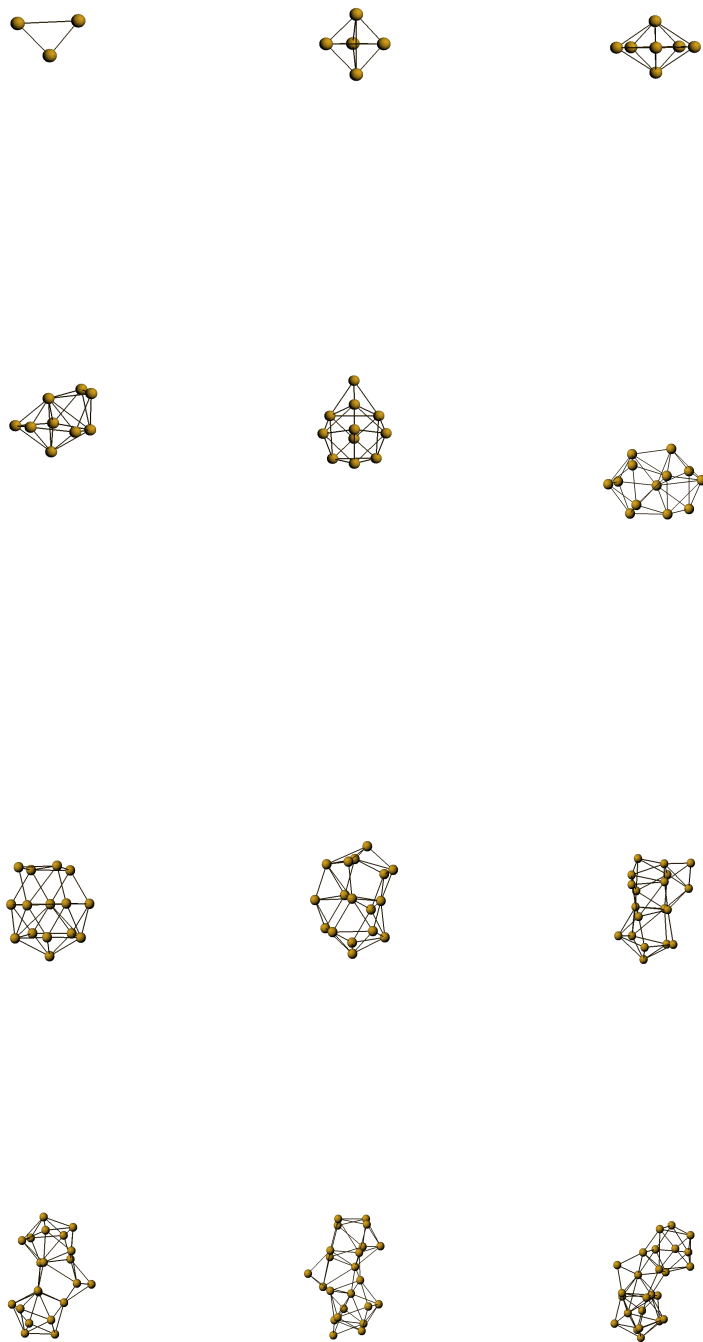


Figure 3.5: The optimized geometries of the energetically lowest isomers of odd numbered  $Si_n$  clusters for odd  $3 \leq N \leq 25$

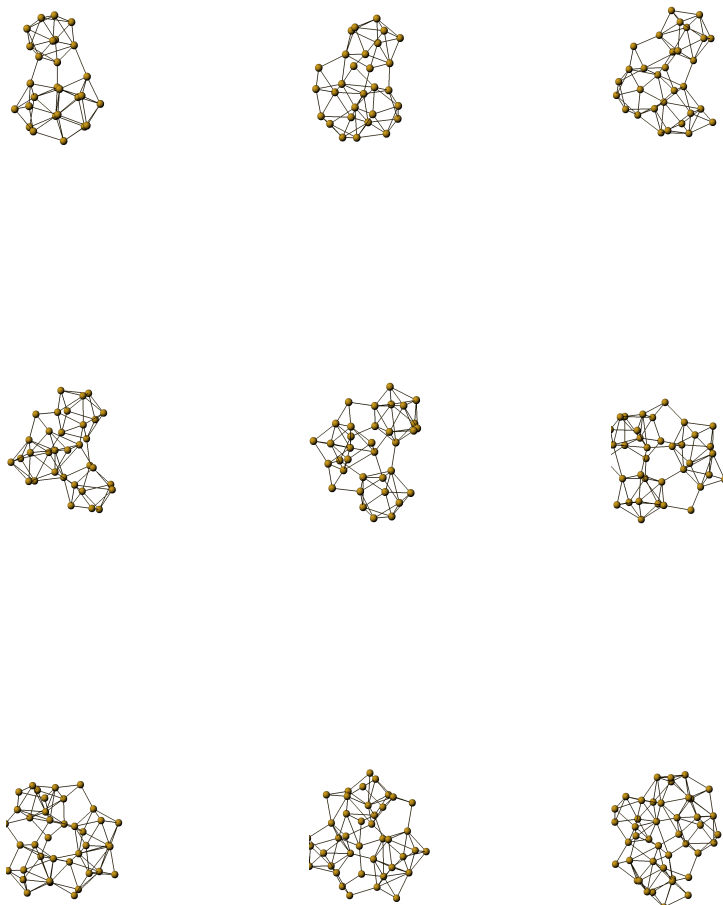


Figure 3.6: The optimized geometries of the energetically lowest isomers of odd numbered  $\text{Si}_n$  clusters for odd  $27 \leq N \leq 43$

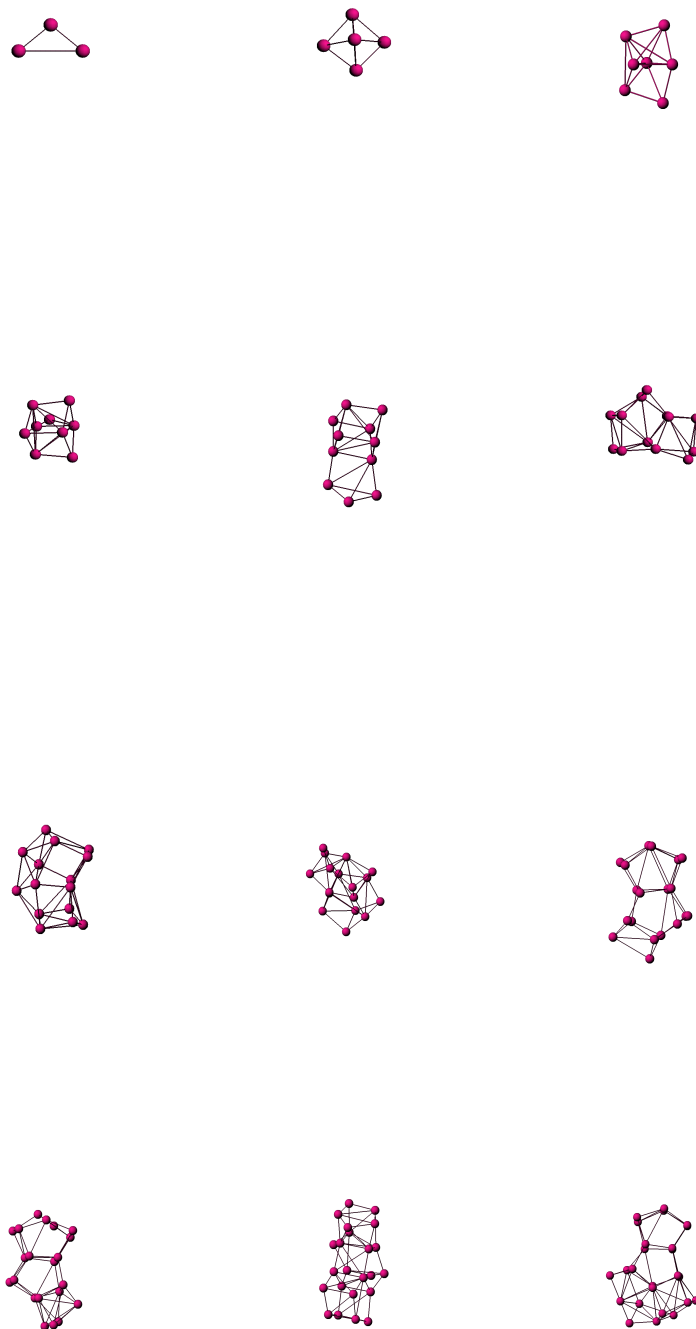


Figure 3.7: The optimized geometries of the energetically lowest isomers of odd numbered  $Ge_n$  clusters for odd numbered clusters  $3 \leq N \leq 25$

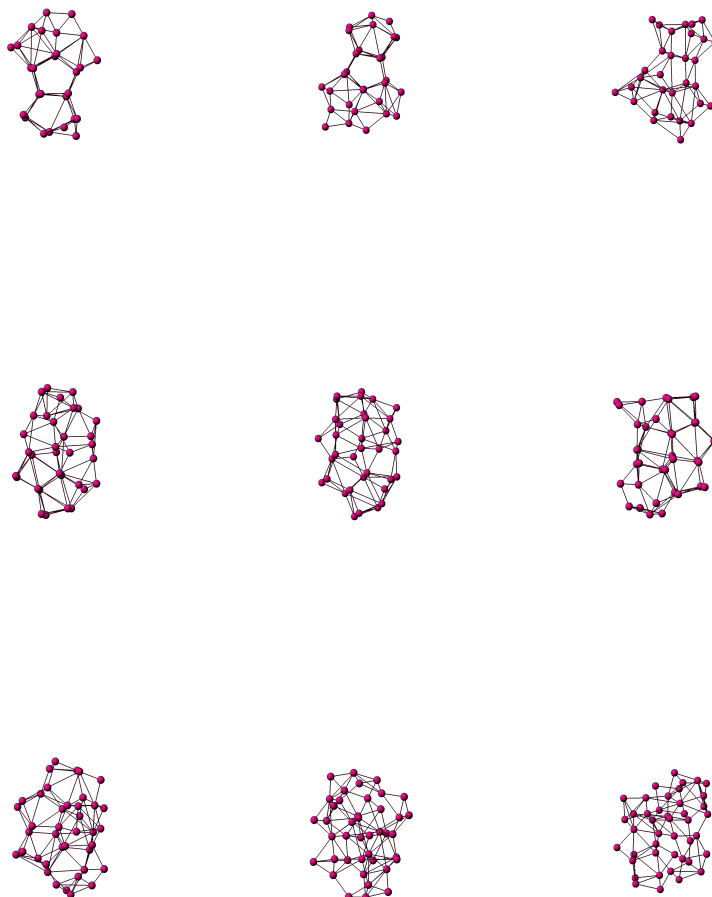


Figure 3.8: The optimized geometries of the energetically lowest isomers of  $\text{Ge}_n$  clusters for odd numbered clusters  $27 \leq N \leq 43$

## Chapter 4

---

# Tools For Structural Analysis

---

As a result of the optimization of different structures of clusters, we get larger amount of numbers, mainly about total energies of clusters and the nuclear coordinates. Now the next very important part is to extract useful information from these larger amount of numbers. In this chapter, we shall discuss some of the means that have been used for the purpose of extracting information from numerical results. All these methods will be discussed separately and results for each of our system clusters will be analyzed afterwards.

### 4.1 Structural Similarity

In this section we shall discuss, how we can compare the similarity between two cluster structures with  $N$  units (or atoms) and  $N-1$  units plus an extra unit. This is important to know because in this way we can check if clusters show a regular growth in which unit after unit is added to a given core or, whether the cluster is similar to a piece of infinite, periodic crystal or of some other larger system (high symmetry object like icosahedron). Due to structural relaxations, the two cluster structures can only be approximately identical and not exactly. For this purpose, we have applied similarity functions here, which are discussed as below. We have applied two similarity functions based on interatomic distances and radial distances. For similarity function, we calculate all the possible distances  $d_{ij}$  (between every two atoms  $i$  and  $j$ ) for the  $(n-1)$ -atomic cluster and sort them. Subsequently, we consider all possible distances for the  $n$  atom cluster and calculate  $d_{ij}$ .

The smallest value of  $q_1$  with

$$q = \left[ \frac{1}{N} \sum_{i=1}^N (d_{ij} - d'_{ij})^2 \right]^{1/2} \quad (4.1)$$

defines the similarity index of  $n$  th atom cluster,

$$s_1 = (1 + q_1)^{-1} \quad (4.2)$$

This index is one for a cluster that is obtained by adding a single atom to the  $(n - 1)$ -atom cluster, and approaches 0 for very different structures. In equation [4.1], we have first divided the coordinates for Si and Ge with a constant (5.85 a.u for Si and 6.10 a.u for Ge) so as to scale the coordinates. By dividing through this number, the influence of different bond lengths in both clusters is minimized. Otherwise, structural related clusters with slightly different interatomic distances would have values of similarity function that suggest less equivalence than there actually is. For the second similarity function which depends on radial distances of the atoms, we calculated the center for each cluster by

$$R_0 = \frac{1}{n} \sum_{i=1}^n R_i \quad (4.3)$$

and then sorted all the  $r_i$  for  $n$ -atom and  $r'_i$  for  $n-1$  atom clusters. Similarity Function is then calculated as above

$$q = \left[ \frac{1}{N} \sum_{i=1}^N (r_{ij} - r'_{ij})^2 \right]^{1/2} \quad (4.4)$$

and

$$s_2 = (1 + q_1)^{-1} \quad (4.5)$$

Similarity Functions calculated individually for each cluster system will be discussed in next section.

## Similarity Functions For $Si_n$ Clusters

Figure [4.1] shows similarity functions based on interatomic distances and based on radial distances separately for pure  $Si_n$  clusters. In this figure, we can see some clear peaks of clusters. There is clear low peak at  $Si_6$  in the upper channel of Figure [4.1] representing the dissimilarity between 5-atom and 6-atom clusters. This peak does not occur at lower channel of Figure [4.1] as dissimilarity is caused mainly by different interatomic distances and not so strongly by different radial distributions. In upper channel of Figure [4.1] there is also a significant peak at  $Si_{15}$  which means that in  $Si_{14}$  and  $Si_{15}$  the radial distances change marginally by adding an atom to the hollow  $Si_{14}$  structure. This peak is absent in lower channel. There is another sharp peak in lower channel of Figure [4.1] for  $Si_{27}$  indicating that when an atom is added to  $Si_{26}$ , it is located away from the center of the cluster that is why the radial distances are altered. This peak is not so profound in upper channel of Figure [4.1]. There is very sharp peak at  $Si_{20}$  in both the channels indicating that when an atom is added to  $Si_{19}$ , both center and interatomic distances are changed when we get  $Si_{20}$  structure. The average value of similarity function (when interatomic distances are sorted) for  $n > 20$  is 0.87. This indicates that clusters are structurally related to each other when interatomic distances are sorted. In contrast similarity function (when radial distances are sorted) has average value of 0.78 for  $n > 15$  which means that radial agreement is less good than that of interatomic distances. This is because a slightly moved atom changes the center of mass and causes therefore deviations in all values  $r_i$  whereas in the same case the interatomic distances  $d_{ij}$  are changed for that specific  $i$ .

We have compared  $Si_n$  cluster structures with a spherical fragment of the fcc crystal when the center of the fragment is placed at, (upper panel) the position of an atom, (middle panel) the middle of nearest neighbors, (lower panel) the center of the cube as plotted in figure [4.2]. For clusters to be structurally similar, similarity function should be above 0.8, but here we don't see any kind of similarity between  $Si_n$  and fragment of fcc crystal.

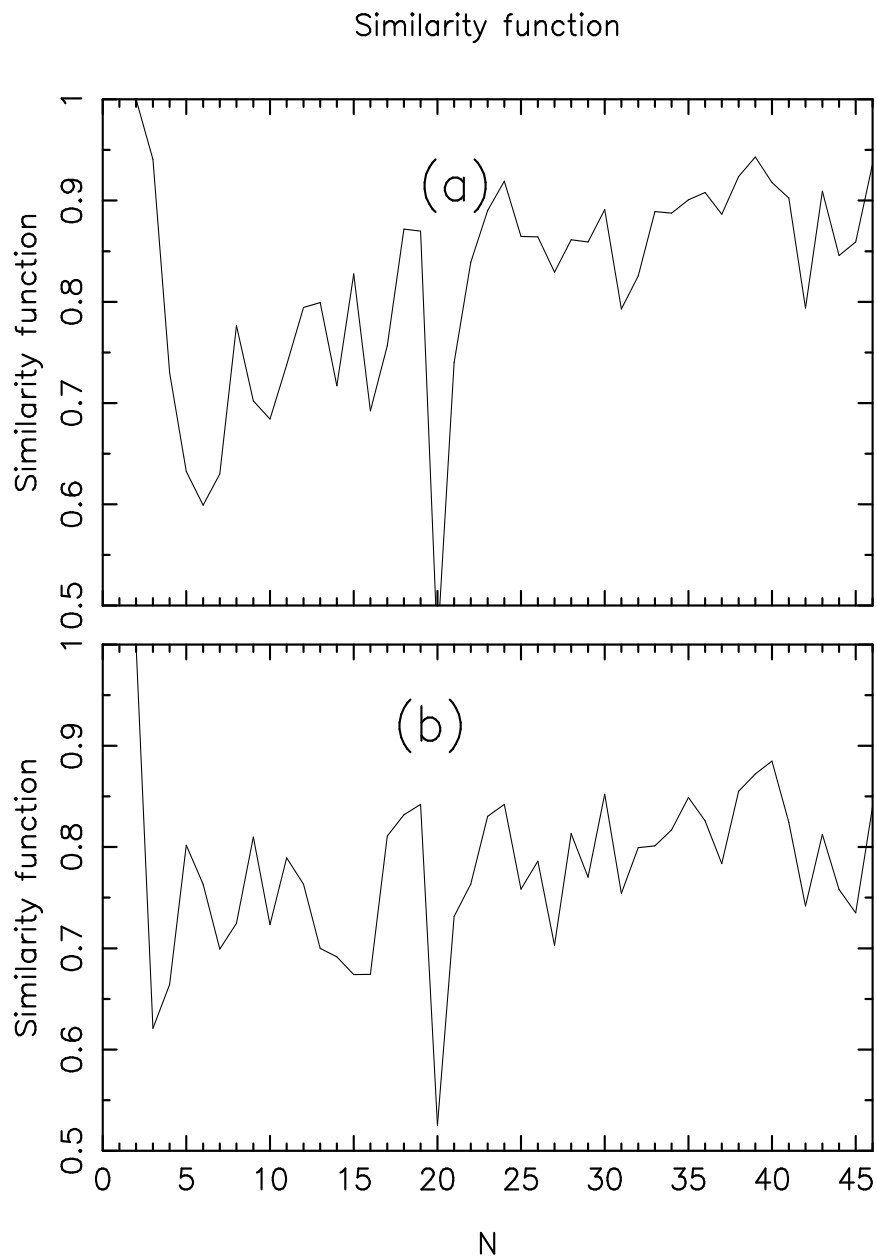


Figure 4.1: Similarity Functions for  $Si_n$  cluster (upper channel) is based on interatomic distances, (lower channel) is based on radial distances

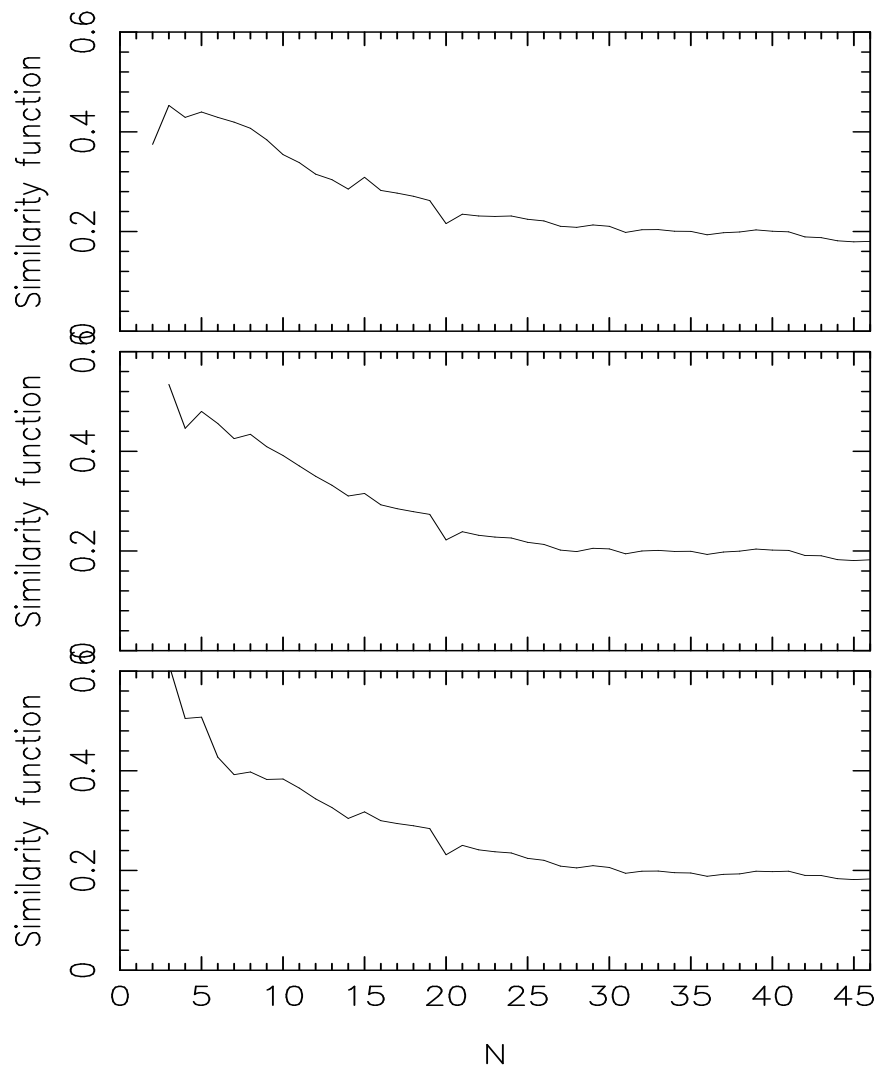


Figure 4.2: Each panel shows the similarity function for the  $S_{i_n}$  clusters when comparing with a spherical fragment of the fcc crystal when the center of the fragment is placed at, (upper panel) the position of an atom, (middle panel) the middle of nearest neighbor bond, (lower panel) the center of the cube

### Similarity Functions For $Ge_n$ clusters

Here we will try to look at the similarity functions drawn from Ge clusters. In Figure [4.3], we have plotted similarity function for pure  $Ge_n$  clusters in which upper channel shows similarity function based on interatomic distances while lower channel shows similarity function based on radial distances. There are prominent low peaks in lower channel for  $Ge_{18}$  and  $Ge_{32}$  which means that these clusters differ from the structures of  $Ge_{17}$  and  $Ge_{31}$  respectively as their radial distances are altered. The corresponding peaks in upper channel are less prominent in both the cases indicating that interatomic distances are not very much changed when an atom is added to both of these structures. There is another very low peak for  $Ge_{11}$  atom cluster for both the functions indicating change in both radial distances and interatomic distances when an extra atom is added to  $Ge_{10}$ . As the cluster size grows, we can observe that similarity function is not a smooth function especially when radial distances are sorted. This means that with increasing  $n$  clusters are not structurally related to each other and they are not built up atom by atom. The value of  $s_1$  for  $Ge_n > 20$  is 0.85 which reflects structural similarity in clusters with more than 20 atoms. The average of similarity function based on radial distances is 0.76 indicating that radial agreement is less good than that of interatomic distances as in case of pure  $Si_n$  clusters. A comparison with fragment of fcc crystal does not show any similarity like the  $Si_n$  clusters.

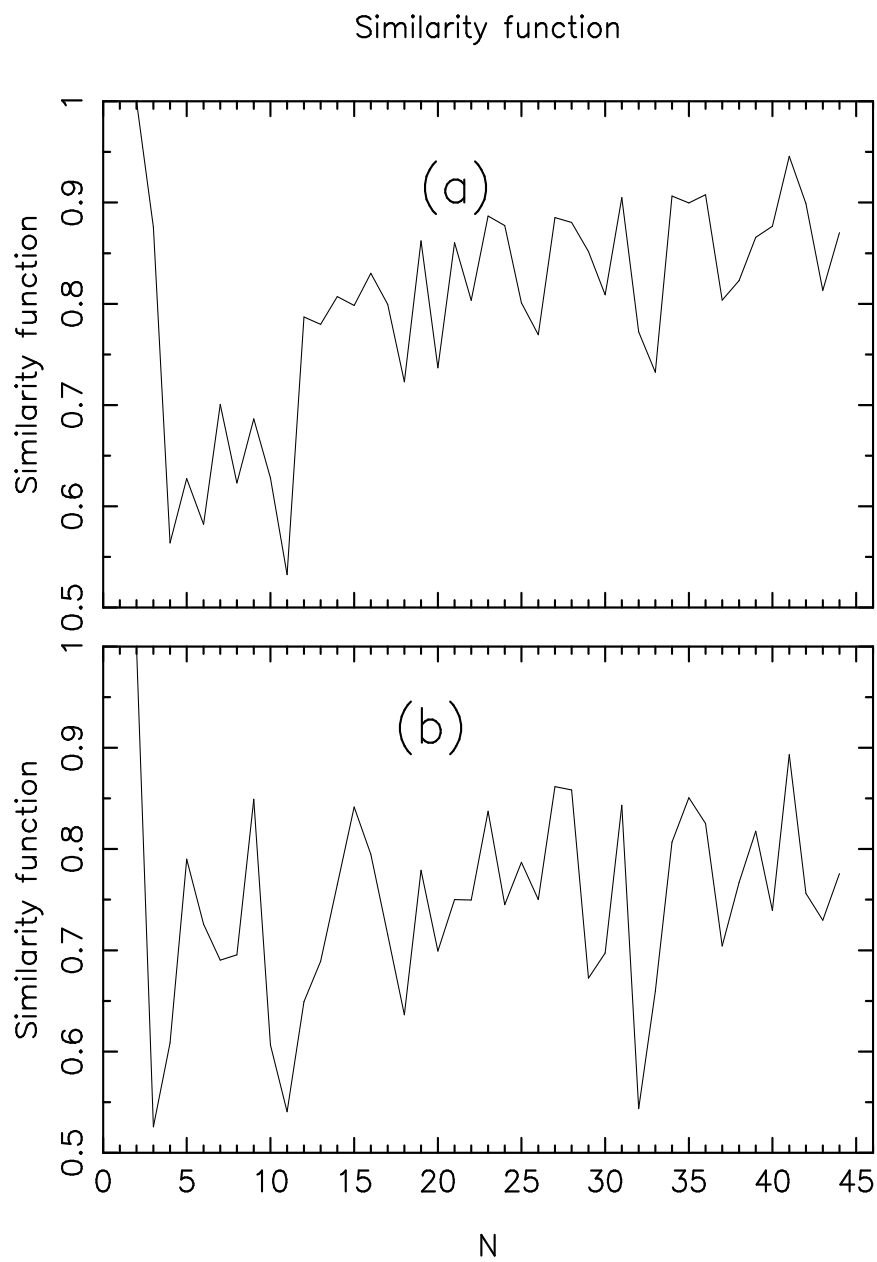


Figure 4.3: Similarity Functions for  $Ge_n$  clusters (upper channel) is based on interatomic distances, (lower channel) is based on radial distances

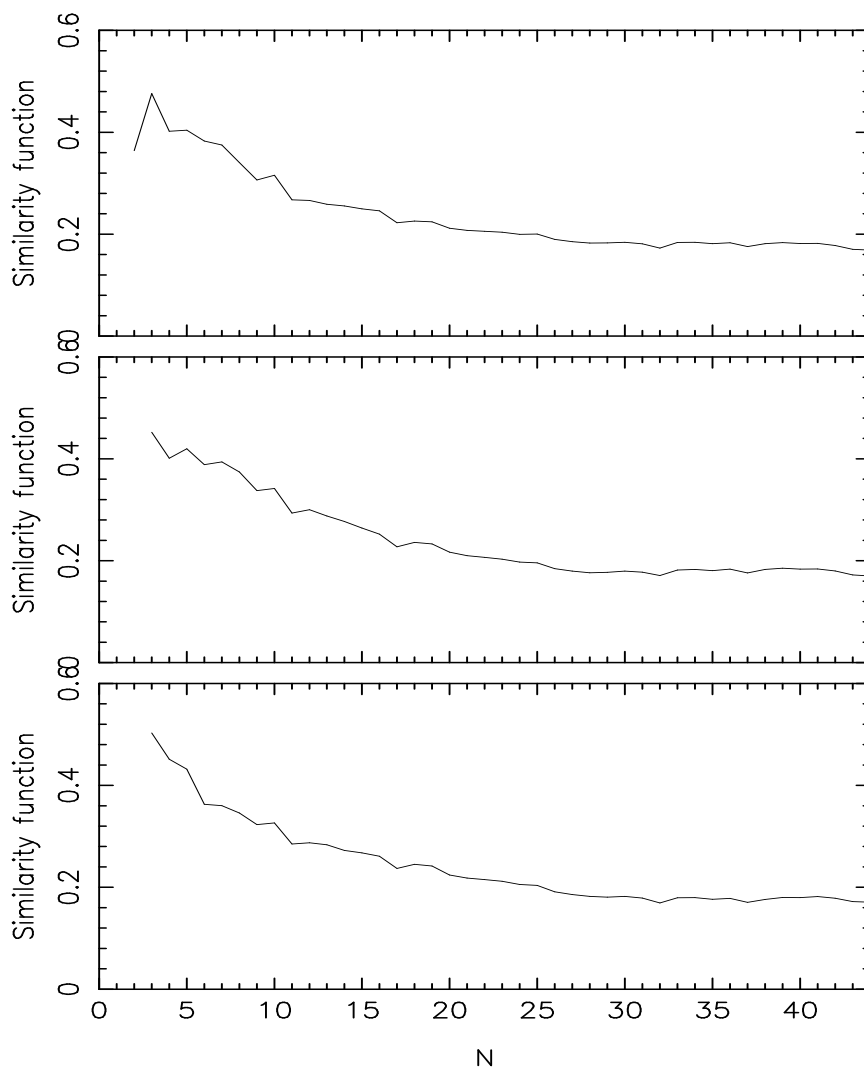


Figure 4.4: Each panel shows the similarity function for the  $Ge_n$  clusters when comparing with a spherical fragment of the fcc crystal when the center of the fragment is placed at, (upper panel) the position of an atom, (middle panel) the middle of nearest neighbor bond, (lower panel) the center of the cube

### Similarity Function for $Si_n$ , $Ge_n$ , and $Si_nGe_n$ clusters

Here we will present a comparison of similarity function analysis for  $Si_n$ ,  $Ge_n$  and  $Si_nGe_n$  clusters. In order to compare these three different cluster systems, we have divided their coordinates with a constant (5.85 *a.u* for Si and 6.1 *a.u* for Ge and for  $Si_nGe_n$  cluster with 5.96 *a.u*). In this way we have scaled our coordinates for all the structures and minimized the influence of different bond lengths on these cluster structures. Then we took average of separation to the center for each cluster structure.

$$q = \left[ \frac{1}{N} \sum_{i=1}^N (r_i^A - r_i^B) \right]^{1/2} \quad (4.6)$$

$$s_1 = (1 + q_1)^{-1} \quad (4.7)$$

Comparison of structures of pure  $Si_n$  and pure  $Ge_n$  clusters is plotted in Figure [4.5]. Here we can observe that comparison between pure  $Si_n$  and pure  $Ge_n$  clusters is very poor. This means that both the cluster systems follow different growth patterns. Comparable structures from Similarity function comparison between  $Si_n$  and  $Ge_n$  clusters are at size  $n=5,6,8,10$  and 14. Similar comparisons between structures of pure  $Si_n$  clusters and bimetallic  $Si_nGe_n$  and those of pure  $Ge_n$  clusters and bimetallic  $Si_nGe_n$  are plotted in figures [4.6] and [4.7] respectively. In case of similarity function between pure  $Si_n$  and binary  $Si_nGe_n$  clusters, we can see that overall similarity between the structures is very poor. Binary clusters and pure  $Si_n$  clusters do have structural similarity in the size range  $n \leq 10$ . Same is the case for similarity comparison between pure  $Ge_n$  and binary  $Si_nGe_n$  clusters. Cluster structures show similarity in the small size range but as the sizes of clusters grows, cluster structures become more and more dissimilar. From the similarity function analysis between binary  $Si_nGe_n$  and pure  $Si_n$  and  $Ge_n$  clusters, it is clear that binary clusters show very poor similarity with their elemental counter parts. This means that binary clusters follow different growth processes compared to their atomic species.

## Similarity function

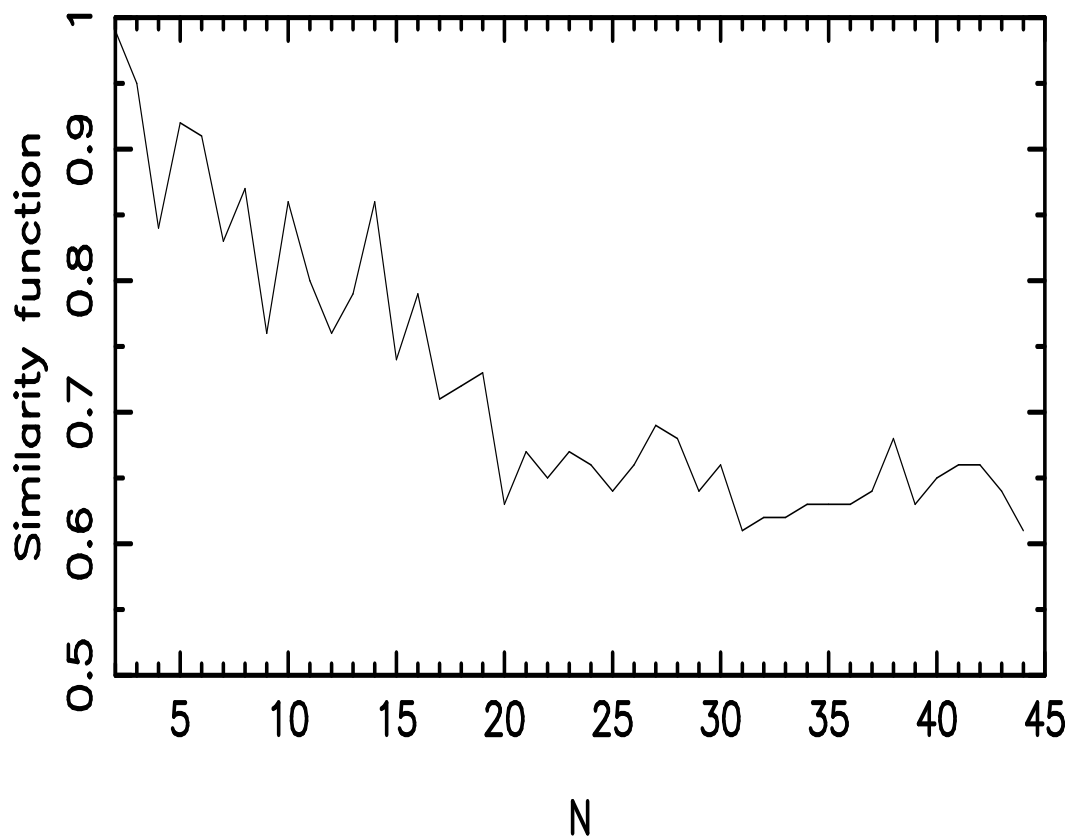


Figure 4.5: Similarity Function between  $S_i_n$  and  $G_e_n$  clusters : Here N=number of atoms

## Similarity function

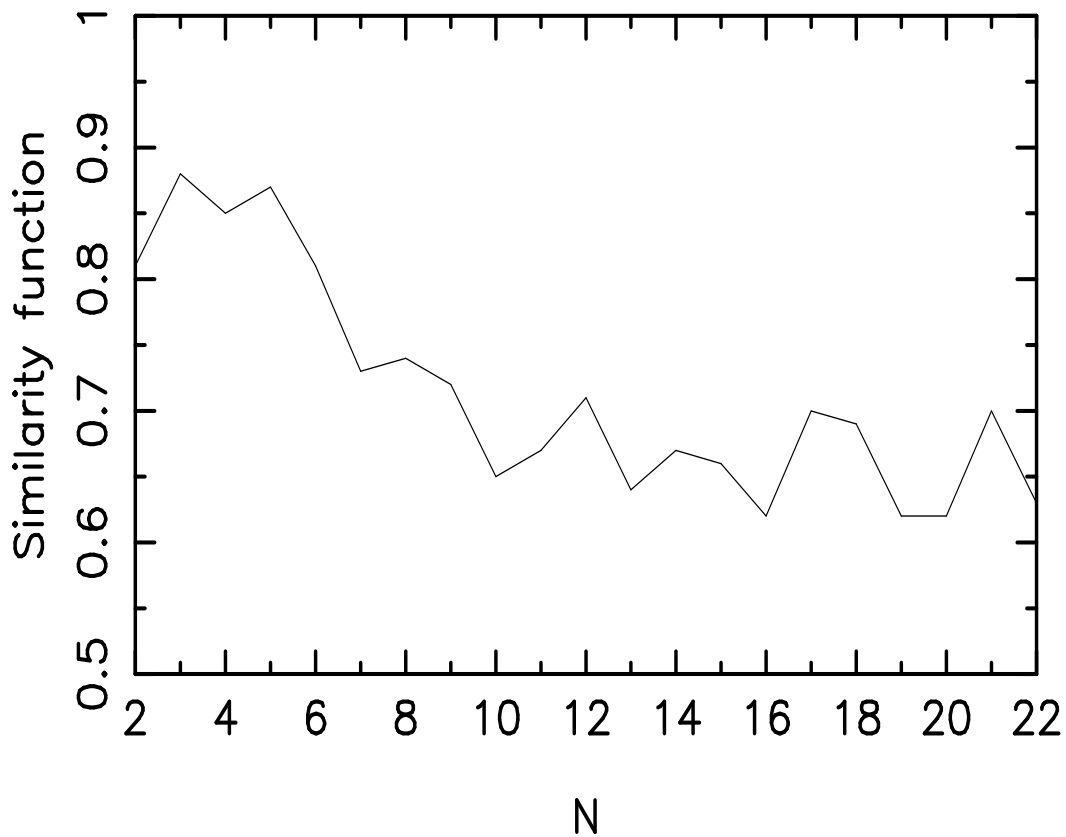


Figure 4.6: Similarity Function between  $Si_n$  and  $Si_nGe_n$  clusters: Here N= Number of units of Si-Ge

## Similarity function

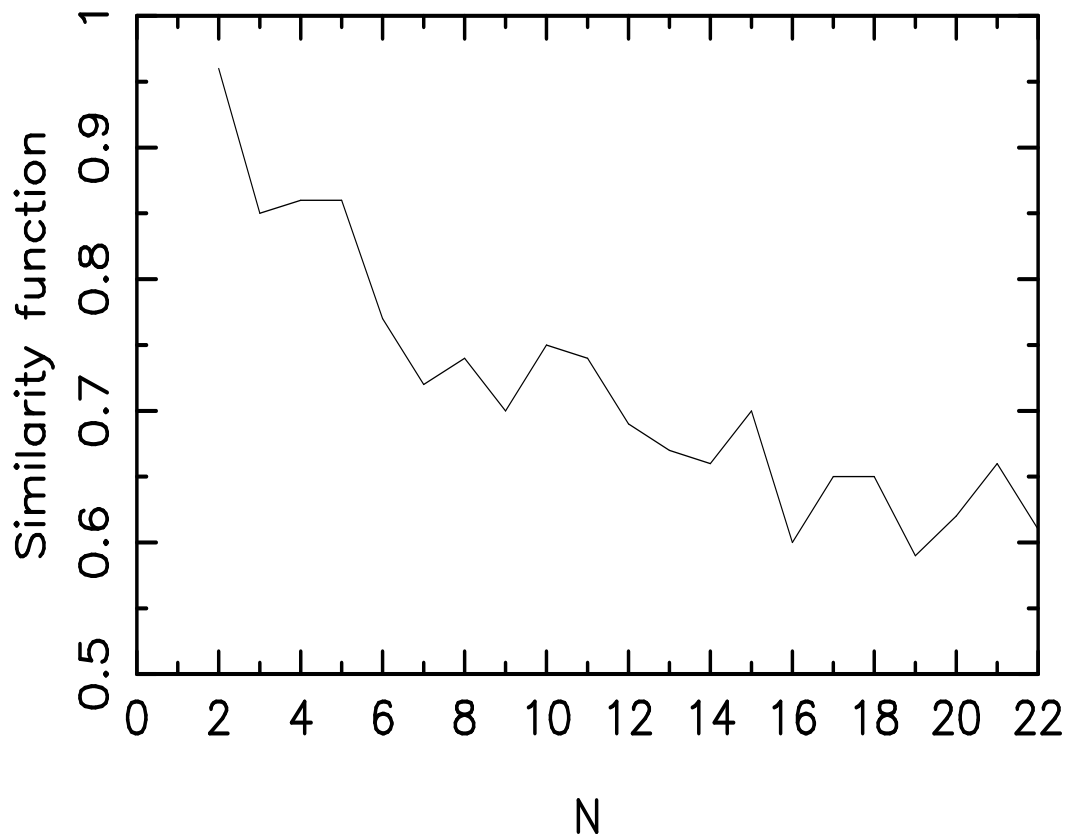


Figure 4.7: Similarity Function between  $Ge_n$  and  $Si_nGe_n$  clusters: Here N= Number of units of Si-Ge

## 4.2 Common Neighbor Analysis

We have used Common Neighbor Analysis to analyze our cluster structures in detail. This idea was originally used by Faken and Johansson [71] for single-atomic clusters. CNA performs a simple geometric analysis of the nearest neighbors around a reference pair of atoms in given structure. A cutoff distance is defined and common neighbors which are separated by less than this distance are considered as bonded. As a result of this analysis we try to get following set of indices for a given pair of atoms in a given cluster structure.

1. Number of shared nearest-neighbors  $i$
2. Number of bonds between shared neighbors  $j$
3. Number of bonds in longest bond-chain formed by shared neighbors.  $k$
4. In case of hetero-atomic clusters, we use this index which tells us about the type of initial reference pair, whether is of A-A type or B-B type or A-B type.  $l$

A cut-off distance is chosen for each cluster (5.85 *a.u* for  $Si_n$ , 5.96 *a.u* for  $Si_nGe_n$  and 6.11 *a.u* for  $Ge_n$  clusters systems). Main idea is to get different sets of indices for each cluster structures and then try to compare these with crystal lattice structures to check for any sort of similarity, if any. In the monoatomic bulk fcc structure, an atom has 12 nearest neighbors. With each of them it shares ( $i=4$ ) common neighbors of which two pairs of atoms are connected by a geometric bond ( $j=2$ ) and as the longest chain of bonds in neighbors in this case is only one so fcc structure has  $12 \times (4:2:1)$  sets of indices. Compared with the monoatomic CNA there are more informations to be sorted during the analysis of binary systems. In addition to detection of geometric bonds and the longest chain of bonds, it is necessary to store the type of the initial reference pairs. In this way it will be possible to distinguish between ordered and disordered binary structures and regions consisting of only one atomic type, as for example in the case of phase segregation. Here we recognized very many different sets of indices for all the clusters. We have plotted all these indices for pure  $Ge_n$  and for pure  $Si_n$  clusters in figures [4.08] and [4.09] respectively. For bimetallic homogeneous  $Si_nGe_n$  clusters, we have divided the indices into three sets depending on the type of initial reference pair, as mentioned above and plotted that in figures [4.10], [4.11] and [4.12].

While comparing CNA for pure  $Si_n$  and  $Ge_n$  clusters, we can see that pure  $Si_n$  have very many different sets of indices as compared to pure  $Ge_n$  clusters. This means that pure  $Si_n$  have more compact structures as compared

to pure  $Ge_n$  clusters. This has been confirmed in our radial distance analysis where we see that individual atoms in  $Ge_n$  clusters are scattered over a wide range from the center of mass  $R_0$ . In case of pure  $Si_n$  we see very many different curves for different indices and some of them are lying at the base in Figure [4.9]. These low lying curves represent the indices like (3,2,2),(3,3,3),(4,3,3), and (4,4,4) which means that pairs of atoms are surrounded by these many different ways. Such indices are mostly present in the size range  $N < 20$ . This is also proved by our radial distance analysis as we see a difference in pattern for radial distances as we move from  $Si_{19}$  to  $Si_{20}$  atom cluster. Most stable  $Si_n$  clusters structures are also found in this size range.

As mentioned above, we have divided our CNA for bimetallic  $Si_nGe_n$  clusters into three sets depending on the type of pairs *i.e.*, if the initial reference pairs are both Si-Si type or Ge-Ge type or Si-Ge type. This is done in-order to check what are the preferential sites for both Silicon or Germanium atoms in binary  $Si_nGe_n$  clusters *i.e.*, whether they tend to stay around same kind of atoms or they move towards opposite atoms (mixed alloy formation). We found that when the initial pairs are both silicon atoms, then we don't see very many different curves in common neighbor analysis. This is very interesting finding as it means that Si atoms do not show tendency to form more bonds with other Si atoms in binary clusters. We see more number of curves in CNA when the initial pairs are Ge-Ge or Si-Ge. This means that there is a strong tendency for both Si and Ge to form bonds with each other in binary clusters. In order to get more clear picture about this we have also plotted coordination number analysis for three different cluster systems.

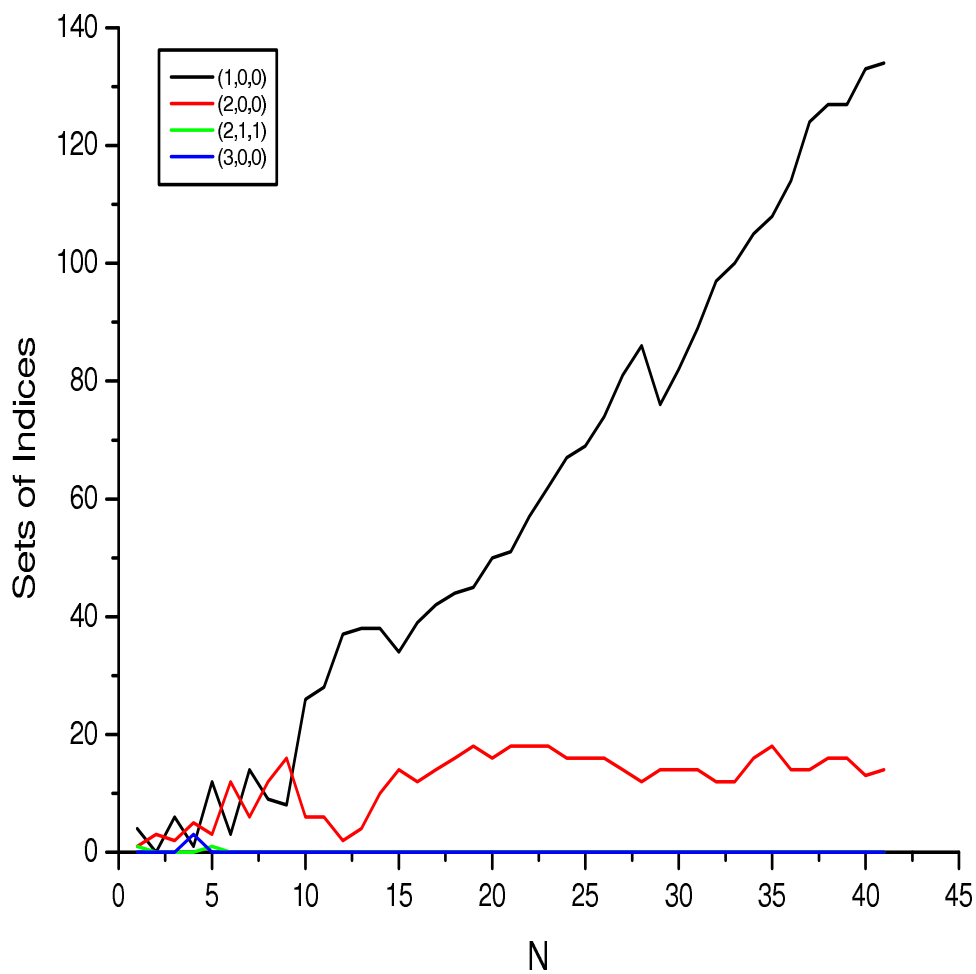


Figure 4.8: Common Neighbor Analysis for  $Ge_n$  clusters : Here N = Number of Atoms

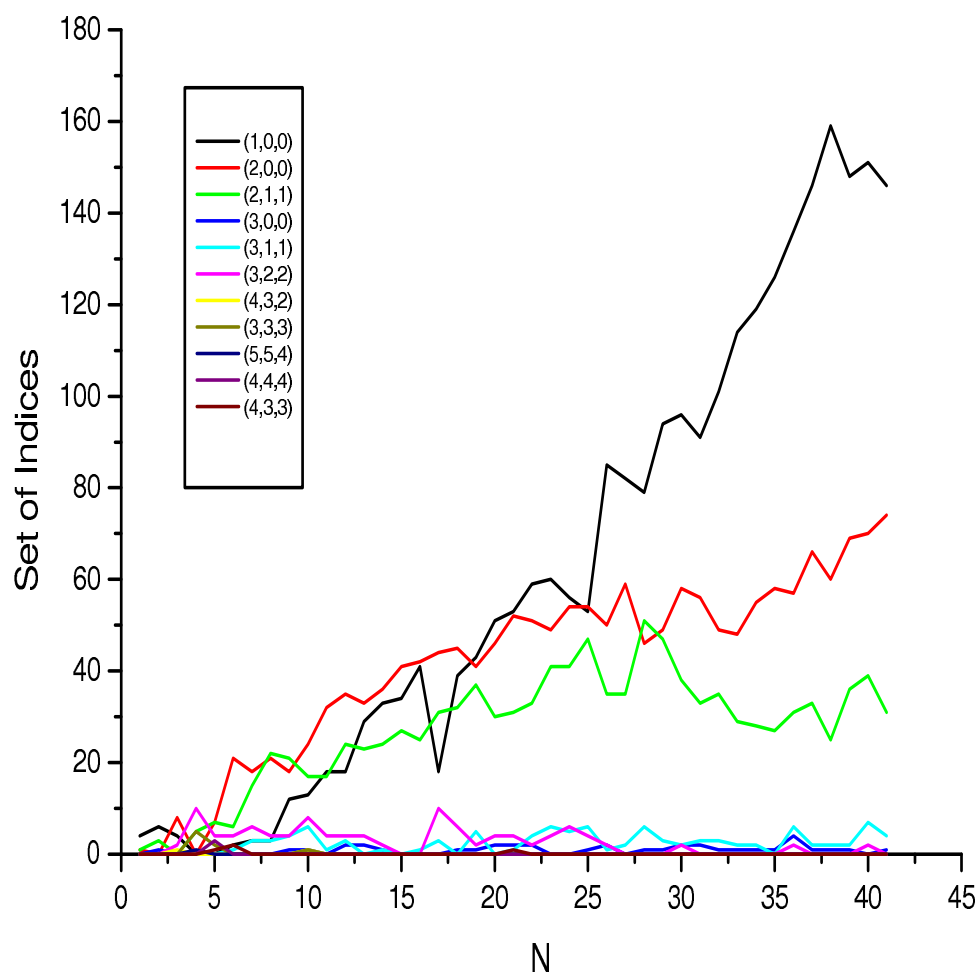


Figure 4.9: Common Neighbor Analysis for  $S_{i_n}$  clusters : Here N = Number of Atoms

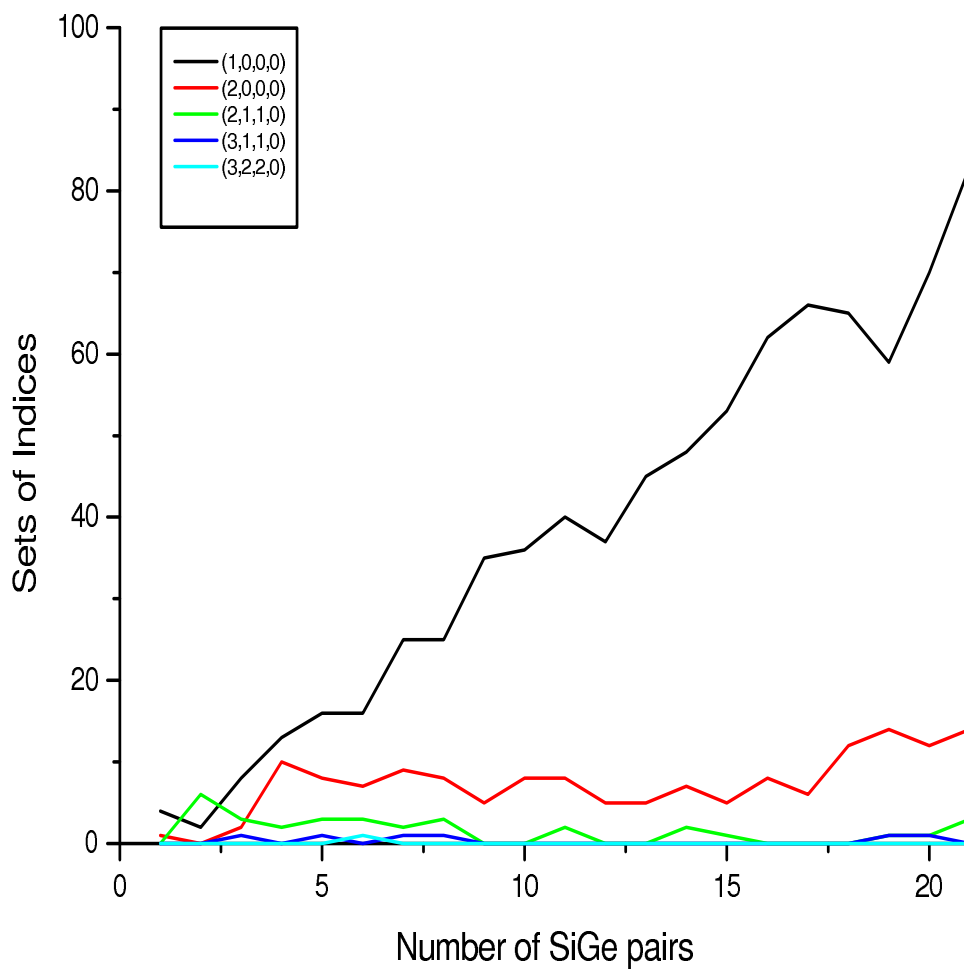


Figure 4.10: Common Neighbor Analysis for  $Si_nGe_n$  clusters when initial pairs are Si-Ge : Here  $N$  = Number of Si-Ge units

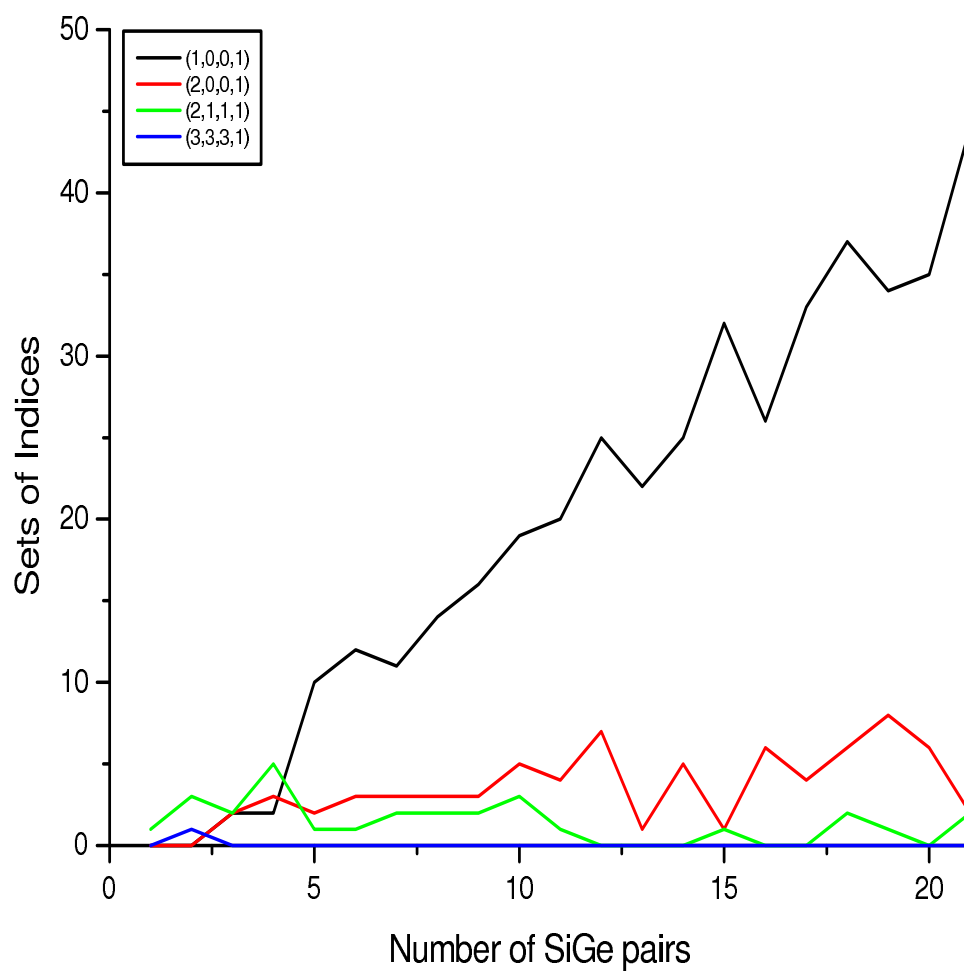


Figure 4.11: Common Neighbor Analysis for  $Si_nGe_n$  clusters when initial pairs are both Si : Here  $N =$  Number of Si-Ge units

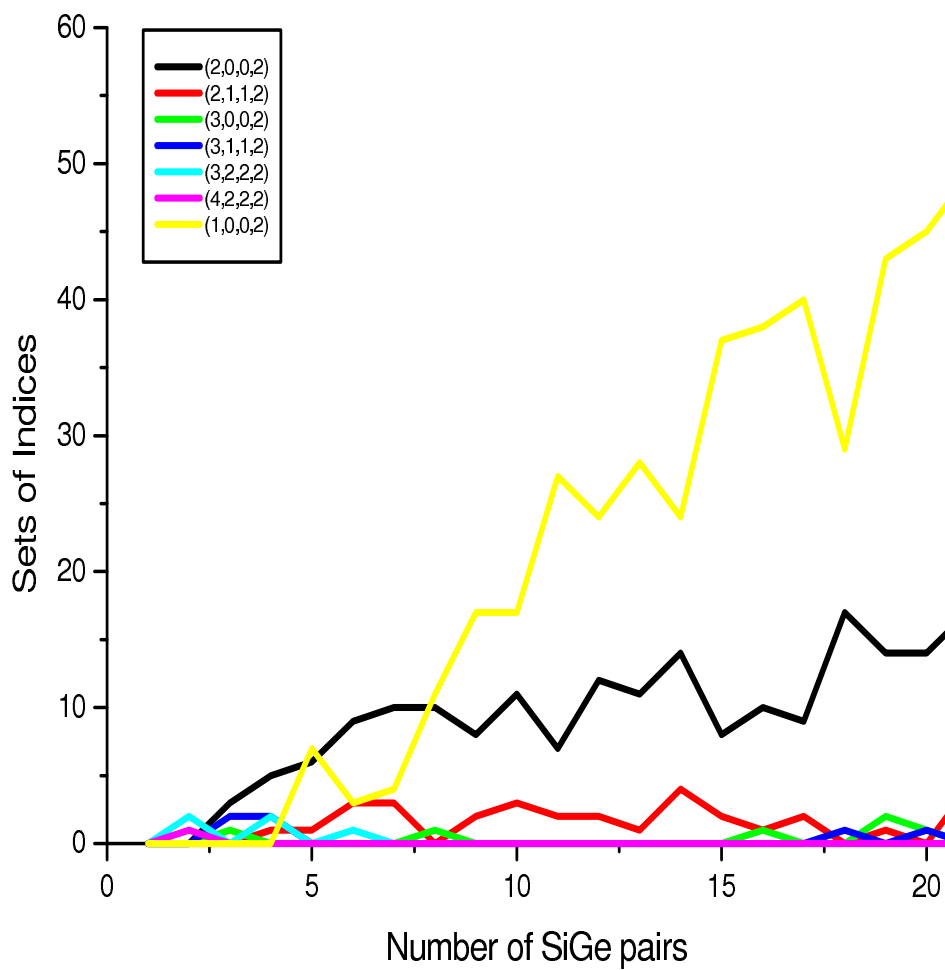


Figure 4.12: Common Neighbor Analysis for  $Si_nGe_n$  clusters when initial pairs are both Ge : Here  $N =$  Number of Si-Ge units

In Figure [4.13], [4.14], [4.15], and [4.16] we have plotted %age coordination number of Ge having Ge, Ge having Si, Si having Si and Si having Ge atoms as their neighbors in the binary  $Si_nGe_n$  clusters. This will give us more clear picture of distribution of atomic species in binary  $Si_nGe_n$  clusters. From these four figures its clear both Si and Ge show strong tendency for having Ge and Si atoms as their neighbors respectively in binary  $Si_nGe_n$  clusters. Also Si shows a decaying curve in Figure. [4.15] which means that Si has very less tendency to form bond with other Si atoms in binary clusters. Ge shows more tendency for other Ge and Si atoms as obvious from Figure [4.13]. From this coordination number analysis we can see that binary  $Si_nGe_n$  clusters prefers to form mixed alloy structures. The total %age coordination numbers for Si and Ge in binary  $Si_nGe_n$  clusters are plotted in figure [4.17] and [4.18] respectively. Figures [4.19] and [4.20] show total %age neighbors of Silicon and of Germanium in pure  $Si_n$  and  $Ge_n$  clusters. The overall coordination number of Silicon decreased from 5 to 3 in mixed clusters where as that of Ge atoms increased from 3 to 4 or even 5 atoms. This figure clearly explains that Si bonds are reduced in binary clusters as compared to atomic  $Si_n$  clusters. J.Tarus *et.al*, [57] have studied the segregation in Si-Ge clusters and for  $Si_{15}Ge_{15}$  they found that coordination number for Silicon and Germanium is three where as for this structure we have found that average coordination around Si is approximately equal to three which is in good agreement with their result. Further more study from Abtew *et.al*, [72] reveals that when they have homogeneous composition for both Si and Ge, Germanium atoms wants to have four fold coordination and that has been found by our result also. To give an example of total coordination number analysis, we have plotted total neighbors of both Si and Ge verses distance of Si and Ge from center for  $Si_{22}Ge_{22}$  cluster in Figures [4.21] and [4.22]. These figures also show tendency of both Si and Ge to have opposite atoms as their neighbors in binary  $Si_{22}Ge_{22}$  cluster.

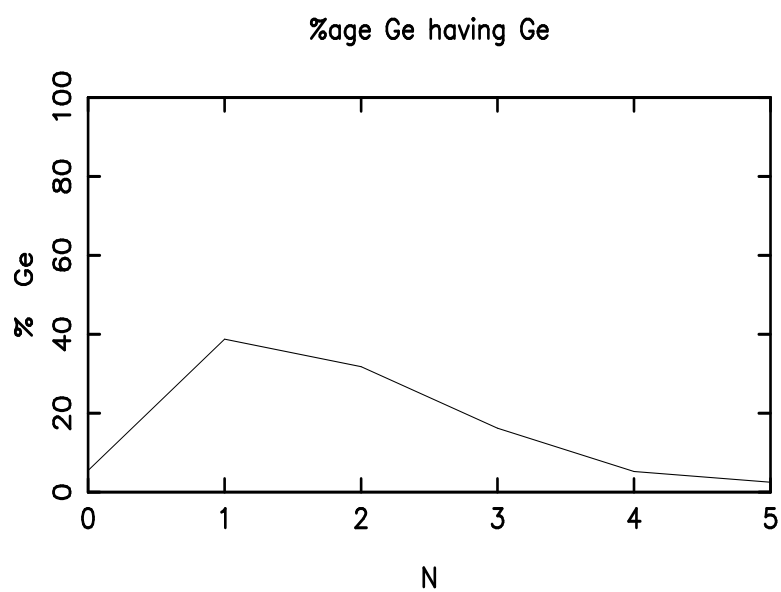


Figure 4.13: % Coordination Number : Here N = Number of Ge neighbors around Ge atoms in binary  $Si_nGe_n$  clusters

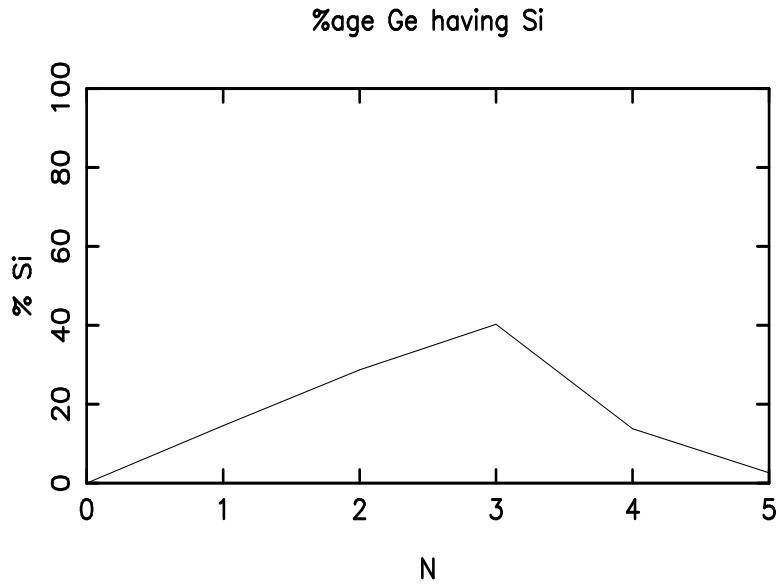


Figure 4.14: % Coordination Number : Here  $N$  = Number of Si neighbors around Ge atoms in binary  $Si_nGe_n$  clusters

### 4.3 Stability Function

DFTB calculations gives us total energy as a function of size of the cluster  $E_B(N)$ . In figure [4.23],[4.24] and [4.25], we show  $\frac{E_B(N)}{N}$  as a function of  $N$  for the globally optimized structures of pure  $Si_n$ , pure  $Ge_n$  and binary  $Si_nGe_n$  cluster structures respectively. As we can see from relative total energy per unit  $\frac{E_B(N)}{N}$  as a function of  $N$  that all the curves are more or less monotonically decreasing as a function of  $N$  with few exceptions in all the cluster systems. This statement means that any cluster is stabler than two separated fragments, but by just looking at total energy per unit we can not say that which cluster structures are particularly stable.

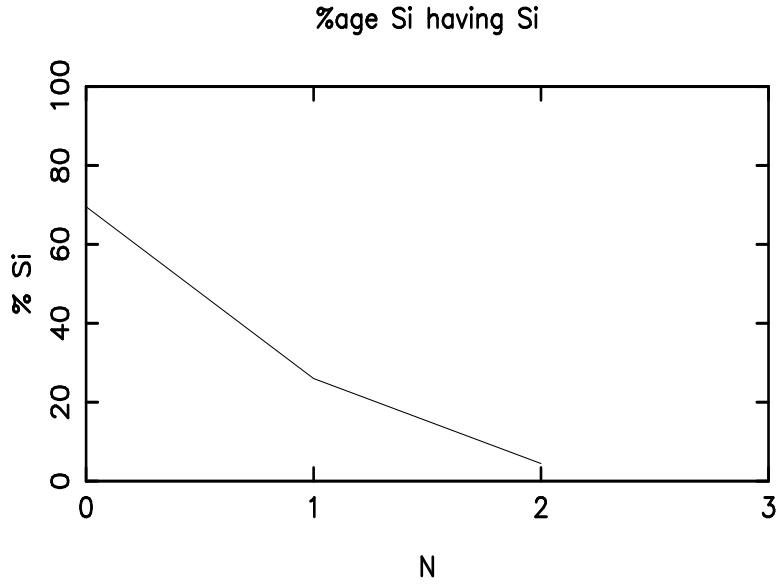


Figure 4.15: % Coordination Number : Here N = Number of Si neighbors around Si atoms in binary  $Si_nGe_n$  clusters

For binary  $Si_nGe_n$  clusters we have studied 22 different structures with each having same number of both Si and Ge atoms. Each of this structures has different number of Si-Si, Ge-Ge and Si-Ge bonds. We have solved equation [4.8] so as to find bond energies  $E_{Si-Si}$ ,  $E_{Ge-Ge}$  and  $E_{Si-Ge}$ . We have found that energy for single Si-Ge unit comes out to be -2.4 eV which is in good agreement with atomic energies of both Si and Ge which is -2.17 eV. The fit of equation [4.8] gives  $E_{Si-Ge} \cong E_{Ge-Ge} > E_{Si-Si}$ , which means that its more favorable for Si-Ge and Ge-Ge bonds to be present in binary  $Si_nGe_n$  cluster as compared to Si-Si bonds. This observation is in accordance with the CNA analysis [section:4.2] and earlier structural discussion, in which we observe that Si has no tendency to have Si as a neighbour where as Ge shows more tendency for Si-Ge and Ge-Ge bonds. Here we observe that bond energies also predict the formation of mixed alloy structures for binary  $Si_nGe_n$  clusters. Our results also match with the findings of Abu *et.al*, [59] who have also found that  $E_{Ge}$  is lower than  $E_{Si}$  so that Ge atoms wants to be incorporated to the Ge-Si core-shell structures.

$$\sum_n [E_n - (n_0 E_0 + N(n)_{Si-Si} E_{Si-Si} + N(n)_{Ge-Ge} E_{Ge-Ge} + N(n)_{Si-Ge} E_{Si-Ge})]^{1/2} = 0 \quad (4.8)$$

In case of pure clusters we have also calculated the energies for  $n$ -fold coordination by solving the equations [4.9] and [4.10] for pure  $Si_n$  and  $Ge_n$

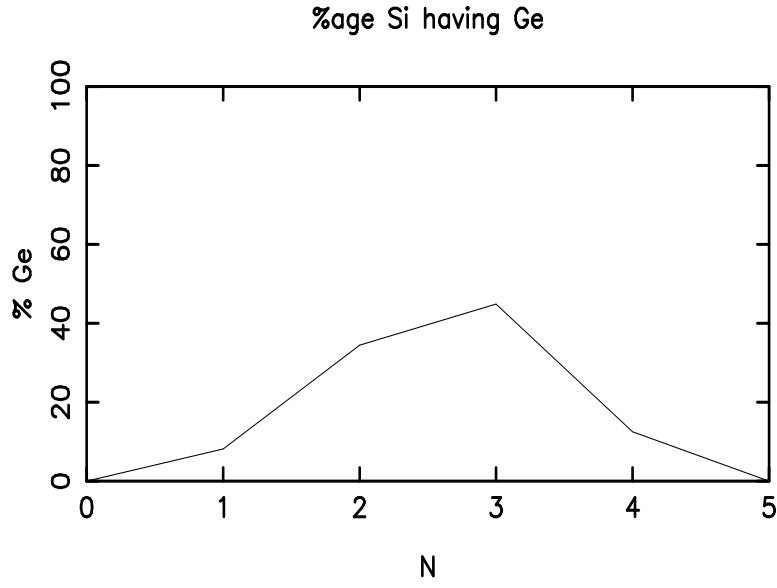


Figure 4.16: % Coordination Number : Here N = Number of Ge neighbors around Si atoms in binary  $Si_n Ge_n$  clusters

clusters. Our results show very small difference in the  $n$ -fold coordination energies.

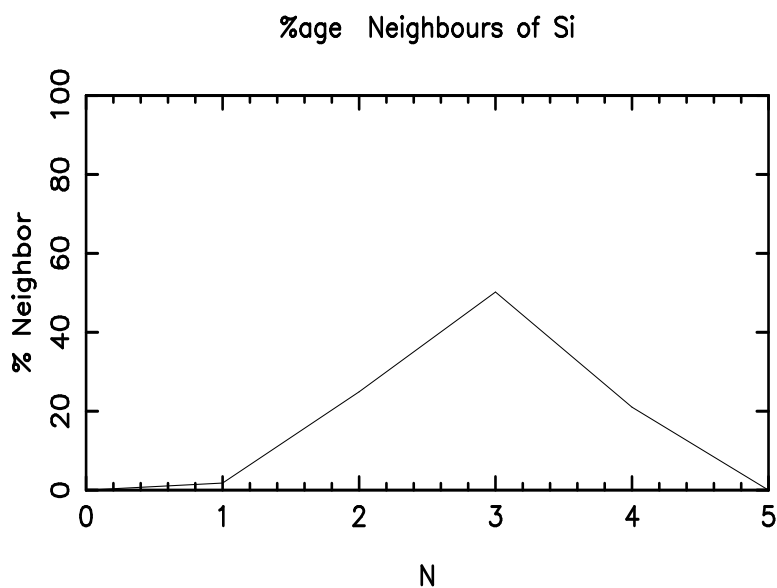
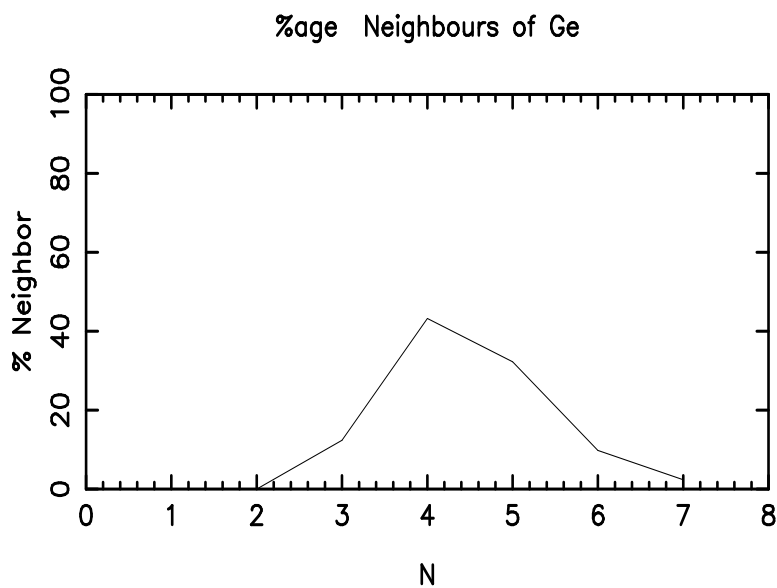
$$\frac{\partial}{\partial E_{ik}} \sum_m [E_{tot}(Si_m) - \sum_i n_{mi} E_i]^{1/2} = 0 \quad (4.9)$$

$$\frac{\partial}{\partial E_{ik}} \sum_m [E_{tot}(Ge_m) - \sum_i n_{mi} E_i]^{1/2} = 0 \quad (4.10)$$

In order to identify such particularly stable structures for our cluster systems, we have used so called stability function defined as,

$$E_{stab} = E_{n+1} + E_{n-1} - 2E_n \quad (4.11)$$

Here we compare the total energy of the cluster of  $N$  units with structures of  $N+1$  and  $N-1$  units and this function gives a highest peak when the  $N$  atom cluster is particularly stable. We have plotted the stability functions for pure  $Si_n$ , pure  $Ge_n$  and binary  $Si_n Ge_n$  clusters in Figures [4.26], [4.27], and [4.28] respectively. For pure  $Si_n$  clusters, we have found that clusters with those  $n=7,16,34$  and  $38$  are particularly stable where as with  $n=17,25,39$  are particularly unstable. Similarly stable Germanium clusters are with those  $n=5,16,29$  and  $39$ , while particularly unstable are those with  $n=6,15,28,39$ . Binary Si-Ge clusters don't show extra stability as evident from the stability function peaks. We can identify clusters

Figure 4.17: % Total Coordination Number of Si in  $\text{Si}_n\text{Ge}_n$  clustersFigure 4.18: % Total Coordination Number of Ge in  $\text{Si}_n\text{Ge}_n$  clusters

with  $n=10,14,12,24,28$  are more stable over other structures. Here we want to mention that Stability Function is meant to identify particularly stable structures, however it does not give any detailed explanation for the reason behind particular stability.

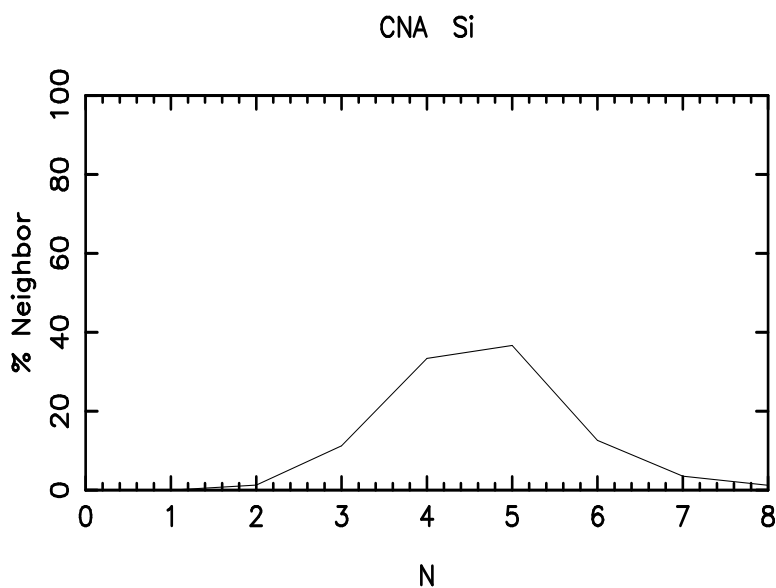


Figure 4.19: % Total Coordination Number in pure  $Si_n$  clusters

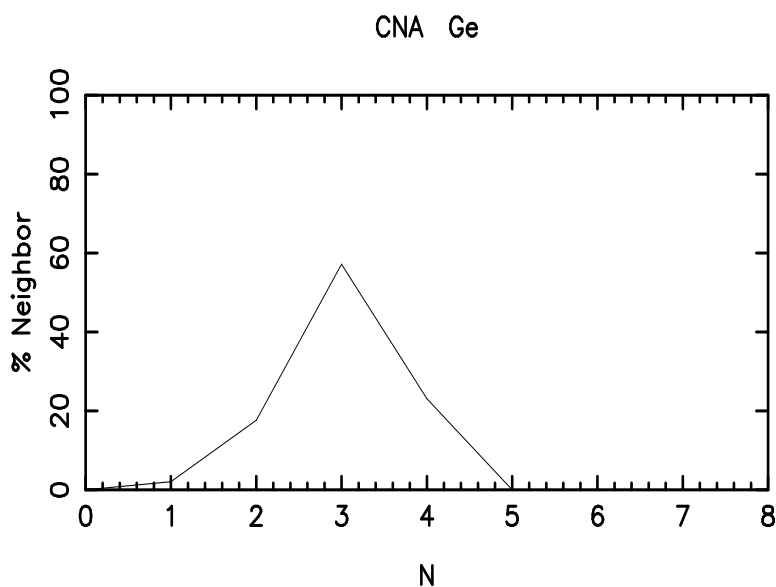


Figure 4.20: % Total Coordination Number in pure  $Ge_n$  clusters

## HOMO-LUMO Gap Analysis

HOMO-LUMO Gap gives information about the electronic properties of clusters. The HOMO-LUMO gap ( $E_{gap}$ ) *i.e.*, the energy gap between the highest occupied molecular orbital (HOMO) and the lowest unoccupied molecular orbital (LUMO), for pure  $Si_n$ , pure  $Ge_n$  and for binary  $Si_nGe_n$

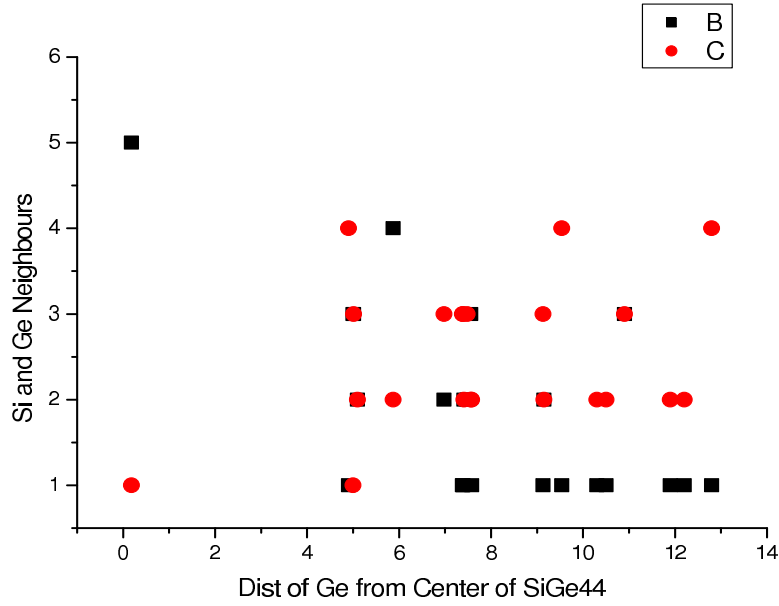


Figure 4.21: Total Coordination Number of Ge atoms in  $\text{Si}_{22}\text{Ge}_{22}$ , Here we have calculated distance of all Ge atoms from center of  $\text{Si}_{22}\text{Ge}_{22}$  cluster and plotted all its neighbors. Here C = Silicon and B = Ge

clusters are shown in Figures [4.29],[4.30] and [4.31] respectively. For all clusters, we have found relatively wider gap for small clusters and narrower for the larger ones. This can be due to the presence of higher number of surface atoms and therefore higher number of dangling bonds in larger clusters. From the HOMO-LUMO Gap figures, it is evident that gap is size dependent and also for smaller clusters band gap is relatively large and for larger ones its narrower. For Silicon clusters, HOMO-LUMO Gap shows maxima at  $n = 5,7,10,14,16$  in the size range  $n \leq 20$  which correlates very well with the maxima of stability function of  $\text{Si}_n$  clusters (Fig: 4.26). For Germanium clusters also, HOMO-LUMO Gap correlates fairly well with the stability function maxima of  $\text{Ge}_n$  clusters (Fig: 4.27). For Germanium clusters, HOMO-LUMO Gap shows maxima at  $n=5,7,8,14,16$ , and 19 in the size range  $n \leq 20$ . We have not found correlation between stability and band gap for binary  $\text{Si}_n\text{Ge}_n$  except for four and eight atomic binary clusters. We have found the widest gap in small Silicon clusters to be 1.6 eV where as smallest gap is found for larger clusters which is 0.4 eV. Marta B. Ferraro *et.al*, [74] have studied medium sized  $\text{Si}_n$  clusters in the size range  $\text{Si } 18 \leq n \leq 60$  and they are reported widest band gaps as 2.25 eV and 1.8 eV respectively where as smallest gaps as 1 eV and 0.76 eV respectively.

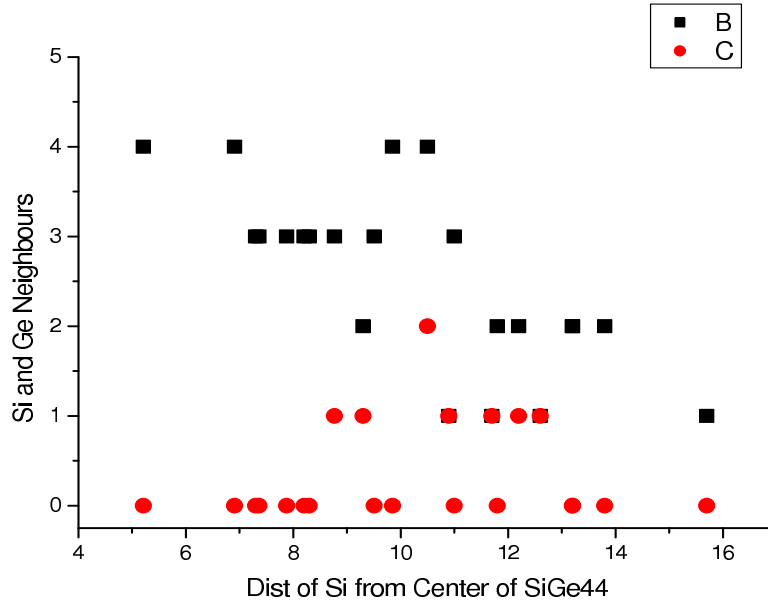


Figure 4.22: Total Coordination Number of Si atoms in  $\text{Si}_{22}\text{Ge}_{22}$ , Here we have calculated distance of all Si atoms from center of  $\text{Si}_{22}\text{Ge}_{22}$  cluster and plotted all its neighbors. Here C = Silicon and B = Ge

The gaps of pure clusters of  $\text{Ge}_n$  clusters have the same trend as those of pure  $\text{Si}_n$  clusters, only slightly narrower, which was reported earlier by Melnikove *et.al*, [73]. For very small clusters, Ge gap is slightly narrower than Si clusters. We have found the widest gap in small germanium clusters to be 1.6 eV where as smallest gap is found for larger clusters which is 0.3 eV. Studies of Zhong-Yi Lu *et.al*, [75] for size range upto  $n=13$  for both Si and Ge clusters have found widest Gap as 2.2 eV and 2.1 eV respectively. For binary cluster  $\text{Si}_n\text{Ge}_n$  we have found the same trend as elemental clusters but larger  $\text{Si}_n\text{Ge}_n$  binary clusters have wider gap as compared to both  $\text{Si}_n$  and  $\text{Ge}_n$  clusters.

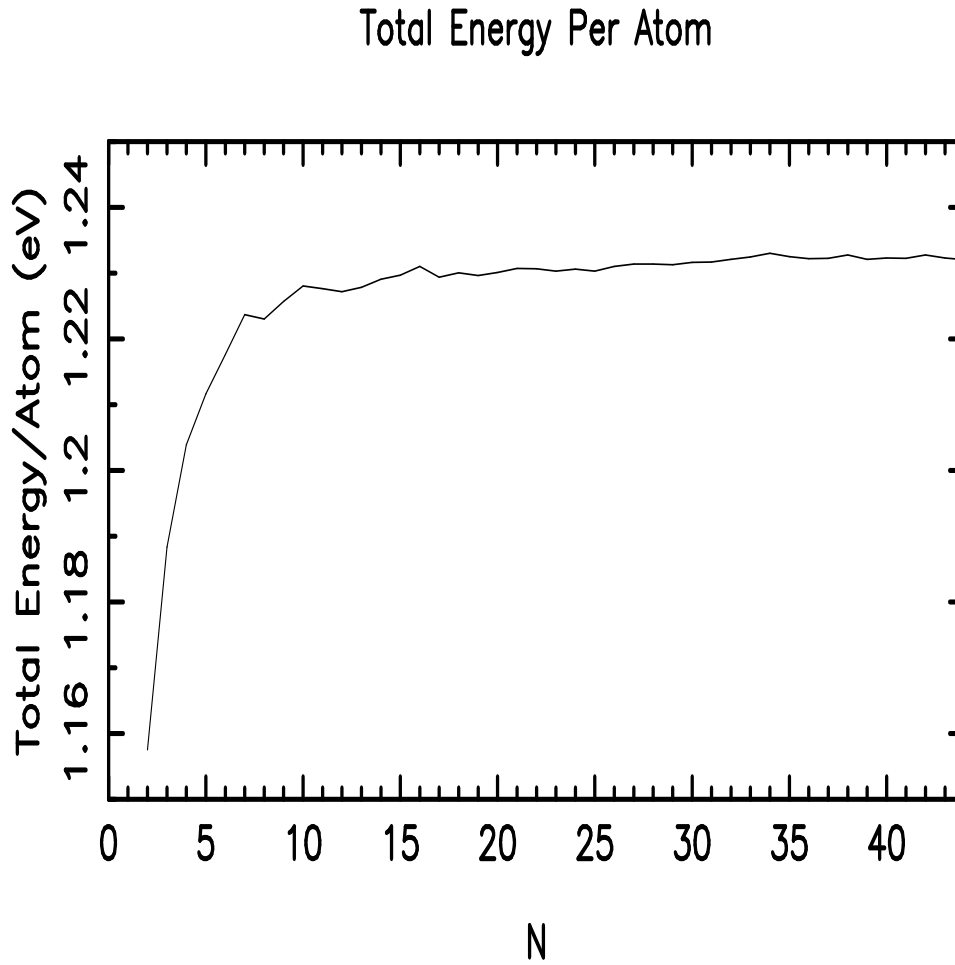


Figure 4.23: Variation in the total energy per atom for  $Si_n$  clusters : Here  $N$ = Number of Atoms

## 4.4 Radial Distribution Function

Radial distribution functions are very important as they give valuable informations about the structure of clusters. The radial distribution is defined as follows. For each atom of our cluster systems, we calculate the distance to the center of mass (positioned at  $R_0$ )

$$\vec{R}_0 = \frac{1}{n+m} \sum_{j=1}^{n+m} \vec{R}_j \quad (4.12)$$

and, subsequently, for each atom its so-called radial distance

$$r_j = |\vec{R}_j - \vec{R}_0|, \quad j = 1, 2, \dots, n+m \quad (4.13)$$

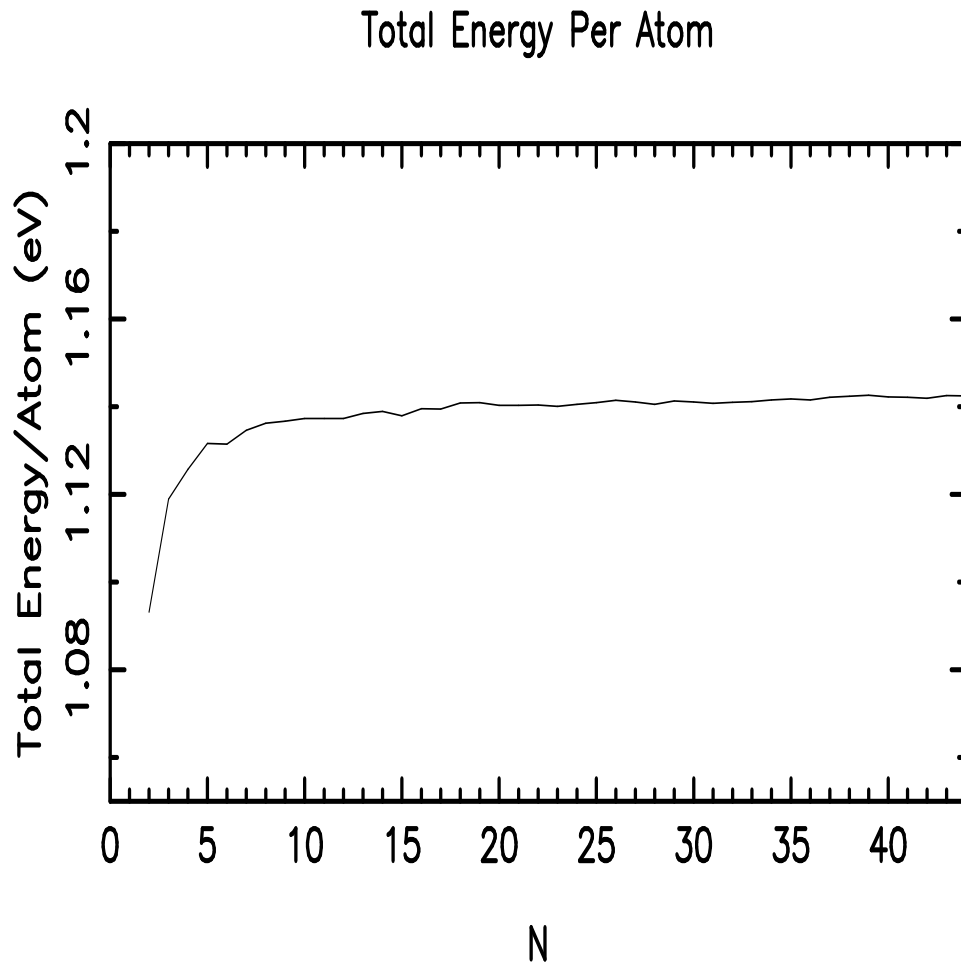


Figure 4.24: Variation in the total energy per atom for  $Ge_n$  clusters : Here  $N$ = Number of Atoms

where  $R_i$  being the position of  $i$ th atom, is calculated. Subsequently all these  $n$  distances are displayed in one diagram and shown as a function of the cluster size (number of atoms  $n$ ). One aspect is clear from the radial distribution analysis that, for all cluster systems, *i.e.*,  $Si_n$ ,  $Ge_n$ , and  $Si_nGe_n$ , the radius of the cluster is increasing with increasing  $n$ . The growth pattern of all the three cluster systems is different. For homogeneous  $Si_nGe_n$  clusters, we can see that radial distances for the different  $Si_nGe_n$  clusters are relatively large (accept for  $Si_5Ge_5$ ). We can see more distances in radial distribution function for binary clusters compared to atomic clusters in the small size range except for  $Si_5Ge_5$ . Stability Analysis shows that  $Si_5Ge_5$  is relatively stable structure along with few other cluster structures compared to other  $Si_nGe_n$  clusters. This suggests that  $Si_nGe_n$  clusters have

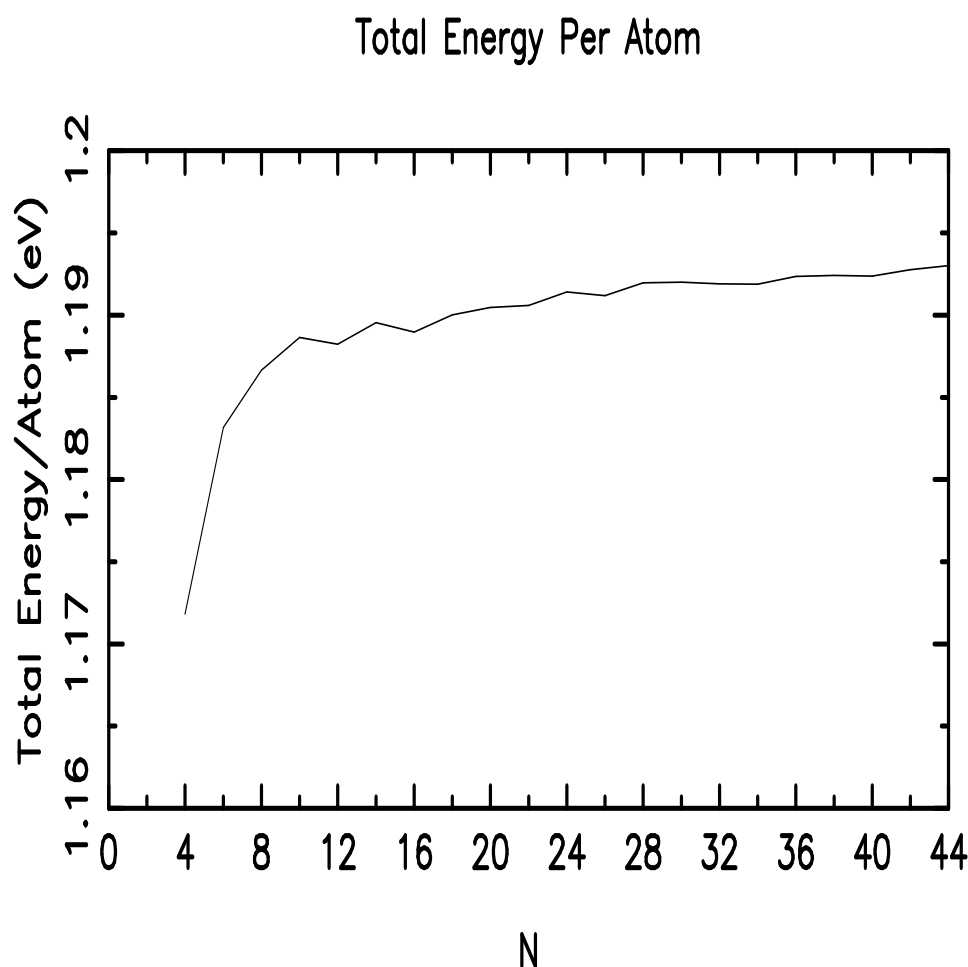


Figure 4.25: Variation in the total energy per atom for  $Si_nGe_n$  clusters : Here N= Number of Atoms

overall very low symmetry and that is confirmed by the point group analysis of available structures. In case of pure  $Si_n$  clusters we see that clusters in the size range  $N < 20$  are less scattered (more compact) as compared to  $Ge_n$  clusters in the same size range. Stability analysis predicts some stable clusters for  $Si_n$  clusters in this size range. After  $N > 20$  both the cluster systems have wide range of distances from the center, meaning very low symmetric structures. In radial distribution function of  $Si_n$  cluster we can see a major difference in the distances of cluster  $Si_{19}$  and  $Si_{20}$ . This change is also identified in similarity function analysis of pure  $Si_n$  cluster. If we look at the structures of both clusters we will find that  $Si_{19}$  has a different structure compared to  $Si_{20}$  which has two separate  $Si_{10}$  units. Point group analysis of pure  $Si_n$  and pure  $Ge_n$  clusters is shown in tables [3.2] and [3.3]

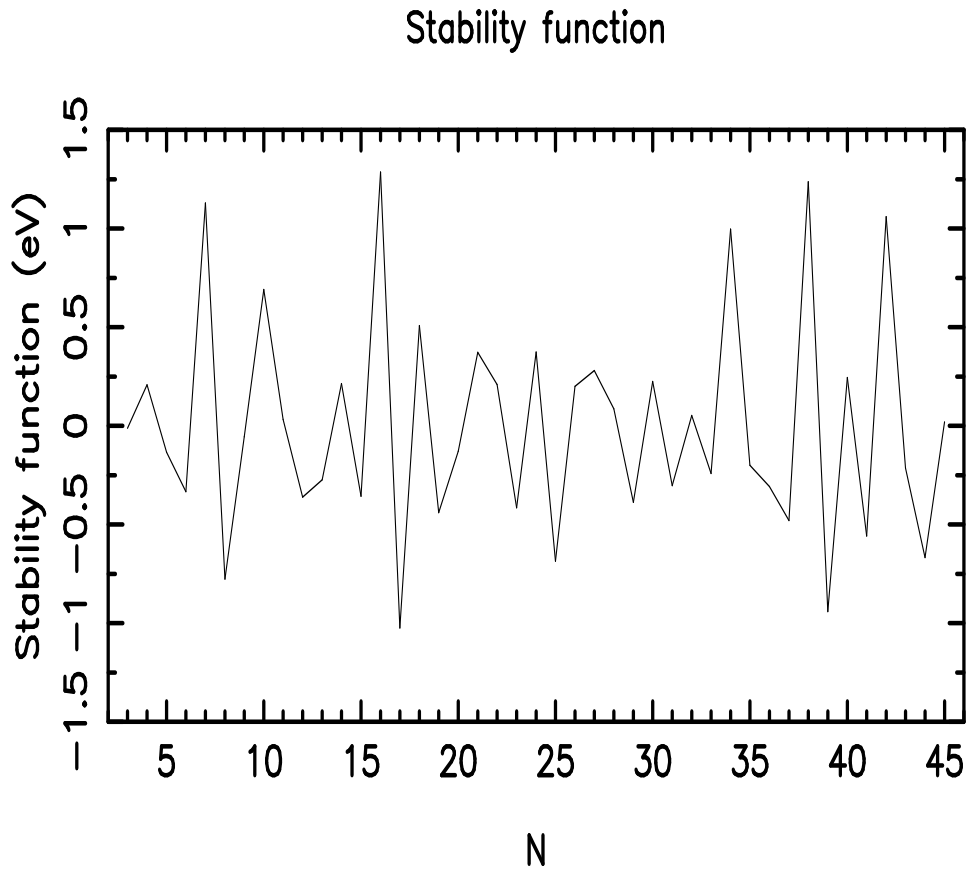


Figure 4.26: Stability Function which has maxima (minima) for particular stable (unstable) structure for  $Si_n$  clusters : Here  $N =$  Number of Atoms

respectively. One more thing that we can notice from radial distribution of  $Ge_n$  clusters is that besides having more irregular radial distances from the center as compared to  $Si_n$  clusters, they have some how shell structures specially in the size range  $22 < N < 31$ . The radial distribution functions for pure  $Si_n$ , pure  $Ge_n$  clusters are shown in Figures [4.32] and [4.33] respectively. For binary  $Si_nGe_n$  clusters we have divided the radial distribution functions into two types based on distances of Silicon and Germanium from the center and are plotted in figures [4.35] and [4.36].

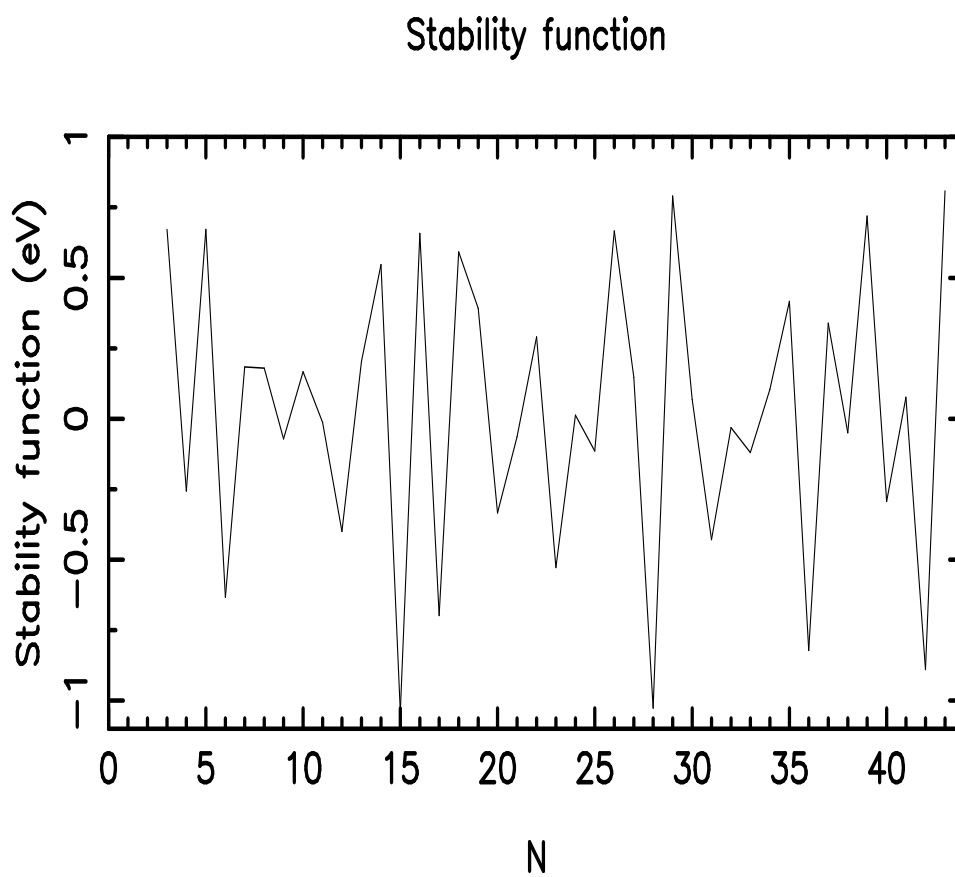


Figure 4.27: Stability Function which has maxima (minima) for particular stable (unstable) structure for  $Ge_n$  clusters : Here  $N =$  Number of Atoms

We have divided the radial distribution function of  $Si_nGe_n$  clusters into two parts on the basis of distances of Silicon atoms and Germanium atoms from the center so that we can clearly observe, how both Silicon and Germanium atoms orient themselves in bimetallic clusters. Here we can observe that for smaller units up-till 12 atom cluster Ge atoms are lying close to the center where as Si tend to move away from the center. The same trend is followed for larger clusters as we can see very few points for Si atoms lying close to the center. Reason behind this can be size difference between Ge and Si as Germanium is heavier element than Silicon.

## Stability Function

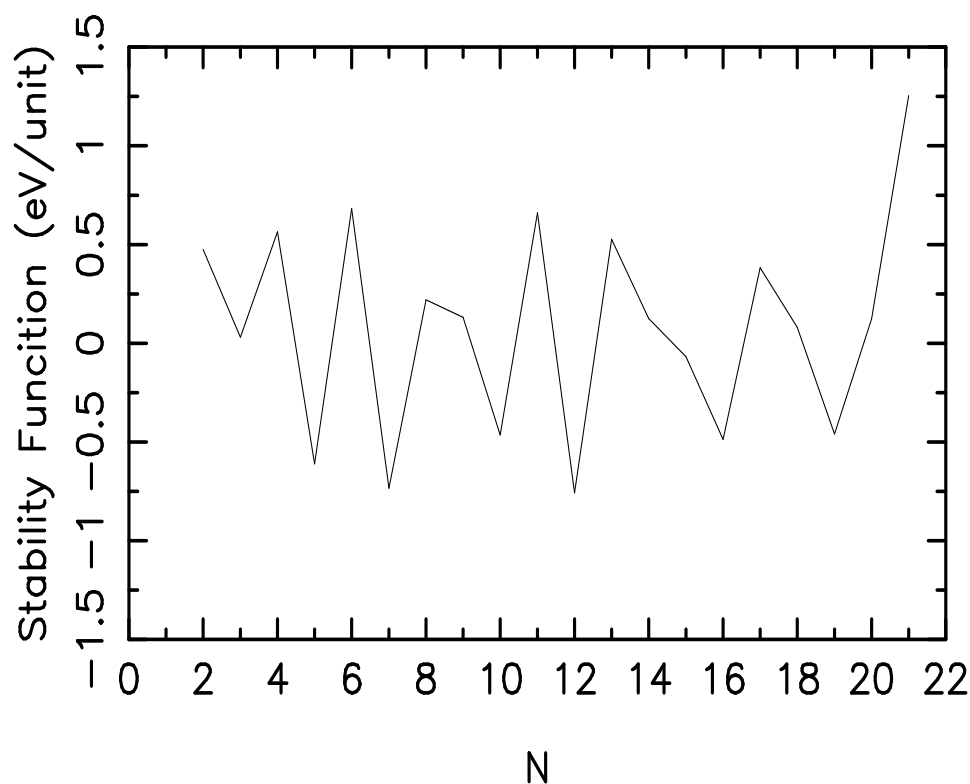


Figure 4.28: Stability Function which has maxima (minima) for particular stable (unstable) structure for  $\text{Si}_n\text{Ge}_n$  clusters : Here  $N$  = Number of Si-Ge units

## 4.5 Shape Analysis

For the structural Analysis of Clusters, the overall shape and its size dependence is also of significant importance. To study this in more detail we calculate for a given  $n$ -atom cluster the eigenvalues  $I_{\alpha\alpha}$  of the matrix containing the moments of inertia  $\sum_{i=1}^n s_i t_i$ . Here  $s$  and  $t$  are the  $x, y, z$  coordinates in a coordinate system centered at the center of mass  $R_0$  defined in equation [4.6]. From the eigenvalues  $I$ , we analyze the overall shape of the cluster. Three identical eigenvalues suggest a spherical shape, whereas two large and one small value suggest a lens like shape, and two small and one large value suggest a cigar-like shape. In Figure [4.37] and [4.38] (for pure  $\text{Si}_n$  and pure  $\text{Ge}_n$  clusters) we show the average eigenvalues (scaled by  $N^{5/3}$ , which is the scaling a spherical jellium would possess) together with

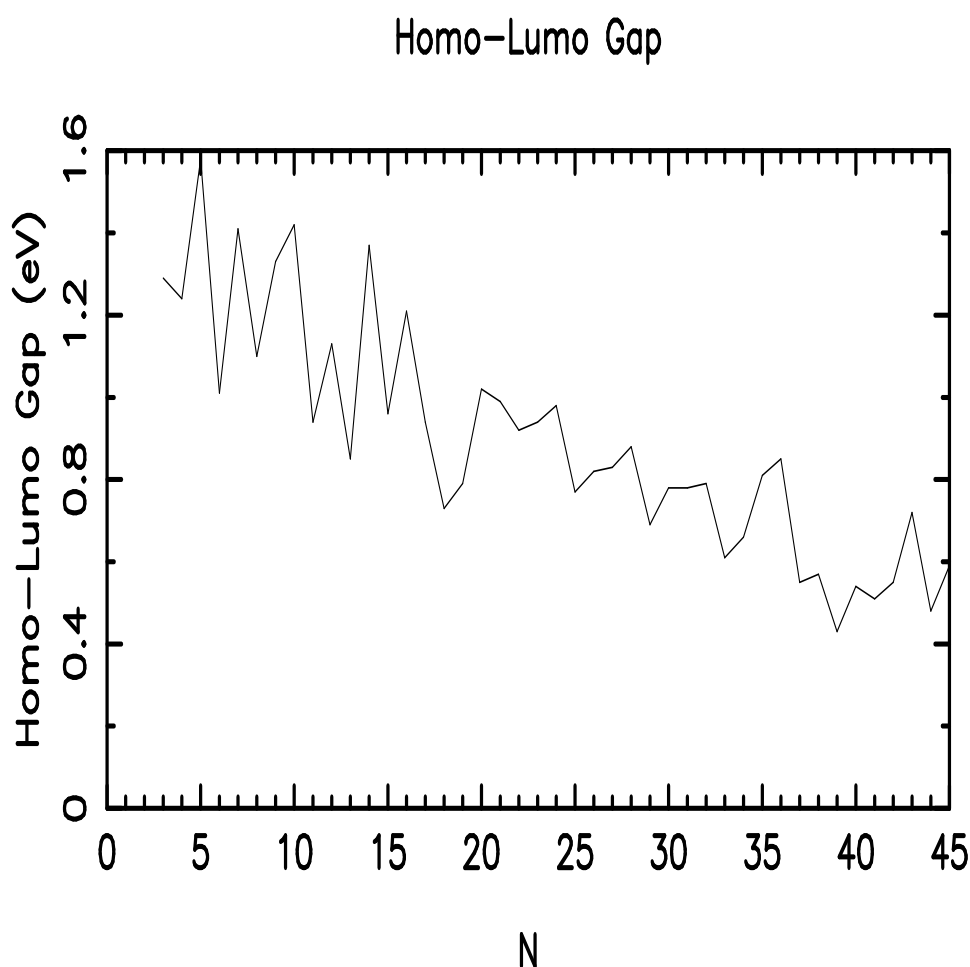


Figure 4.29: HOMO-LUMO Gap for Silicon clusters : Here N = Number of Atoms

marks indicating the overall shape. Also the largest difference between the eigenvalues is shown. We see that no cluster has an overall spherical shape, in agreement with the point group analysis of  $Si_n$  clusters and of pure  $Ge_n$  clusters from Tables [3.02] and [3.03] respectively. However the largest difference of the eigenvalues takes particularly low values for  $n=5,10,15,41$  for  $Si_n$  clusters and for  $N=5,10,42,44$  for  $Ge_n$  clusters. Some of these clusters are particularly stable so we can say that stability is roughly related to the spherical structure of these clusters. This is explained by radial distance analysis as we can see that for  $Si_5$  and  $Si_{10}$  there are few radial distances showing that these are symmetric clusters.

Here we would like to mention that, general conclusions about the semiconductor studies are given in the last part of this thesis (Chapter 6)

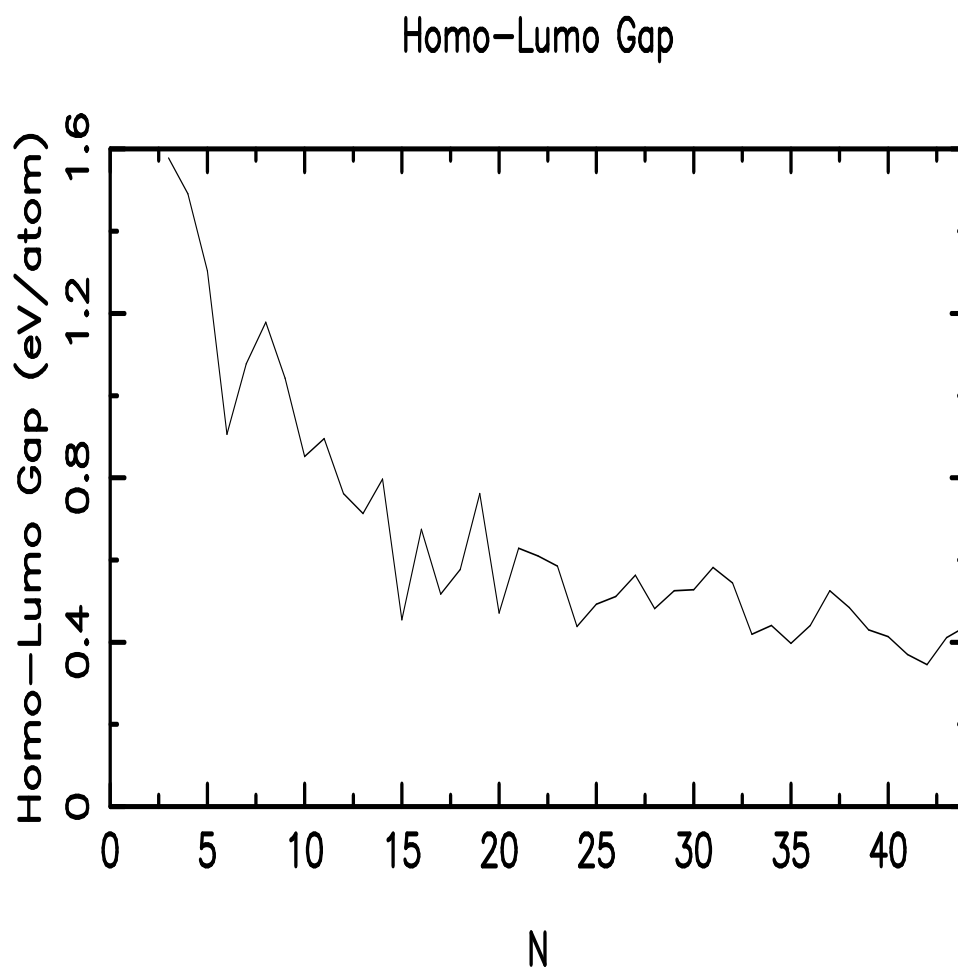


Figure 4.30: HOMO-LUMO Gap for Germanium clusters : Here N = Number of Atoms

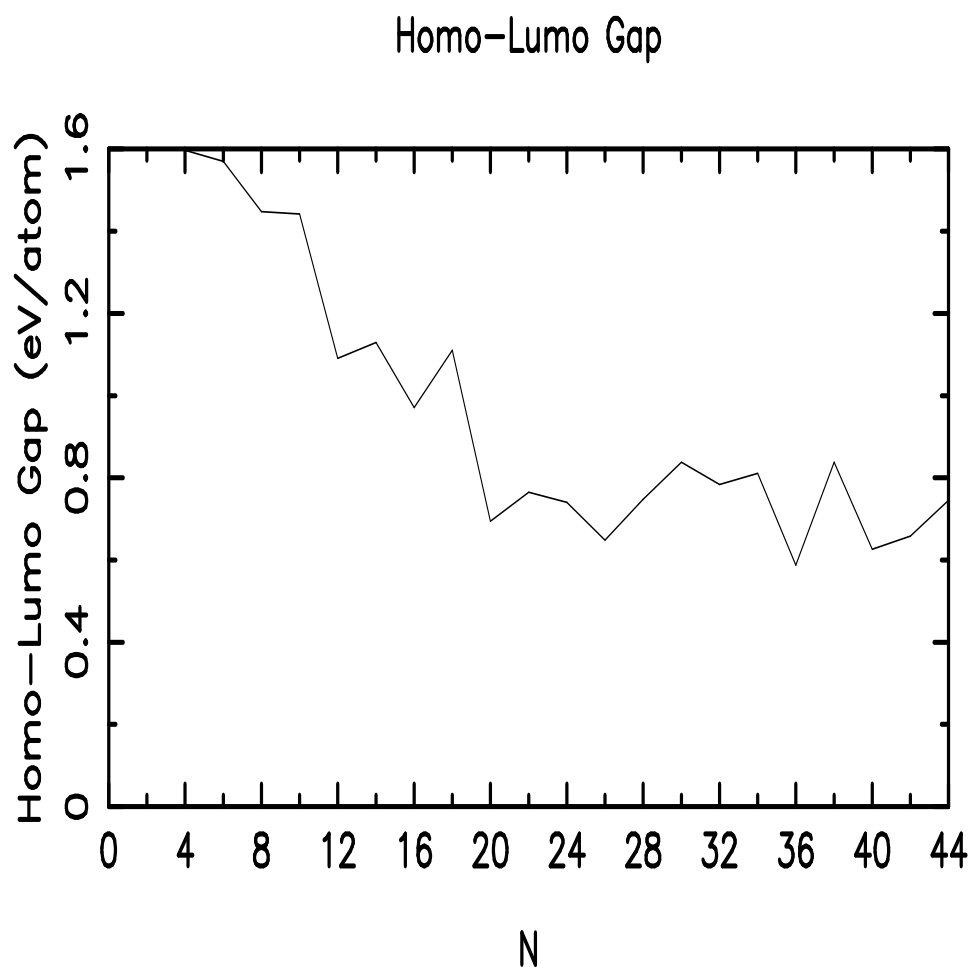


Figure 4.31: HOMO-LUMO Gap for Silicon Germanium binary clusters :  
Here N = Number of Atoms

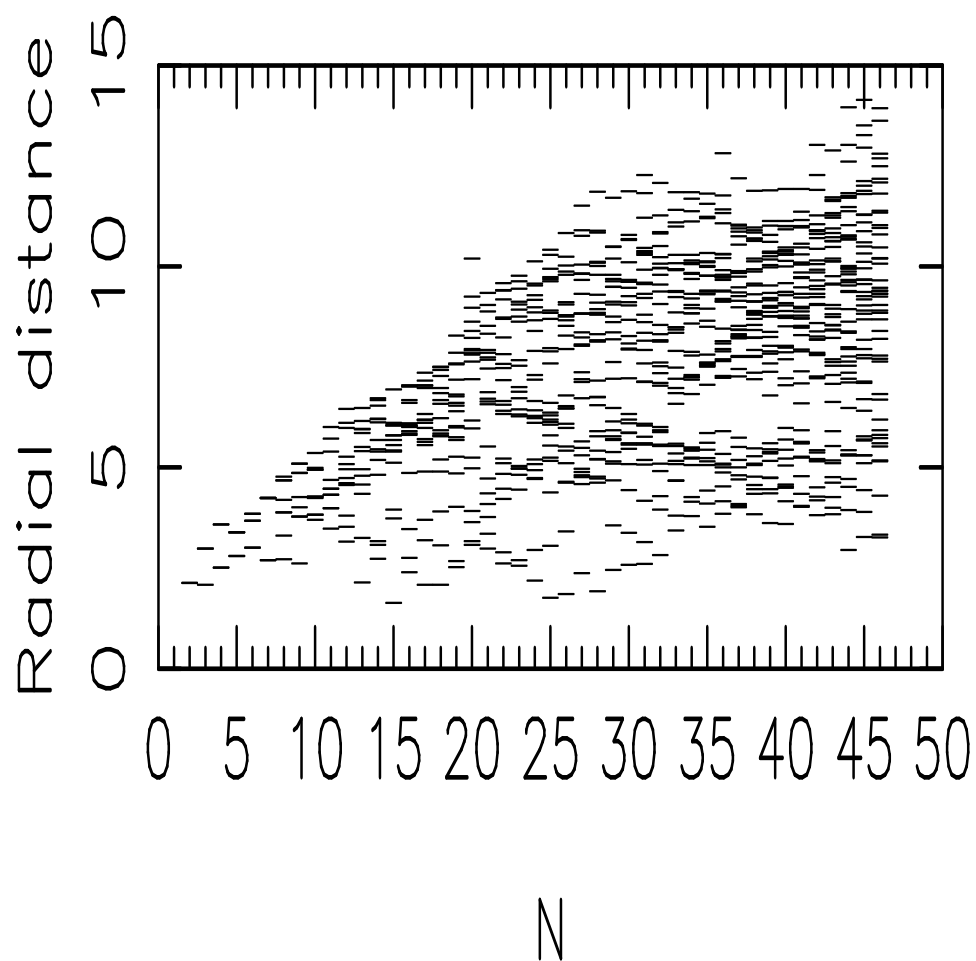


Figure 4.32: Radial Distribution Function for  $\text{Si}_n$  clusters : Here  $N$  = Number of Atoms

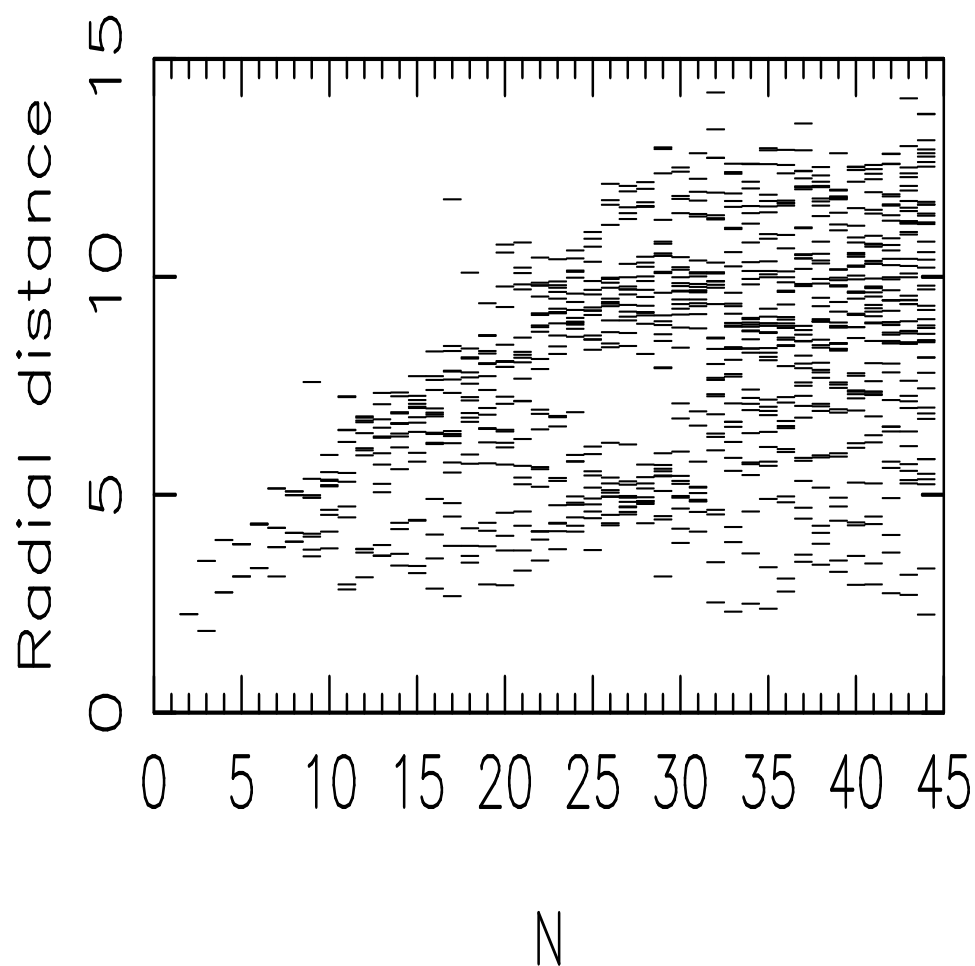


Figure 4.33: Radial Distribution Function for  $Ge_n$  clusters : Here  $N =$  Number of Atoms

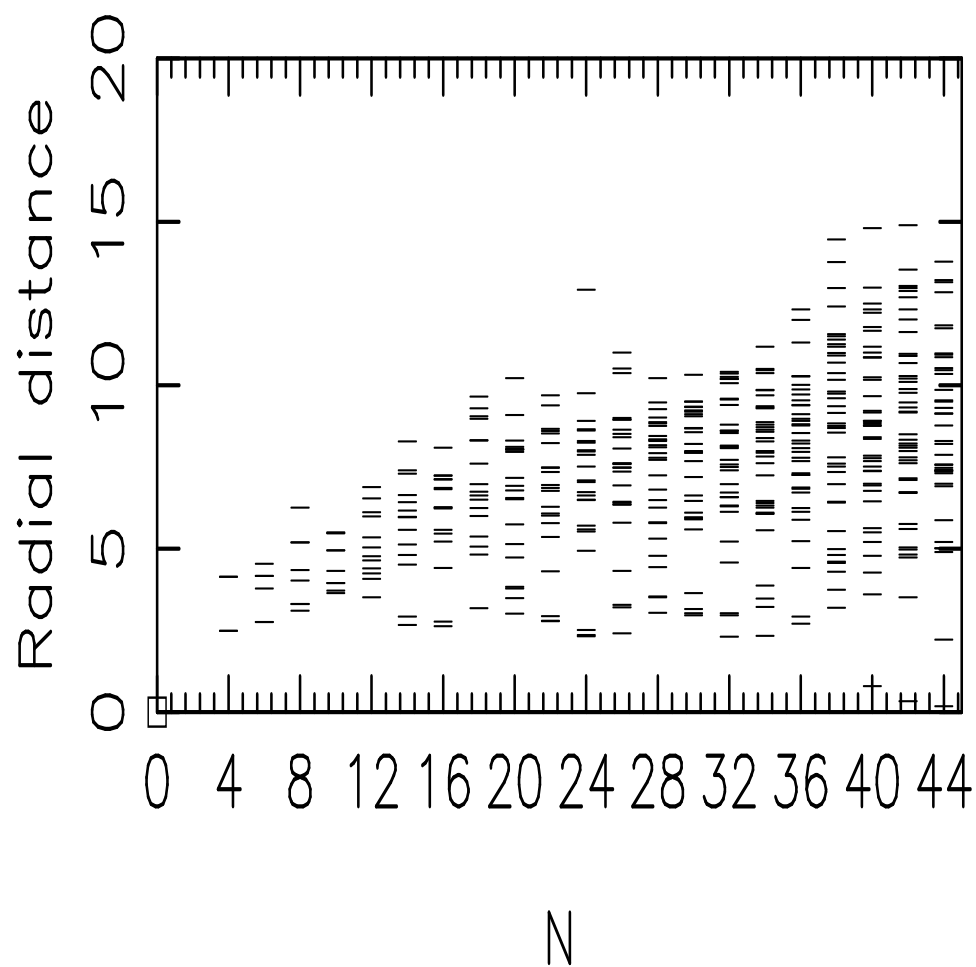
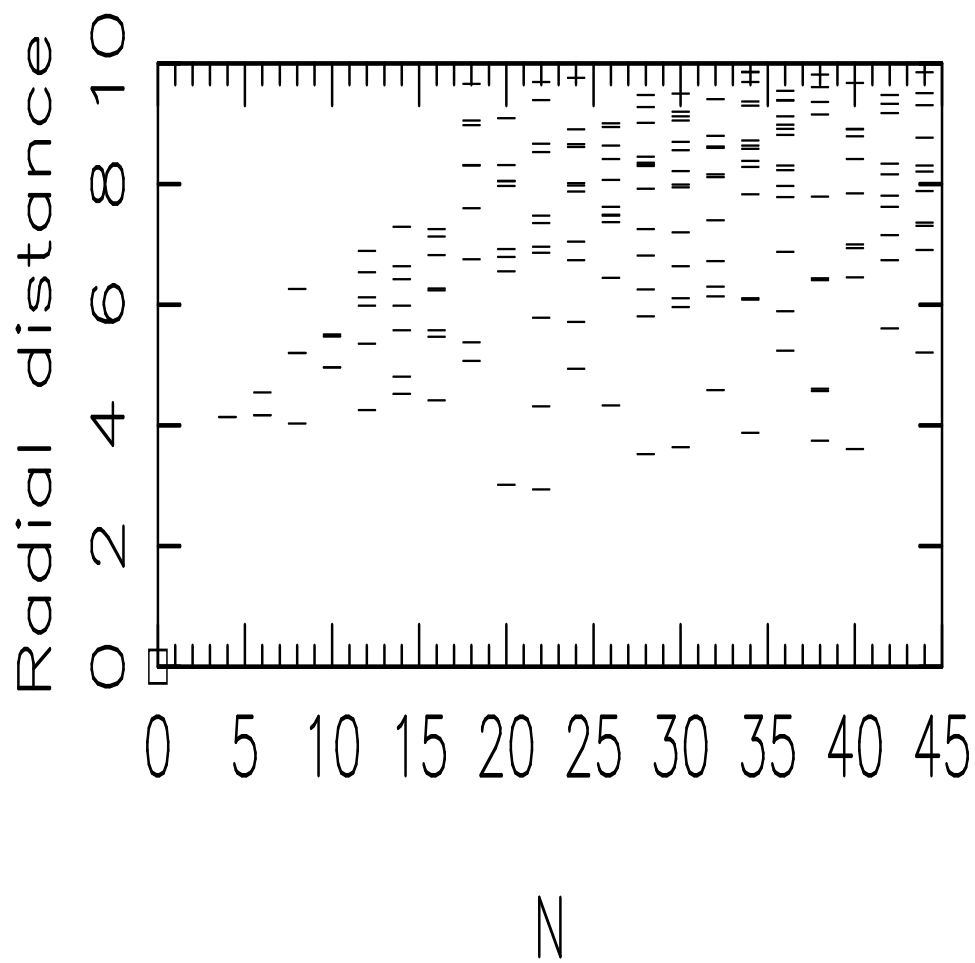


Figure 4.34: Radial Distribution Function for  $\text{Si}_n\text{Ge}_n$  clusters : Here N = Number of Atoms

Figure 4.35: Radial Distribution for Si in  $\text{Si}_n\text{Ge}_n$  clusters

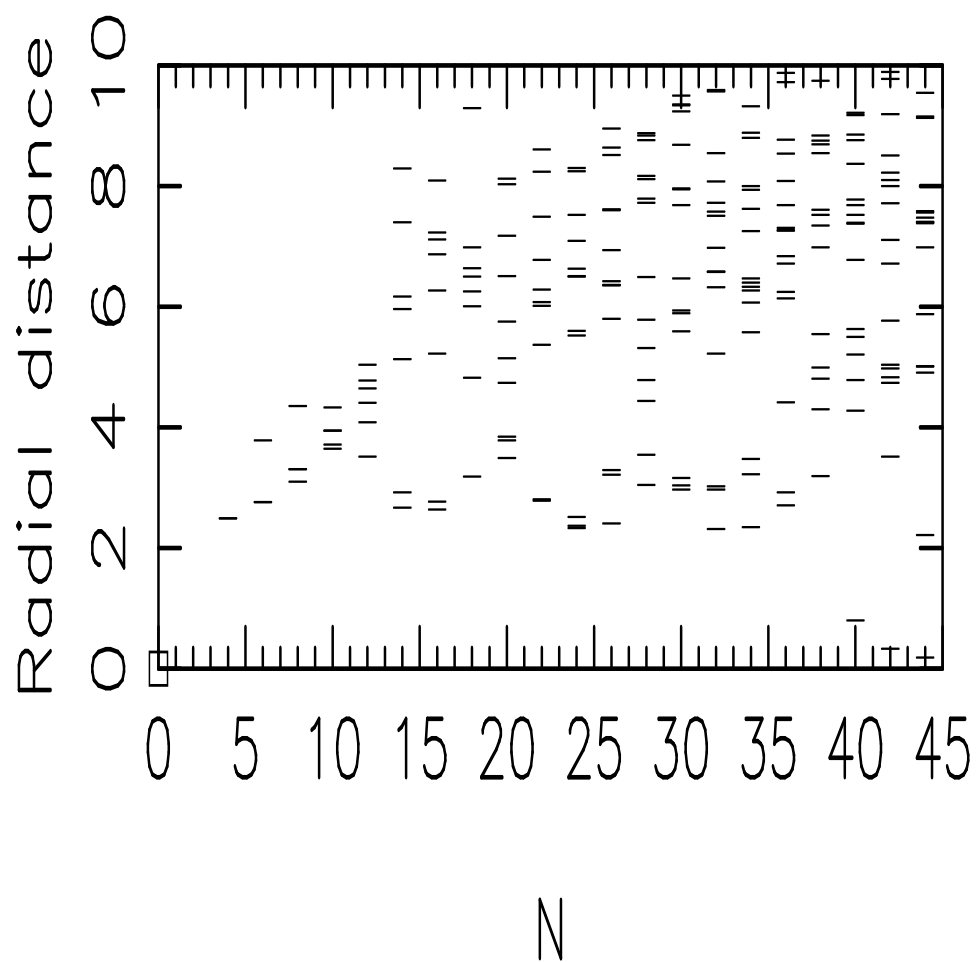
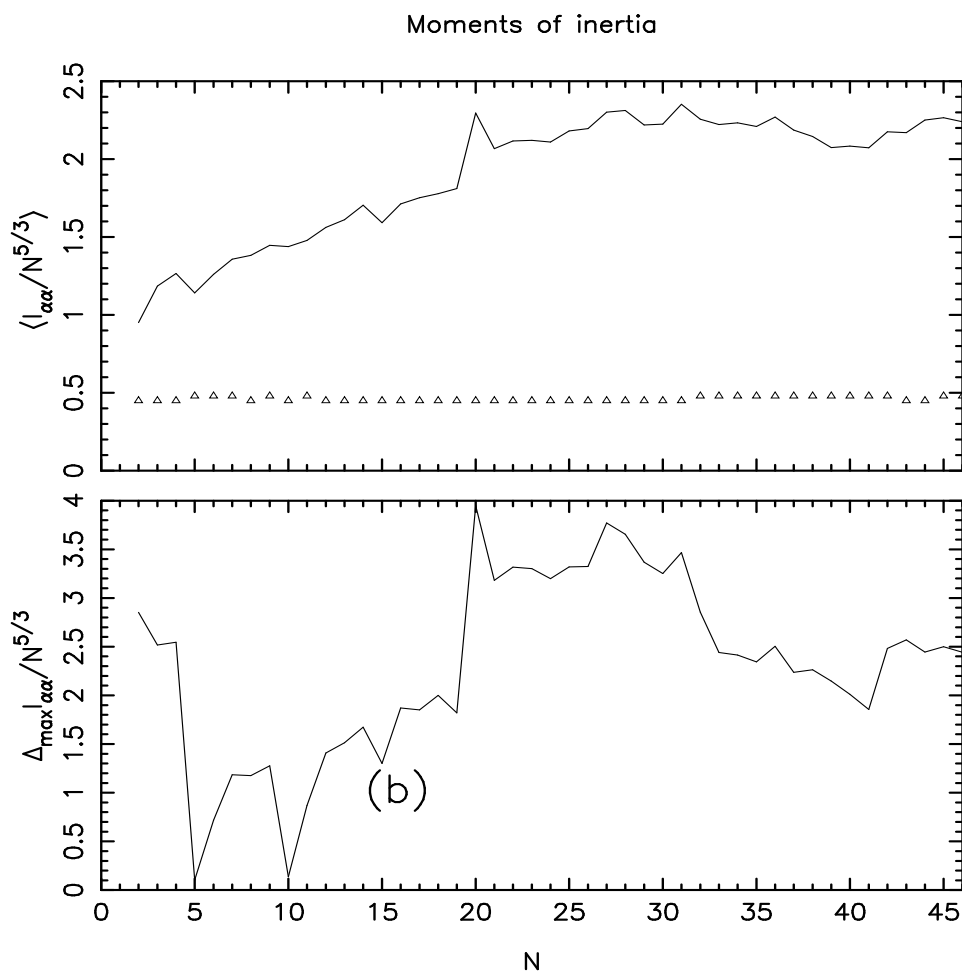


Figure 4.36: Radial Distribution for Ge in  $\text{Si}_n\text{Ge}_n$  clusters

Figure 4.37: Shape Analysis for  $Si_n$  clusters : Here  $N =$  Number of Atoms

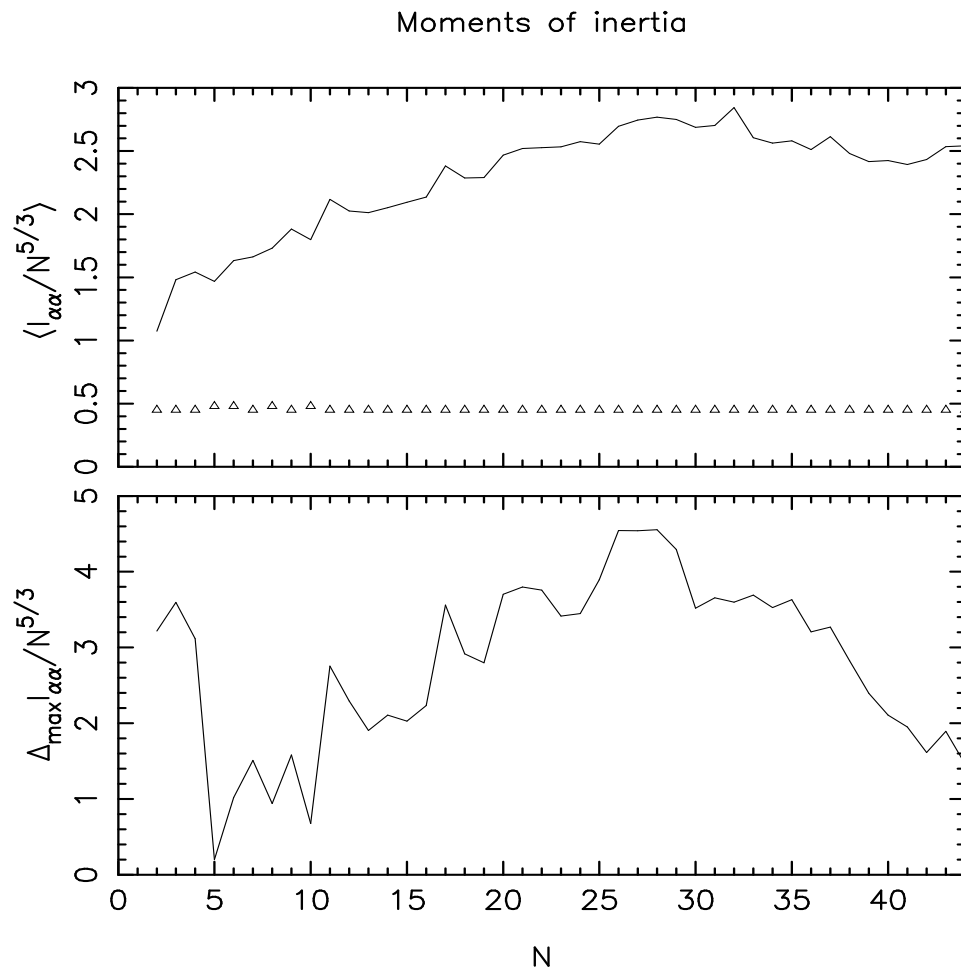


Figure 4.38: Shape Analysis for  $Ge_n$  clusters : Here  $N$  = Number of Atoms

## Chapter 5

---

# Properties of $\text{Cu}_n$ Clusters

---

### 5.1 Introduction

In second part of our research work, we will present results of theoretical studies of properties of  $\text{Cu}_n$  clusters in medium size range ( $2 \leq N \leq 36$ ). The evolution of structures and properties of metal clusters has been a subject of great interest in the past few years [86]-[94]. Clusters can serve as a convenient model for a systematic understanding of properties of materials at nanoscale level. Of the metal clusters, transition metals (TM) clusters are particularly interesting since they have been widely used as catalysis in many heterogeneous catalytic reactions [95, 96].

In this chapter, we present theoretical studies on the structural evolution of medium sized copper clusters ( $n < 37$ ). Small copper clusters have been a subject of intense theoretical and experimental studies. While the first principles based calculations were generally restricted to  $\text{Cu}_n$  ( $n \leq 10$ ) [61, 93, 94, 97, 98, 99] larger Copper clusters up to  $n = 55$  were systematically investigated with the tight-binding method assuming the clusters follow an icosahedra growth pathway [63]. Massobrio *et.al*, [60, 93] performed the first DFT calculations using the Car-Parinello Method and the local-density approximation (LDA) to study  $\text{Cu}_n$  with  $n \leq 10$ . They used the cluster geometries that had been used earlier for  $\text{Na}_n$  and  $\text{Ag}_n$  clusters, which were re-optimized for  $\text{Cu}_n$  clusters. K.Jug *et.al*, [99] used the generalized gradient approximation (GGA) to study the relative stability of a number of cluster isomers upto  $n=10$ . Similarly Fernández *et.al*, [123] examined the selected cluster geometries up to  $n=13$ , and for  $n=20$ , using

GGA to compare and contrast the properties of  $\text{Cu}_n, \text{Ag}_n$  and  $\text{Au}_n$ . Guvelioglu *et.al.*, [124] investigated the  $\text{H}_2$  chemisorption on  $\text{Cu}_n$  up to  $n=15$ , using DFT-based study. In intermediate size range, Darby *et.al.*, [125] used a genetic algorithm to find the optimal structures for  $n=10-56$ , representing the energy surfaces with the Gupta Potential. M.Kabir *et.al.*, [63, 126, 128] have used tight-binding based molecular dynamics approach to study the size range  $n=3-55$ . Denitsa *et.al.*, [102] has used embedded-atom method (EAM) in the version of Daw, Baskes, and Foiles (DBF) to study the  $\text{Cu}_n$  clusters in the size range  $n=2-150$ . M.Yang and K.A.Jackson *et.al.*, [127] have used unbiased search based on DFT to study the structural evolution of  $\text{Cu}_n$  clusters in the size range  $n=8-20$ . In this work, we have studied the optimized geometries of  $\text{Cu}_n$  clusters in the size range ( $2 \leq N \leq 36$ ). To identify the ground-state structures of  $\text{Cu}_n$ , we have used density functional tight binding method (DFTB) as described in chapter 2. The DFTB Hamiltonian includes 3d and 4s orbitals for each atom. Hamiltonian and overlap matrix elements are based on DFT results for isolated atoms. The repulsive pair potential in the model was fit to reproduce DFT results for the Cu dimer. Cu crystal has fcc structure with lattice parameter  $a=3.67 \text{ \AA}$ , where as we have produced here  $a=3.61 \text{ \AA}$ . The global minima structures were obtained using so called genetic algorithms which was found to provide an efficient tool for the global geometry optimization. The geometric algorithm for structural optimization has been explained in section [2.3] of present work. In the next section we will present structures of  $\text{Cu}_n$  clusters and then discuss them separately and compare them with the available data.

## 5.2 Structures of Cu clusters: Cu<sub>2</sub> to Cu<sub>36</sub>

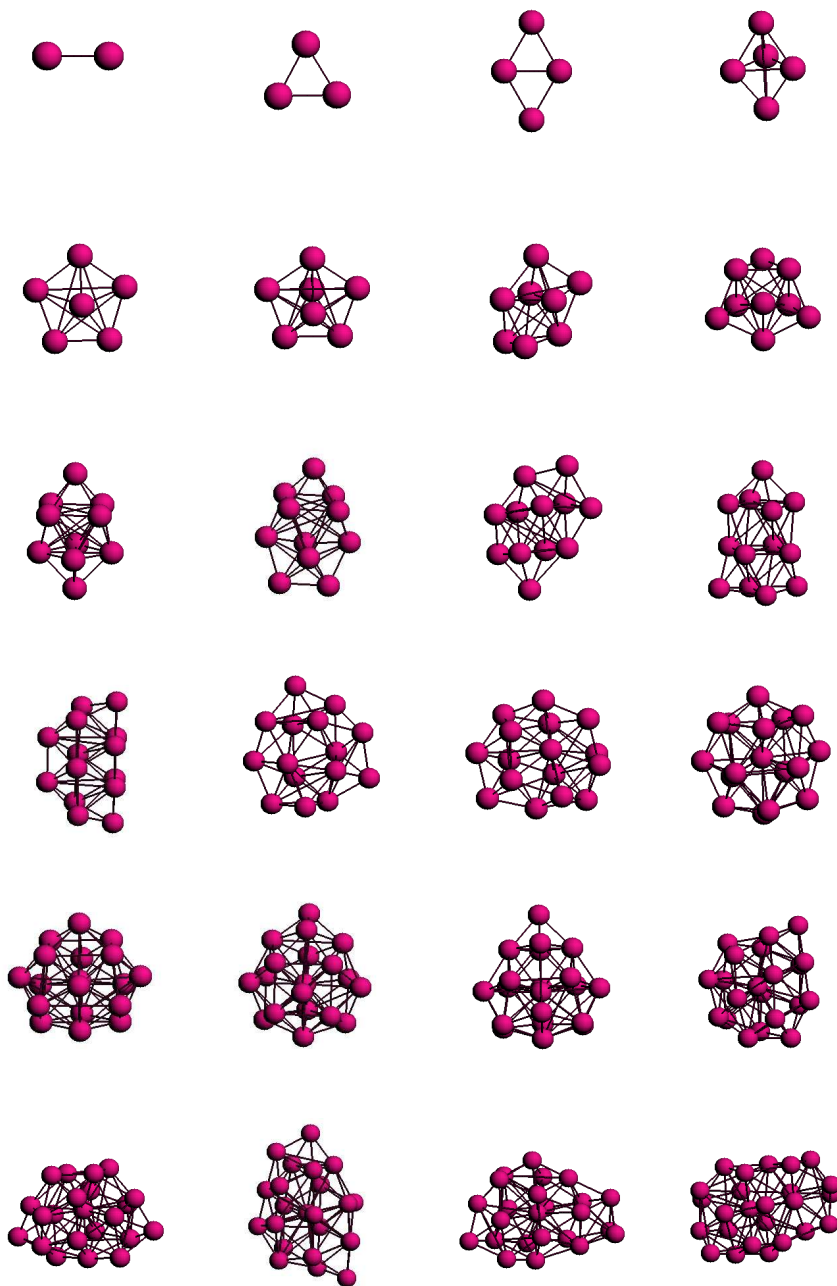
The structures of the small Cu<sub>n</sub> clusters upto Cu<sub>9</sub> except Cu<sub>5</sub> are similar to those obtained from first principles theoretical work on Cu<sub>n</sub> clusters. The optimized bond-length for Cu<sub>2</sub> dimer comes out to be 4.11 *a.u.*, where as its experimental value is 4.22 *a.u.* Table [5.1] shows the comparison between bond length of the Cu dimer with other approaches. The Cu<sub>3</sub> is equilateral triangle (point group D<sub>3h</sub>), where as Cu<sub>4</sub> cluster is predicted to be having planer rhombus (D<sub>2h</sub>) structure. These structures are also predicted by other studies [63, 93, 101, 124, 126]. We have investigated Cu<sub>5</sub> to be having trigonal bipyramid (D<sub>3h</sub> symmetry) structure. This structure is different from DFT based studies [124] but is not new structure of Cu<sub>5</sub> cluster as it is predicted by EAM studies in the version of DBS by Denitsa *et.al*, [102]. In the case of Cu<sub>6</sub> cluster we have found flat pentagonal pyramid C<sub>5v</sub> to be the most stable structure which is also predicted by M.Kabir *et.al*, [63] by TBMD studies. How ever this differs from the results found by H.Cheng [124] (DFT studies) and Denitsa [102] who predict planer trapezoidal (C<sub>2v</sub> symmetry) and octahedron (O<sub>h</sub> symmetry) respectively for Cu<sub>6</sub> cluster. For Cu<sub>6</sub> local-density approximation with in molecular dynamics performed by Massobrio *et.al*, [93] predicts two trigonal bipyramid where as tight binding linear muffin-tin-orbital calculation performed by Lammers *et.al*, [101] predicts square bipyramid structure. We have found the pentagonal bipyramid with D<sub>5h</sub> symmetry to be the most stable structure for Cu<sub>7</sub> cluster. This prediction is in well agreement with other first principle studies. For Cu<sub>8</sub> we have found bicapped octahedron with D<sub>2d</sub> symmetry to be lowest energy structure. This structure is also found by Denitsa *et.al*, [102] as the most stable structure. Cu<sub>8</sub> is predicted to be having capped pentagonal bipyramid (C<sub>s</sub>) structure by M.kabir *et.al*, [63] who carried out tight binding based molecular dynamics approach for Cu<sub>n</sub> cluster studies. Studies by Lammers *et.al*, [101] gives anti-prism structure to Cu<sub>8</sub>. For Cu<sub>9</sub> we have obtained D<sub>3h</sub> symmetry where as M.Kabir *et.al*, [63] found the BPB with capping atom on the non adjacent faces with C<sub>2</sub> symmetry where as Denitsa *et.al*, [102] found C<sub>2v</sub> symmetry for Cu<sub>9</sub>. For Cu<sub>10</sub> we have found D<sub>4d</sub> structure while in case of M.Kabir *et.al*, [63], they found tri-capped pentagonal bipyramid structure where as Denitsa *et.al*, [102] found C<sub>3v</sub> symmetry of Cu<sub>10</sub> cluster. For smaller Cu<sub>n</sub> clusters we have produced the structures which are reported in earlier works. The structures of optimized Cu<sub>n</sub> clusters are presented in figure [5.1] and [5.2]. M.Kabir *et.al*, [63] suggested that copper clusters for 10 ≤ n ≤ 55 adopt an icosahedral structure using tight-binding calculation

Cu dimer Bond-length comparison	
Method	Bond Length $\text{\AA}$
Here	2.11
DBF/VC	2.13/2.22
ab initio	2.17
exp.	2.22

Table 5.1: Cu dimer Bond-length comparison

which, in contrast is different from our findings. We have obtained structure with  $C_{2v}$  point group for  $Cu_{11}$  cluster which is in very good agreement with the all the four different methods used by Denitsa *et.al*, [102]. Our structure for  $Cu_{12}$  cluster has  $C_s$  symmetry which is same structure found by M.Yang and K.A.Jackson *et.al*, [127] based on density-functional calculation. We have found a symmetric structure with  $C_{2v}$  point group for  $Cu_{13}$  cluster which differs from results from other studies. We have given the point groups of  $Cu_n$  clusters in table [5.2].

In the next section we will discuss various tools used to study size dependent properties of  $Cu_n$  clusters.

Figure 5.1: Structures of Smaller  $Cu_n$  clusters  $2 \leq N \leq 25$

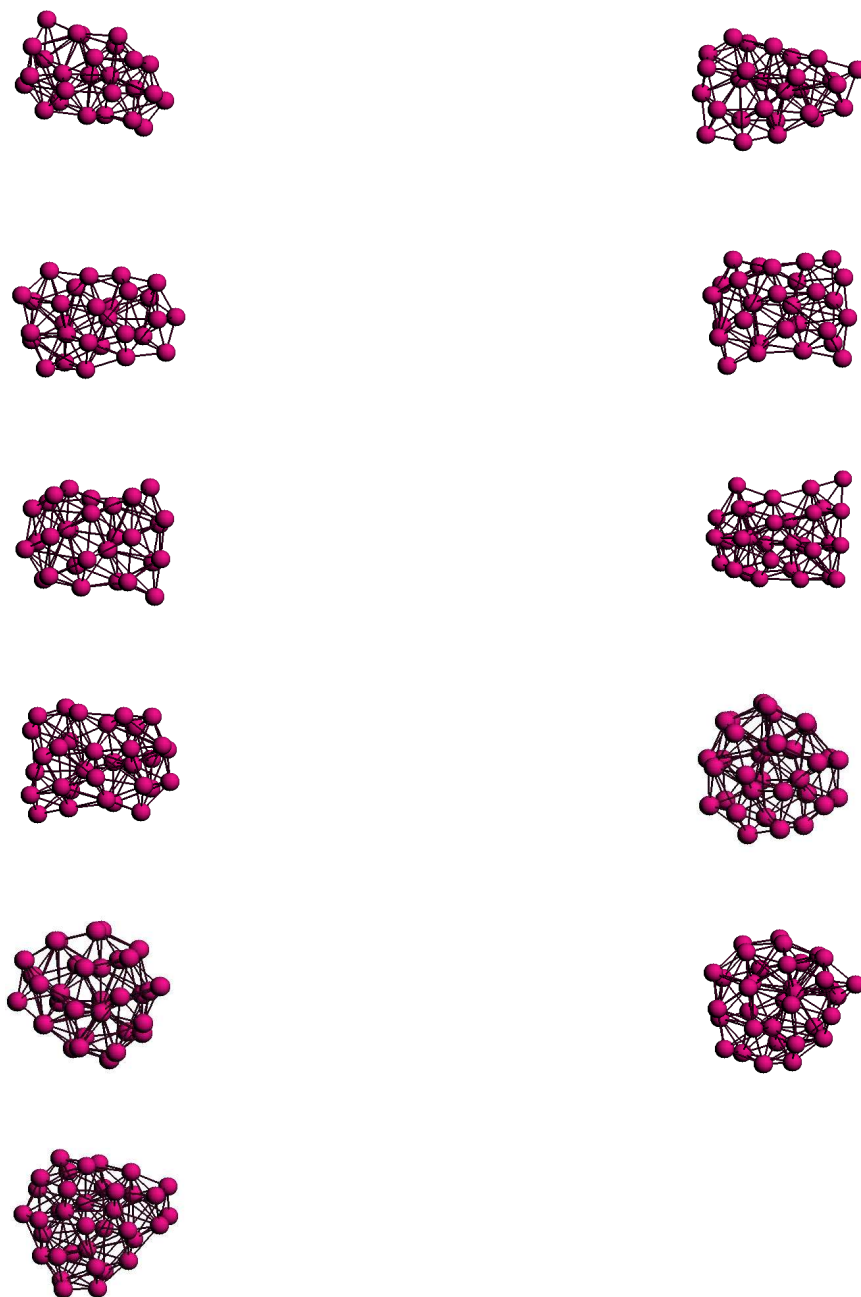


Figure 5.2: Structures of Smaller  $Cu_n$  clusters  $26 \leq N \leq 36$

## 5.3 Tools for Structural Analysis

### Radial Distribution Function

As mentioned in Chapter 4, Radial distribution functions are very important as they give valuable informations about the structure of clusters. The radial distribution is defined as follows. For each atom of  $\text{Cu}_n$  cluster, we calculate the distance to the center of mass (positioned at  $R_0$ )

$$\vec{R}_0 = \frac{1}{n+m} \sum_{j=1}^{n+m} \vec{R}_j \quad (5.1)$$

and, subsequently, for each atom its so-called radial distance

$$r_j = |\vec{R}_j - \vec{R}_0|, \quad j = 1, 2, \dots, n+m \quad (5.2)$$

where  $R_i$  being the position of  $i$ th atom. Subsequently, all these  $n$  distances are displayed in one diagram and shown as a function of the cluster size (number of atoms  $n$ ). We can observe that, in the resulting diagram, radius of the cluster increases with the cluster size  $n$ . Radial Distribution function for  $\text{Cu}_n$  clusters is plotted in figure [5.3]. As mentioned, radius is increasing with increasing number of atoms, although some irregularities do occur and in those cases the cluster radius decreases slightly even if an atom is added. This case be clearly observed in case of  $\text{Cu}_{16}$  and  $\text{Cu}_{17}$ . In most cases this decrease is consistent with a re-organization of the system and an increase in the number of the symmetry elements. The point groups of the clusters are given in the table [5.2].

Secondly with increasing number of atoms per cluster more and more different distances occur. This indicates that these clusters have lower symmetries than those with only a few different distances to the origin. Clusters with  $n \leq 10$  are highly symmetric as we can see few distances in the radial distribution function for this size range. Some stable  $\text{Cu}_n$  clusters are found in this range, as seen in stability function analysis for  $\text{Cu}_n$  clusters. We can observe that clusters in the size range  $16 \leq N \leq 25$  have a shell structure in which one atom is present at the center of the cluster. Clusters have asymmetric arrangement in the size range  $26 \leq N \leq 33$ . In contrast to the smaller cluster (table [5.2]) the larger ones have much lower symmetries. The point groups  $C_1, C_s$ , and  $C_2$  are dominating but there are still some clusters with even D symmetry. However most clusters have at least a mirror plane or even a  $C_2$  axis.

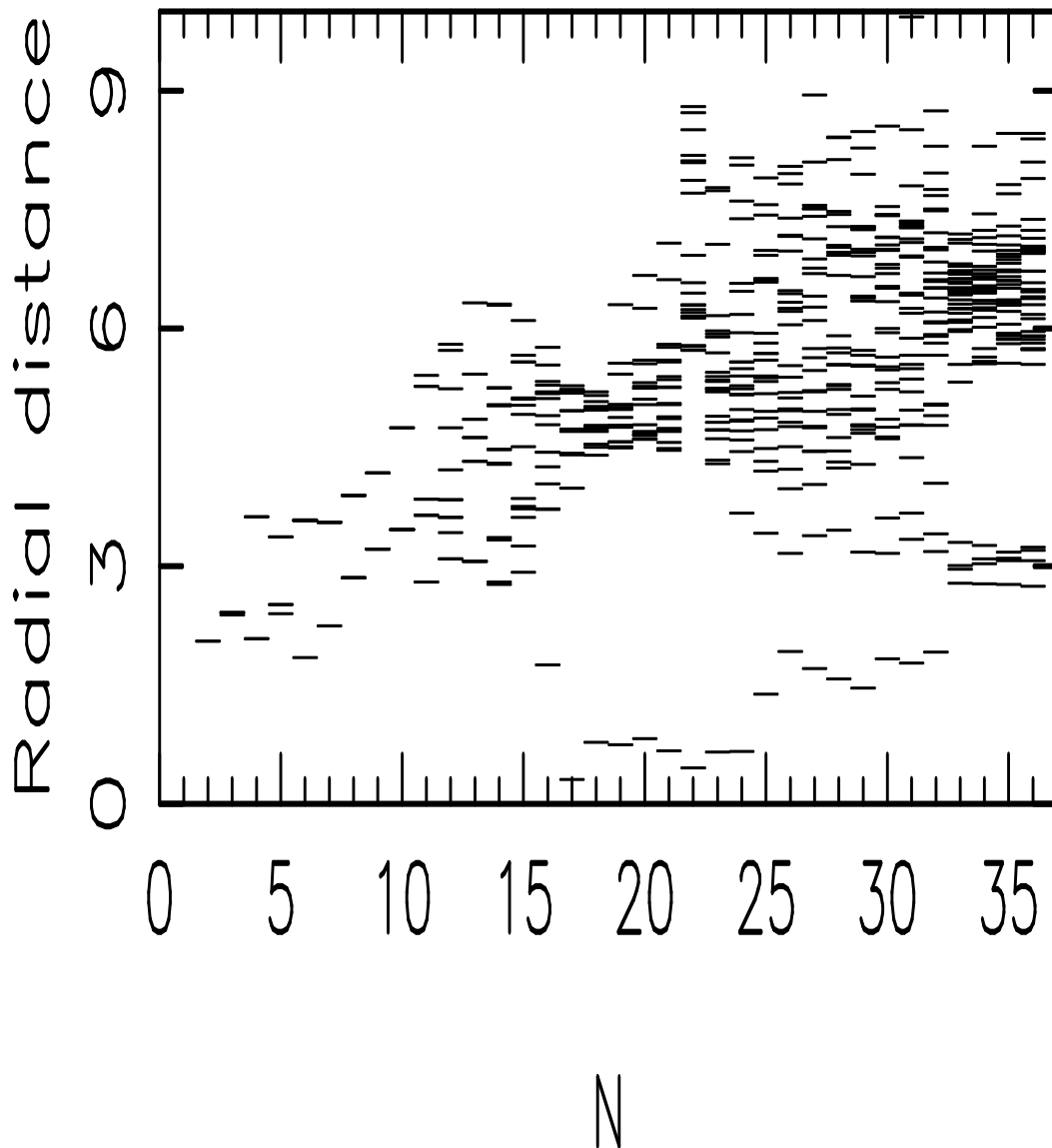


Figure 5.3: Radial Distribution Function for  $Cu_n$  clusters : Here  $N$  = Number of Atoms

### Stability Function

From DFTB calculations we get total energy which is plotted as a function of cluster size  $E_B(N)$ . In Figure [5.4] we show  $\frac{E_B(N)}{N}$  as a function of  $N$  for the globally optimized structures of  $Cu_n$  clusters. As we can see from relative total energy per unit  $\frac{E_B(N)}{N}$  as a function of  $N$  that the curve is more or less monotonically decreasing as a function of  $N$ . This means that any cluster is stabler than two separated fragments. However there are some

Point Group comparison					
n	This work	[102]	[128]	[99]	[127]
3	$D_{3h}$	$D_{3h}$	$C_{2v}(\text{ob.})$	$C_{2v}$	$C_{2v}$
4	$D_{2h}$	$T_d$	$D_{2h}$	$D_2$	$D_2$
5	$C_{2v}$	$D_{3h}$	$D_{3h}$	$C_2$	$C_2$
6	$C_{5v}$	$O_h$	$C_s$	$D_{3h}$	$D_{3h}$
7	$D_{5h}$	$D_{5h}$	$D_{5h}$	$D_{5h}$	-
8	$D_{2d}$	$D_{2d}$	$C_s$	$C_{2v}$	$C_{2v}$
9	$D_{3h}$	$C_{2v}$	$D_{3h}$	$C_s$	$C_{2v}$
10	$D_{4d}$	$C_{3v}$	-	$D_{4d}$	$C_{2v}$
11	$C_{2v}$	$C_{2v}$	-	-	$C_1$
12	$C_s$	$C_{5v}$	-	-	$C_s$
13	$C_{2v}$	$I_h$	-	-	$C_1$
14	$C_2$	$C_{3v}$	-	-	$C_1$
15	$C_1$	$D_{6d}$	-	-	$C_1$
16	$C_1$	$C_s$	-	-	$C_1$
17	$D_2$	$C_2$	-	-	$C_2$
18	$C_s$	$C_s$	-	-	$C_1$
19	$C_s$	$D_{5h}$	-	-	$C_1$
20	$C_s$	$C_s$	-	-	$C_1$

Table 5.2: Point Group comparison for  $Cu_n$  clusters

irregularities in this curve also. The total energies per atom for  $Cu_9$  and  $Cu_{15}$  are particularly high *i.e.*, both clusters are particularly unstable. In order to identify particularly stable cluster structures we have used stability function given in equation [5.3]. In stability function analysis we compare the total energy of the cluster of  $N$  units with structures of  $N+1$  and  $N-1$  units and this function gives a highest peak when the  $N$  atom cluster is particularly stable. The stability function is plotted in Figure [5.5].  $Cu_9$  and  $Cu_{15}$  have the most negative values which indicates that they are particularly unstable. The reason for this particular instability can be the exceptional stability of the  $Cu_{10}$  and  $Cu_{16}$  cluster structures.

$$E_{stab} = E_{n+1} + E_{n-1} - 2E_n \quad (5.3)$$

The second possibility to explain the instability of  $Cu_9$  and  $Cu_{15}$  is that the genetic algorithm did not find the global minima. Particular stable clusters are with those with  $n=4,8,10,14,18,26,30$  and  $33$ , where as particularly unstable are those with  $n=9,15,21,25$  and  $31$ .

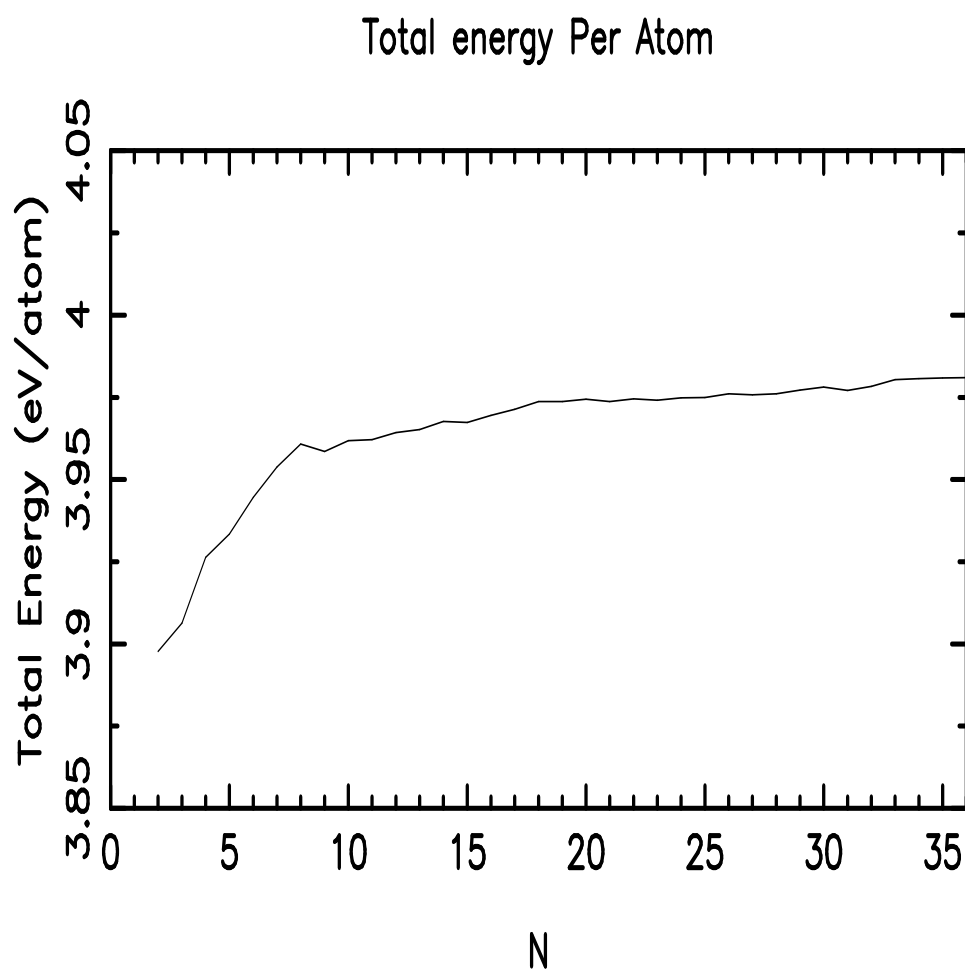


Figure 5.4: Total Energy Per Atom for  $Cu_n$  clusters : Here N = Number of Atoms

### Similarity function

To investigate the growth of  $Cu_n$  clusters, we have used similarity functions, that have been described in chapter 4 (section:4.2). Similarity Functions for  $Cu_n$  clusters are plotted in figure [5.6] .

## Stability function

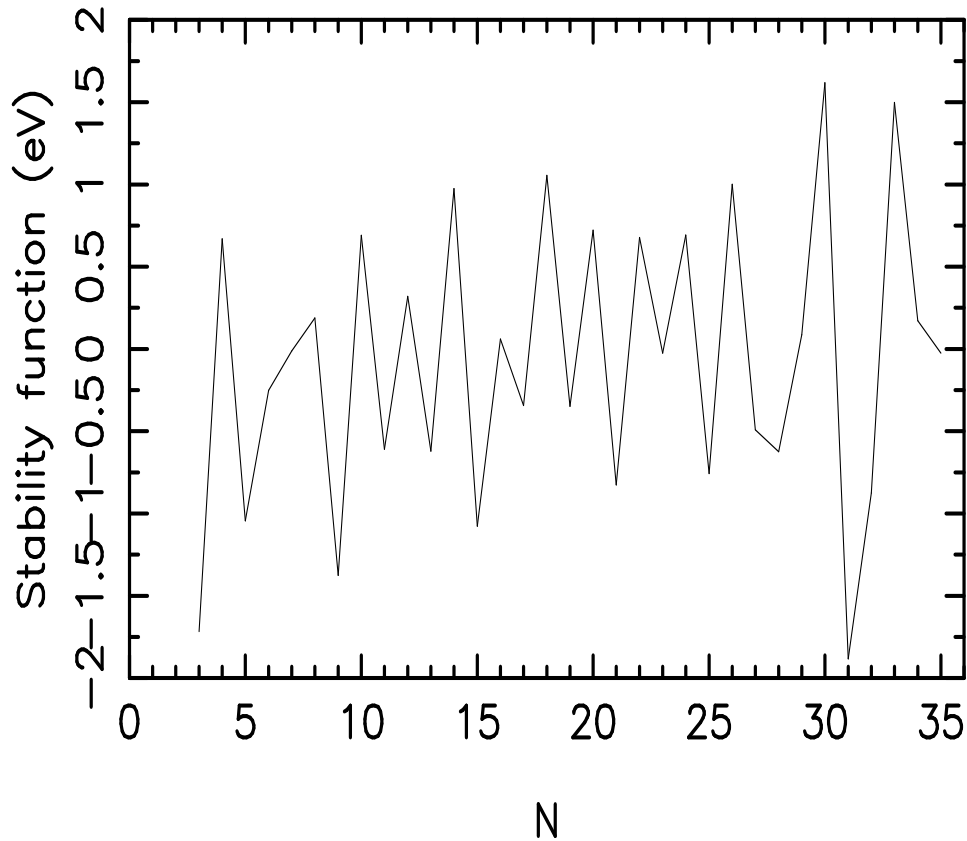


Figure 5.5: Stability Function for  $Cu_n$  clusters : Here  $N =$  Number of Atoms

We can see that structural development is very irregular over the whole range of  $n$  that we have considered here, with some smaller intervals where  $S$  is relatively close to 1. We can see some significant peaks of this function in both the channels. The low peak of  $Cu_6$  in the upper panel means that when an atom is added to  $Cu_5$ , it alters the interatomic distances as it is placed away from the center. This peak is less profound in lower panel. We can also observe clear low peaks at  $Cu_{22}$  and  $Cu_{23}$  which means that both interatomic distances and radial distances are altered with the addition of an atom. The average value of similarity function when interatomic distances are sorted is 0.79 where as it is 0.73 when radial distances are calculated. This means that similarity function analysis between the  $Cu_n$  clusters is poor and clusters are not built atom by atom as the cluster size increases. We have also compared  $Cu_n$  cluster structures with a spherical fragment of

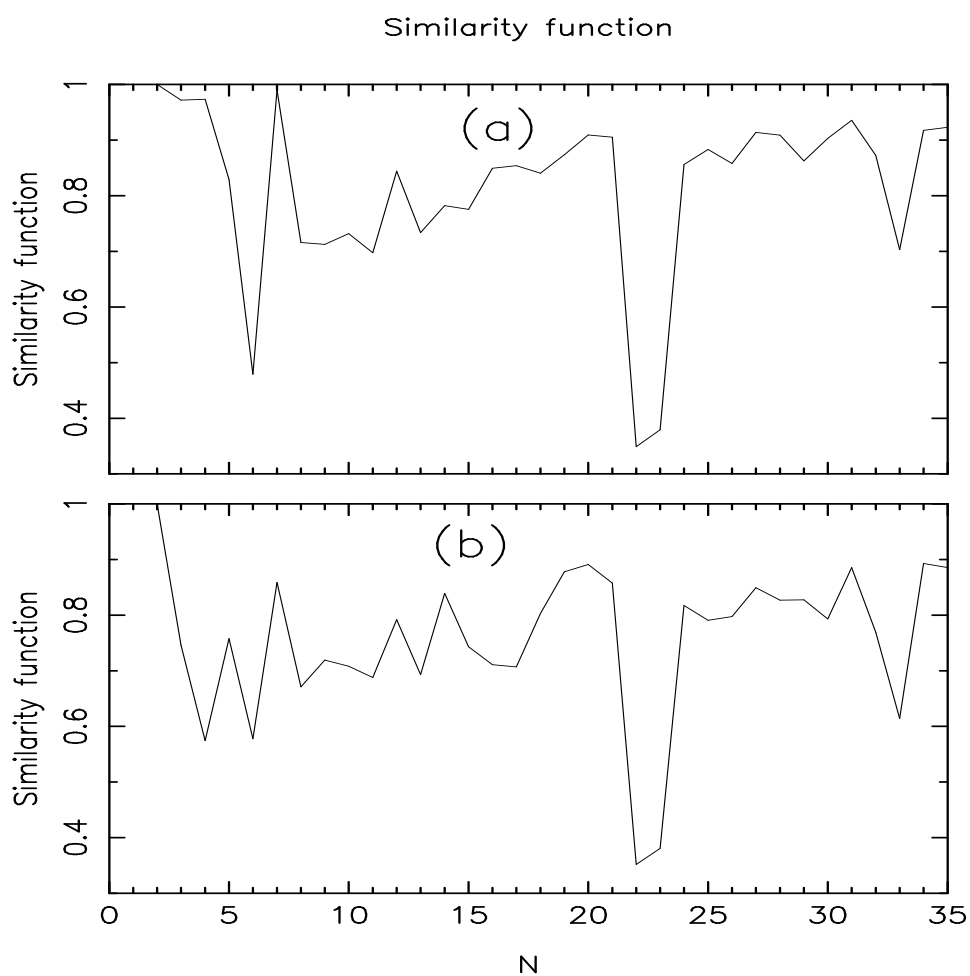


Figure 5.6: Similarity Functions for  $Cu_n$  clusters (a) based on interatomic distances (b) based on radial distances

the fcc crystal and plotted it in figure [5.7]. From the figure it is evident that there is a poor similarity between  $Cu_n$  clusters and spherical fragment of the fcc crystal.

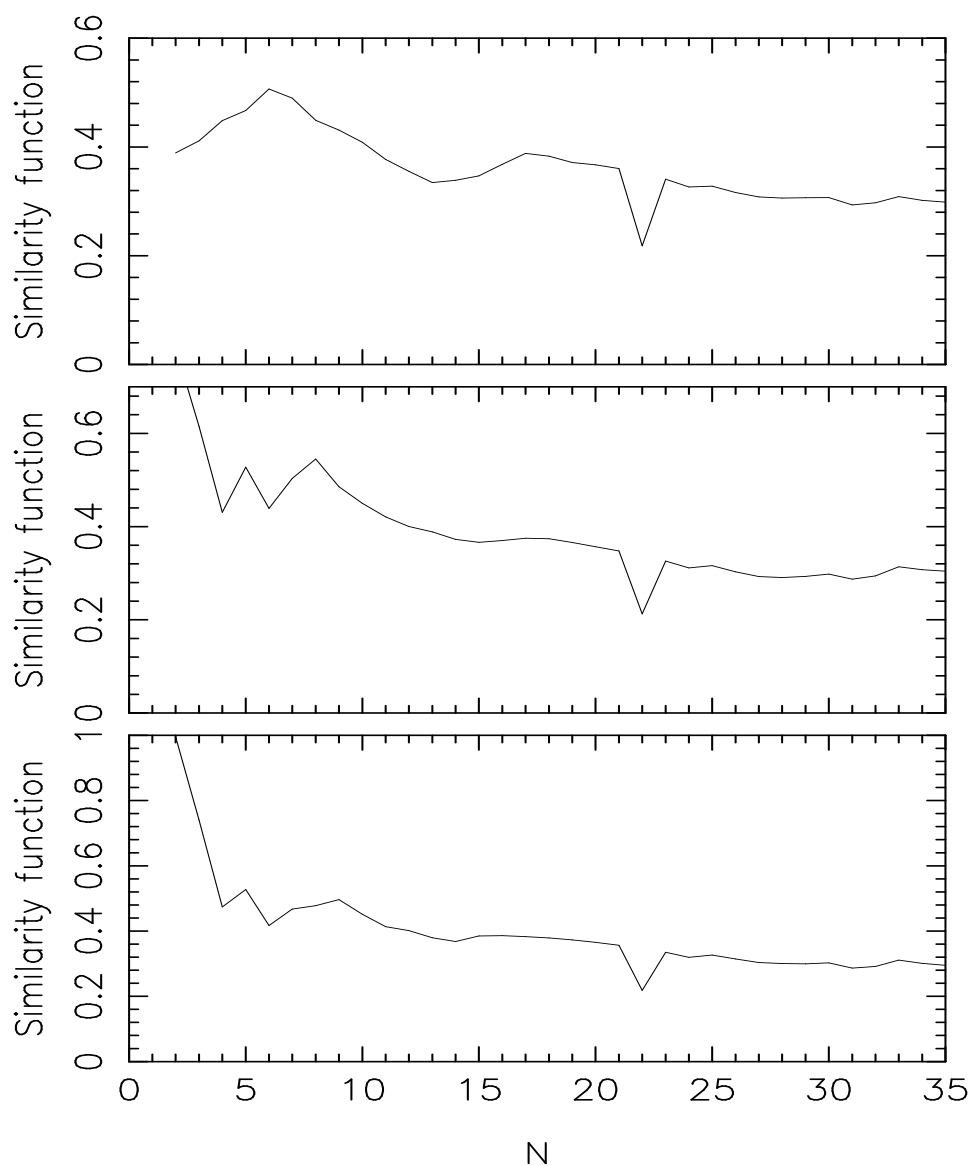


Figure 5.7: Each channel shows the similarity function for the  $Cu_n$  clusters when comparing with a spherical fragment of the fcc crystal when the center of the fragment is placed at, (upper panel) the position of an atom, (middle panel) the middle of nearest neighbor bond, (lower panel) the center of the cube

## HOMO-LUMO Gap

We have plotted the HOMO-LUMO Gap for even numbered  $\text{Cu}_n$  clusters in Figure [5.8]. However, for odd numbered  $\text{Cu}_n$  clusters we have considered two gaps, one between the single-occupied orbital and the lowest completely empty orbital,  $E_{g_2}$  Figure [5.10] and one between the highest completely filled orbital and the single-occupied one,  $E_{g_1}$  Figure [5.9]. We did not find correlation between stability and band gap for  $\text{Cu}_n$  clusters except for even numbered  $\text{Cu}_8$  and  $\text{Cu}_{18}$  clusters.

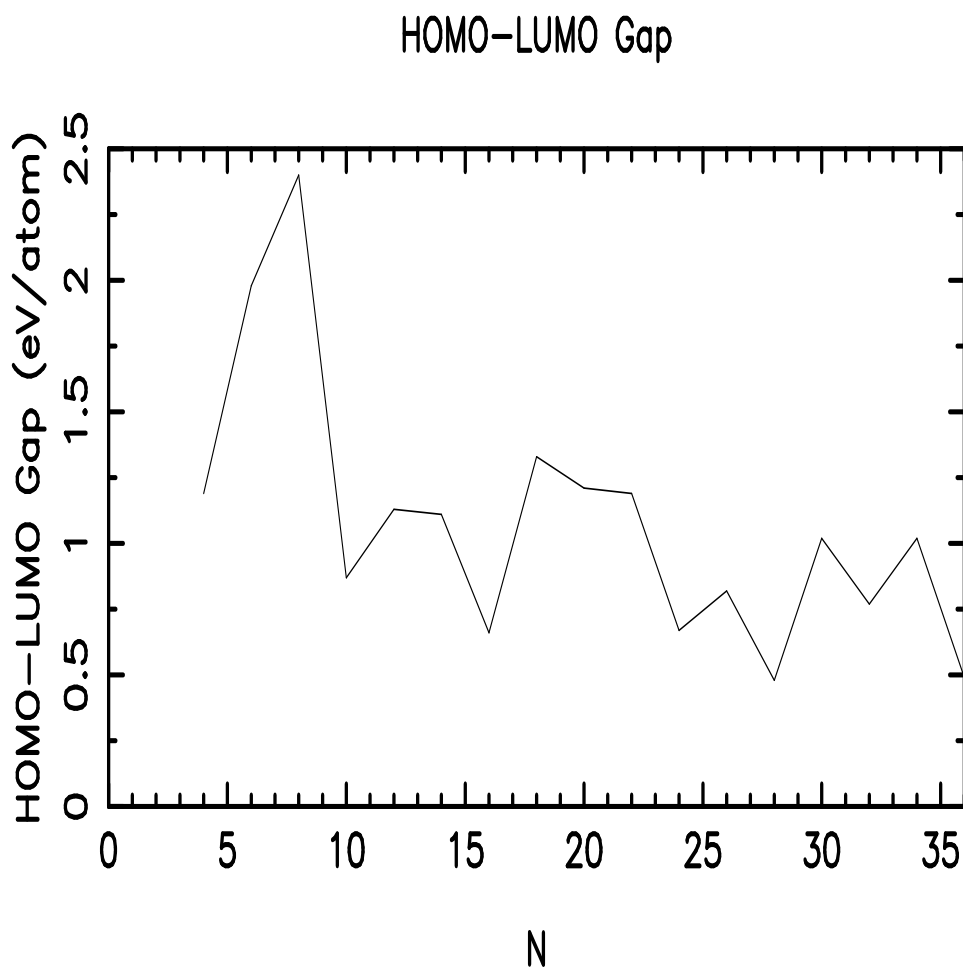


Figure 5.8: HOMO-LUMO Gap for  $\text{Cu}_n$  even clusters

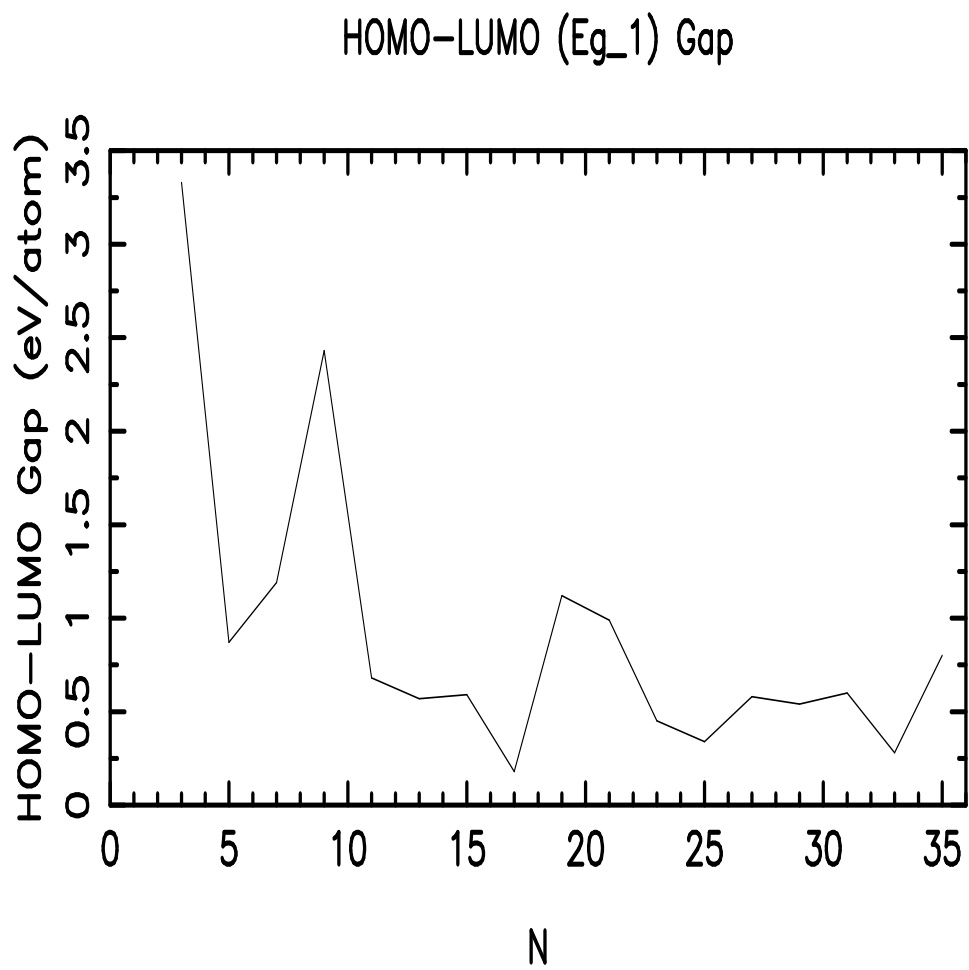


Figure 5.9: HOMO-LUMO Gap for  $Cu_n$  odd ( $E_{g_1}$ ) clusters

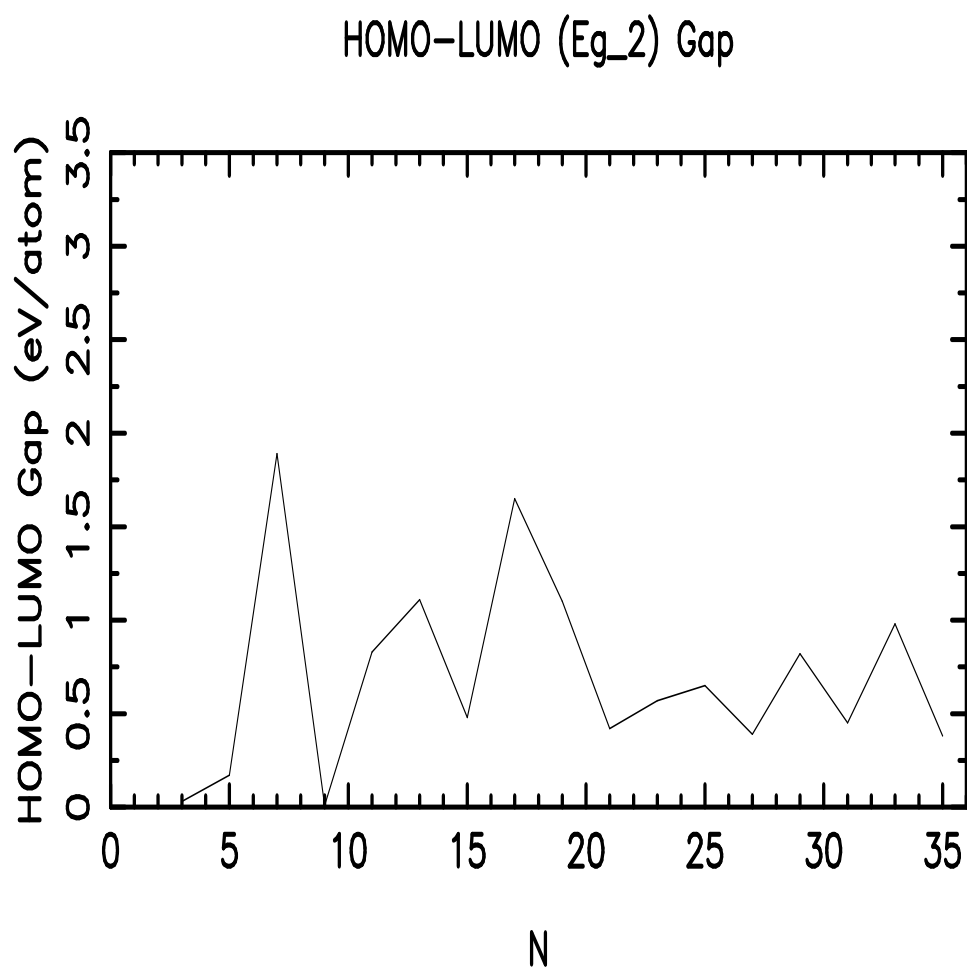
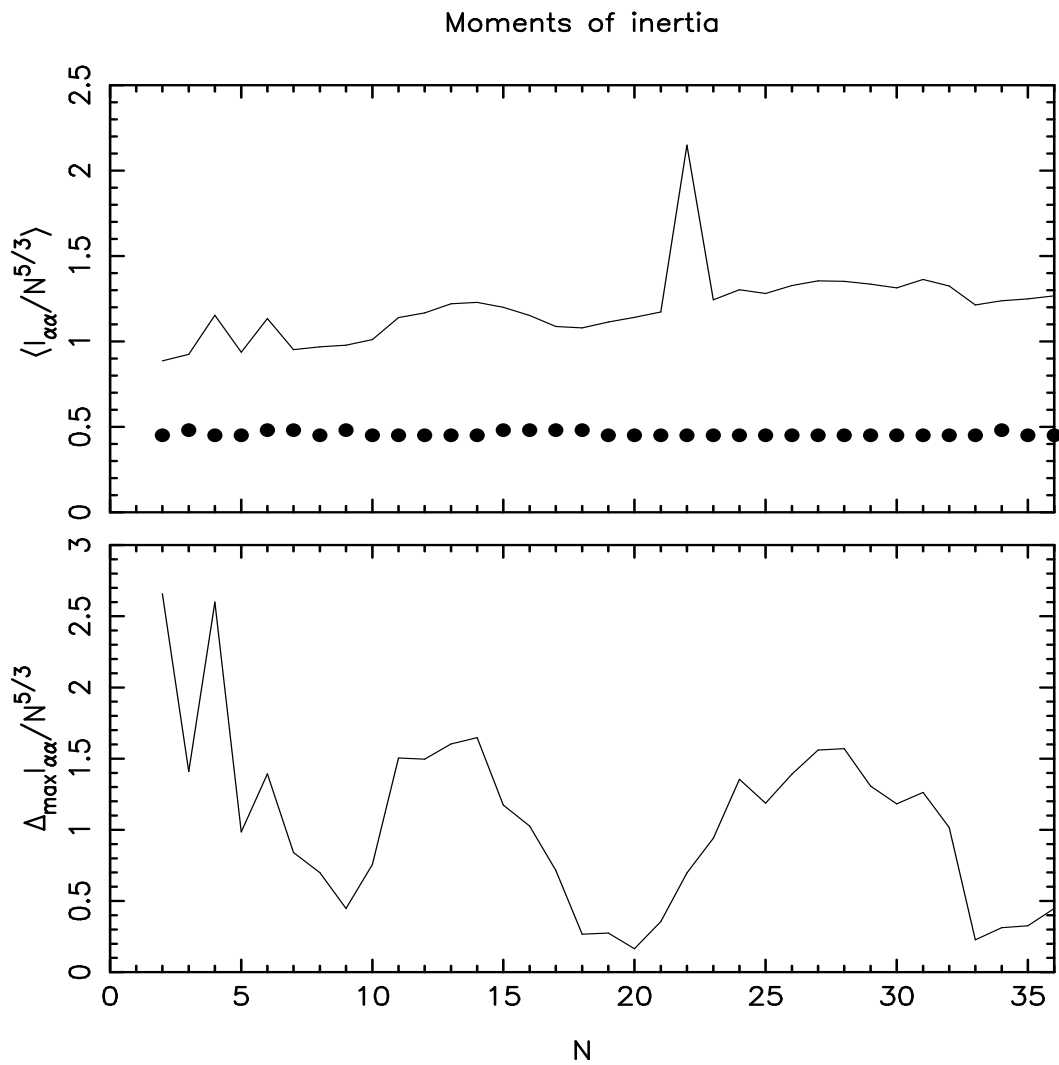


Figure 5.10: HOMO-LUMO Gap for  $Cu_n$  odd ( $E_{g_2}$ ) clusters

## Shape Analysis

For the structural Analysis of Clusters, the overall shape and its size dependence is also of significant importance. To study this in more detail we calculate for a given  $n$ -atom cluster the eigenvalues  $I_{\alpha\alpha}$  of the matrix containing the moments of inertia  $\sum_{i=1}^n s_i t_i$ . Here  $s$  and  $t$  are the  $x, y, z$  coordinates in a coordinate system centered at the center of mass  $R_0$  defined in equation [3.3]. From the eigenvalues  $I$ , we analyze the overall shape of the cluster. Three identical eigenvalues suggest a spherical shape, whereas two large and one small value suggest a lens like shape, and two small and one large value suggest a cigar-like shape. In Figure [5.11] we show the average eigenvalues (scaled by  $N^{\frac{5}{3}}$ , which is the scaling a spherical jellium would possess) together with marks indicating the overall shape. Also the largest difference between the eigenvalues is shown. We see that clusters do not have an overall spherical shape, however the largest difference of the eigenvalues takes particularly low values for  $N=9, 20, 18$  and  $33$  for  $Cu_n$  clusters. Some of these clusters are particularly stable as we can see from stability function analysis so we can say that stability is roughly related to the spherical structure of these clusters.

Figure 5.11: Shape Analysis for  $Cu_n$  clusters : Here N = Number of Atoms



## Chapter 6

---

# Summary and Conclusions

---

In the present work we have investigated structural and electronic properties of different semiconductor and metal cluster systems. These studies have been carried out using density-functional method: a density-functional tight binding program (DFTB). Geometry optimizations were carried out using a genetic algorithm method which proved to be an effective tool in finding global total-energy minimum structures for different cluster systems. It has been observed that optimization of clusters requires more computational efforts as the cluster size grows from smaller to medium size clusters. The genetic algorithm has been applied to optimize pure and binary homogeneous Si-Ge semiconductor clusters upto 44 atoms (22 units) using DFTB method. Same method is used for the total energy calculation of  $\text{Cu}_n$  clusters in the medium size range ( $2 \leq n \leq 36$ ). In this study we have investigated the geometric structures of these clusters and then compared with other results.

We have found that binary  $\text{Si}_n\text{Ge}_n$  clusters follow different growth pattern as compared to pure elemental clusters. This gives rise to formation of mixed disordered alloy structures for binary  $\text{Si}_n\text{Ge}_n$  clusters with low symmetries. Same is the case for pure  $\text{Si}_n$  and  $\text{Ge}_n$  clusters as their cluster structures are different from each other especially as the cluster size grows. These structural differences between semiconductor cluster systems are clearly visible from our similarity functional analysis. Binary  $\text{Si}_n\text{Ge}_n$  clusters, in the size range  $n \leq 8$  have structures which are reported in earlier studies also [55, 105]. Elemental  $\text{Si}_n$  and  $\text{Ge}_n$  clusters also show structural similarity in the size range  $n \leq 10$ . We have found symmetric Copper clusters struc-

tures in the size range  $n \leq 10$  which have been found by some earlier studies [67, 72].

Total energy per atom curves for elemental semiconductors show monotonic decrease as with  $N$ . For binary  $\text{Si}_n\text{Ge}_n$  clusters, total energy per atom curve shows some irregularities for  $\text{Si}_7\text{Ge}_7$  and for  $\text{Si}_9\text{Ge}_9$ . These are particularly visualized in the stability function where these both clusters turn out to be particularly unstable. Total energy per atom for Copper clusters also shows some irregularities at  $\text{Cu}_9$  and  $\text{Cu}_{15}$  which can also be seen in stability function where they both turn to be particularly unstable. Stability Function predicts stable cluster structures for all the cluster systems. For pure  $\text{Si}_n$  clusters, we have found that clusters with those  $n=7,16,34$  and  $38$  are particularly stable where as for Germanium clusters, stable structure are those with  $n=5,16,29$  and  $39$ . Binary  $\text{Si}_n\text{Ge}_n$  clusters do not show extra stability which can be seen from the stability function peaks. Particular stable Copper clusters are with those with even number  $n=4,8,10,14,18,26,30$ .

Overall similarity between the semiconductor cluster systems is very poor as seen from the similarity function analysis drawn for all the cluster systems. Similarity functions used for structural similarity analysis show good agreement when similarity functions are drawn from interatomic distances for pure elemental clusters. This agreement is less profound when radial distances are sorted out.  $\text{Si}_{20}$  and  $\text{Ge}_{11}$  show clear peak low peaks in similarity functions which shows their dissimilarity with  $\text{Si}_{19}$  and  $\text{Ge}_{10}$  clusters. In case of pure clusters, as the cluster size increases we see that peaks in similarity function are not regular especially when radial distances are sorted. This shows that clusters are not structurally related to each other. The similarity between binary  $\text{Si}_n\text{Ge}_n$  and pure clusters is very poor as indicated in Figures [4.5-4.7]. This shows that binary clusters are not structurally related to atomic clusters. Similarity functions for  $\text{Cu}_n$  clusters show clear peak at  $\text{Cu}_{22}$  and  $\text{Cu}_{23}$  clusters. The average value of similarity function for  $\text{Cu}_n$  clusters when interatomic distances are sorted is 0.79 where as it is 0.73 when radial distances are sorted. This shows that both the similarity functions are not perfect for  $\text{Cu}_n$  clusters and clusters can not be regarded as built up atom by atom.

Through Common Neighbor Analysis we have obtained sufficient informations about the geometric structures of different clusters systems. Pure  $\text{Si}_n$  have very many different sets of indices as compared to pure  $\text{Ge}_n$  clusters. This means that pure  $\text{Ge}_n$  clusters have more open cluster structures as compared to  $\text{Si}_n$  clusters. In binary clusters we have found that there are few curves for CNA when initial reference pair were both Si atoms. This

shows that Si does not want to have more neighbor. While in this case, when reference pairs were Si-Ge, or Ge-Ge type, then we have found more different peaks in CNA curve. This shows tendency of Ge to form more Si-Ge and Ge-Ge bonds in binary  $\text{Si}_n\text{Ge}_n$  clusters. This gives rise to mixed alloy structures for binary clusters. We have looked at the total coordination of both Silicon and Germanium in binary clusters. We have found that total percentage coordination of Si decreases from 4 or 5 to 3 in binary clusters compared to elemental clusters whereas for Ge atoms it increases to 4 in binary clusters compared to 3 in pure elemental Ge clusters. This clearly indicates that Si has less tendency to form bonds in  $\text{Si}_n\text{Ge}_n$  clusters whereas Ge shows greater tendency of forming bonds in binary clusters. We have also calculated the bond energies  $i, e$   $E_{\text{Si-Si}}$ ,  $E_{\text{Ge-Ge}}$ ,  $E_{\text{Si-Ge}}$ , in binary  $\text{Si}_n\text{Ge}_n$  clusters.  $E_{\text{Si-Ge}}$  and  $E_{\text{Ge-Ge}}$  in binary  $\text{Si}_n\text{Ge}_n$  clusters has more negative value as compared to  $E_{\text{Si-Si}}$  which explains that Si-Ge and Ge-Ge bonds are more favored as compared to Si-Si bonds. We have found that Ge atoms tend to move towards the center of the  $\text{Si}_n\text{Ge}_n$  clusters. This can be due to more negative value of  $E_{\text{Ge-Ge}}$  compared to  $E_{\text{Si-Si}}$ . Also the size difference between Germanium and Silicon might be another reason for this movement of Ge atoms towards the center.

Radial Distribution function give us distribution of atomic species in different cluster systems. In binary  $\text{Si}_n\text{Ge}_n$  clusters we observe that silicon atoms tend to move away from the center of cluster which is mostly occupied by germanium atoms. In case of  $\text{Si}_n$  clusters we see that clusters in the size range  $N \leq 20$  have compact structures as compared to  $\text{Ge}_n$  clusters in the same size range. Stability Analysis predicts some of stable  $\text{Si}_n$  clusters in this size range. We can also see that radius of cluster increases with increasing  $n$ . Radial distribution function plotted for  $\text{Cu}_n$  clusters shows that  $\text{Cu}_n$  clusters have symmetric structures till the size range  $n=10$  as we can see few distances. From  $\text{Cu}_{15}$  onwards clusters have a shell structure in which one atom is sitting in the center of the cluster.  $\text{Cu}_{33}$  have a compact structure with high stability as seen in stability function. Comparing  $\text{Cu}_n$  clusters with fragment of fcc crystal structure shows a poor similarity between  $\text{Cu}_n$  clusters and fcc piece. We have also performed shape analysis for elemental clusters which gives no clusters with an overall spherical shape in different cluster systems. We have also plotted the second difference in energy which has some low values which correspond to stable clusters. Stability of these clusters can be related to near spherical nature of these clusters.

The HOMO/LUMO gap as function of cluster size shows strong oscillations and it decreases with the increasing cluster size  $n$ . The gaps of pure

clusters of  $Ge_n$  clusters have the same trend as those of pure  $Si_n$  clusters, only slightly narrower, which was reported earlier by Melnikove [63]. For binary  $Si_nGe_n$  clusters we have found the same trend as elemental clusters but larger  $Si_nGe_n$  binary clusters have wider gap as compared to both Si and Ge clusters. For Silicon clusters, HOMO-LUMO Gap shows maxima at  $n = 5, 7, 10, 14, 16$  in the size range  $n \leq 20$  which correlates very well with the maxima of stability function of  $Si_n$  clusters (Fig: 4.26). For Germanium clusters also, HOMO-LUMO Gap correlates fairly well with the stability function maxima of  $Ge_n$  clusters (Fig: 4.27). For Germanium clusters, HOMO-LUMO Gap shows maxima at  $n=5, 7, 8, 14, 16$ , and 19 in the size range  $n \leq 20$ . We have not found correlation between stability and band gap for binary  $Si_nGe_n$  except for four and eight atomic binary clusters. We did not find correlation between stability and band gap for  $Cu_n$  clusters except for even numbered  $Cu_8$  and  $Cu_{18}$  clusters.

---

# Bibliography

---

- [1] A.P.Alivisatos, *Science*. **271**, 933 (1996).
- [2] J.L.Elkind, M.Alford, F.D.Weiss, R.T.Laaksonen and R.E.Smalley, *J.Chem.Phys.* **87**, 2397 (1987).
- [3] M.F.Jarrold, *Science*. **252**, 1085 (1991).
- [4] M.F.Jarrold and V.A.Constant, *Phys.Rev.Lett.* **67**, 2994 (1991).
- [5] M.F.Jarrold and J.E.Bower, *J.Chem.Phys.* **96**, 9180 (1992).
- [6] Q.L.Zhang, Y.Liu, R.F.Curl, F.K.Tittel and R.E.Smalley, *J.Chem.Phys.* **88**, 1670 (1988).
- [7] E.C.Honea, A.Ogura, C.A.Murray, K.Raghavachari, W.O.Sprenger, M.F.Jarrold and W.L.Brown, *Nature(London)*. **366**, 42 (1993).
- [8] K.Fuke, K.Tsukamoto, F.Misaizu and M.A.Sanekata, *J.Chem.Phys.* **99**, 7807 (1993).
- [9] S.Li, R.J.V.Zee, W.Weltner,Jr. and K.Raghavachari, *Chem.Phys.Lett.* **243**, 275 (1995).
- [10] D.Tomanek and M.A.Schlüter, *Phys.Rev.Lett.* **56**, 1055 (1986).
- [11] K.Raghavachari and C.M.Rohlfing, *J.Chem.Phys.* **89**, 2219 (1988).
- [12] P.Ballone, W.Andreoni, R.Car and M.Parrinello, *Phys.Rev.Lett.* **60**, 271 (1988).
- [13] B.C.Bolding and H.C.Andersen, *Phys.Rev.B* **41**, 10568 (1990).
- [14] E.Kaxiras, *Phys.Rev.Lett.* **64**, 551 (1990).

- [15] E.Kaxiras and K.Jackson, *Phys.Rev.Lett.* **71**, 727 (1993).
- [16] P.Ordejón, D.Lebedenko and M.Menon, *Phys.Rev.B* **50**, 5645 (1994).
- [17] I.H.Lee, K.J.Chang and Y.H.Lee, *J.Phys.:Condens.Matter* **6**, 741 (1994).
- [18] A.Bahel and M.V.Ramakrishna, *Phys.Rev.B* **51**, 13849 (1995).
- [19] J.C.Grossman and L.Mitás, *Phys.Rev.Lett.* **95**, 1323 (1995).
- [20] M.R.Pederson, K.Jackson, D.V.Porezag, Z.Hajnal and T.Frauenheim, *Phys.Rev.B* **54**, 2863 (1996).
- [21] A.Sieck, D.Porezag, T.Frauenheim, M.R.Pederson and K.Jackson, *Phys.Rev.A* **56**, 4890 (1997).
- [22] S.Weil, B.N.Barnett and U.Landman, *Phys.Rev.B* **55**, 7935 (1997).
- [23] I.Vasiliev, S.Ögut and J.R.Chelikowsky, *Phys.Rev.Lett.* **78**, 4805 (1997).
- [24] K.M.Ho, A.A.Shvartsbug, B.Pan, Z.Y.Lu, C.Z.Wang, J.G.Wacker, J.L.Fye and W.F.Jarrold, *Nature(London)*. **392**, 582 (1998).
- [25] B.Liu, Z.Y.Lu, B.Pan, C.Z.Wang, K.M.Ho, A.A.Shvartsbug and M.F.Jarrold, *J.Chem.Phys.* **109**, 9401 (1998).
- [26] Y.Luo, J.Zhao and G.H.Wang, *Phys.Rev.B* **60**, 10703 (1999).
- [27] L.Mitás, J.C.Grossman, I.Stich and J.Tobik, *Phys.Rev.Lett.* **84**, 1479 (2000).
- [28] B.X.Li, P.L.Cao and M.Jiang, *Phys.Status Solidi* **218**, 399 (2000).
- [29] Z.Y.Lu, C.Z.Wang and K.M.Ho, *Phys.Rev.B* **61**, 2329 (2001).
- [30] X.Zhu and X.C.Zeng, *J.Chem.Phys.* **118**, 3558 (2003).
- [31] G.Pacchioni and J.Koutecky, *J.Chem.Phys.* **84**, 3301 (1986).
- [32] D.A.Dixon and J.L.Gole, *Chem.Phys.Lett.* **188**, 560 (1992).
- [33] A.B.Anderson, *J.Chem.Phys.* **63**, 4430 (1975).
- [34] J.Harris and R.O.Jones, *Phys.Rev.A* **18**, 2159 (1978).

- [35] J.E.Northrup and M.L.Cohen, Chem.Phys.Lett. **102**, 440 (1983).
- [36] J.E.Kingcade, H.M.Nagarathna-Naik, I.Shim and K.A.Gingerich, J.Phys.Chem. **90**,2830 (1986).
- [37] J.Andzelm, N.Russo and D.R.Salahub, J.Chem.Phys. **87**, 6562 (1987).
- [38] K.Balasubramanian, J.Mol.Spectrosc. **123**, 228 (1987).
- [39] M.S.Islam and A.K.Ray, Chem.Phys.Lett. **153**, 496 (1988).
- [40] K.Balasubramanian, Chem.Rev. **90**, 93 (1990).
- [41] J.Bruna and F.Grein, Mol.Phys. **74**, 1133 (1991).
- [42] D.Dai and K.Balasubramanian, J.Chem.Phys. **96**, 8345 (1992).
- [43] D.Dai, K.Sumathi and K.Balasubramanian, Chem.Phys.Lett. **193**, 251 (1992).
- [44] D.Dai and K.Balasubramanian, J.Chem.Phys. **105**, 5901 (1996).
- [45] A.A.Shvartsburg, B.Liu, Z.Y.Lu, C.Z.Wang, M.F.Jarrold and K.M.Ho, Phys.Rev.Lett. **83**, 2167 (1999).
- [46] P.W.Deutsch, L.A.Curtiss and J.P.Blaudeau, Chem.Phys.Lett, **270**, 413 (1997).
- [47] A.M.Marzzone, Phy.Rev.B **54**, 8 (1996).
- [48] S.Ögut and J.R.Chelikowsky, Phy.Rev.B **55**, 8 (1996).
- [49] C.Jo and k.Lee, J.Chem.Phys. **113**, 17 (2000).
- [50] E.Kikuchi, S.Eshii and K.Ohno, Phy.Rev.B **74**, 195410 (2006).
- [51] J.M.Hunter *et.al*, Phys.Rev.Lett. **73**, 2063 (1994).
- [52] P.L.Tereshchuk, Z.M.Khakimov, F.T.Umarova and M.T.Swihart, Phys.Rev.B **76**, 125418 (2007).
- [53] C.K.Maiti, L.K.Bera, S.Maikap, S.K.Ray and N.B.Chakrabarti, Def.Sci.J. **50**, 299 (2000).
- [54] D.D.Salvador, *et.al*, Phys.Rev.B **61**, 13005 (2000).
- [55] S.D.Li and Z.H.Jin, Chem.J.Chin.Univ.(in chinese) **21**, 1468 (2000).

- [56] S.D.Li, Z.G.Ghao, X.F.Zhao, H.S Wu and Z.H.Jin, Phys.Rev.B **64**, 195312 (2001).
- [57] J.Tarus, M.Tantarimaeki and k.Nordlund, Nuclear Instruments and Methods in Physics Research B **228**, 51 (2005).
- [58] D.Bing, Q.C.Nguyen, X.F.Fan and J.L.Kuo, J.Phys.Chem.A **112(11)**, 2235 (2008).
- [59] A.M.Asaduzzaman and Michael Springborg, Phys.Rev.B **74**, 165406 (2006).
- [60] C.Massobrio, A.Pasquarello and R.Car, Chem.Phys.Lett. **238**, 215 (1995).
- [61] P.Calaminici, A.M.Köster, N.Russo and D.R.Salahub, J.Chem.Phys. **105**, 9546 (1996).
- [62] H.Häkkinen, M.Moseler and U.Landman, Phys.Rev.Lett. **89**, 033401 (2002).
- [63] M.Kabir, A.Mookerjee and A.K.Bhattacharya, Eur. Phys.J.D **31**, 477 (2004).
- [64] P.Blaudeck, Th.Frauenheim, D.Porezag, G.Seifert and E.Fromm, J.Phys.: Condens.Matter **4**, 6389 (1992).
- [65] D.Porezag, Th.Frauenheim, Th.Köhler, G.Seifert and R.Kaschner, Phys.Rev.B **51**, 12947 (1995).
- [66] G.Seifert, D.Porezag and Th.Frauenheim. Int.J.Quant.Chem. **58**, 85 (1996).
- [67] E.Schrödinger, Ann.Phys. **79**, 361 and 489 (1926), Ann.Phys. **80**, 437 (1926), Ann.Phys. **81**, 109 (1926).
- [68] P.Gombás, *Die statistische Theorie des Atoms und ihre Anwendungen*, Springer-Verlag, Wien, (1949).
- [69] P.Hohenberg and W.Kohn, Phys.Rev.A **136**, 864 (1964).
- [70] W.Kohn and L.J.Sham, Phys.Rev.A **140**, 1133 (1965).
- [71] D.Faken and H.Jonsson, Comp.Mat.Sci. **2**, 279 (1994).

- [72] T.A.Abtew and D.A.Drabold, Phys.Rev.B **75**, 045201 (2007).
- [73] D.V.Melnikov and J.R.Chelikowsky, Phys.Rev.B **69**, 113305 (2004)
- [74] Ofelia Ona, V.E.Bazterra, M.C.Caputo, J.C.Facelli, P.Fuentealba and M.B.Ferraro Phys.Rev.A **73**, 053203 (2006).
- [75] Z.Y.Lu, C.Z.Wang and K.M.Ho Phys.Rev.B **61**, 2329 (2000).
- [76] A.A.Shvartsburg, B.Liu, Z.Y.Lu, C.Z.Wang, M.F.Jarrold and K.M.Ho, Phys.Rev.Lett.**83**, 2167 (1999).
- [77] S.Yoo, X.C.Zeng, X.L.Zhu and J.J.Bai, J.Am.Chem.Soc. **125**, 13318 (2003).
- [78] J.Zhao, J.Wang, Jellinek, S.Yoo, and X.C.Zeng, Eur.Phys.J.D. **34**, 35 (2005).
- [79] S.H.Yoo, and X.C.Zeng, Angew.Chem.Int.Ed **44**, 1491 (2005).
- [80] M.Takahashi and Y.Kawazoe, Chem.Phys.Lett. **418**, 475 (2006).
- [81] O.Cheshnovsky, S.H.Yang, C.L.Pettiette, M.J.Craycraft, Y.Liu and R.E.Smalley, Chem.Phys.Lett. **138**, 119 (1987).
- [82] F.Jarrold and V.A.Constant, Phys.Rev.Lett. **67**, 2994 (1991); R.R.Hudgins, M.Imai, M.F.jarrold and P.Dogourd, J.Chem.Phys. **111**, 7865 (1999).
- [83] J.M.Hunter,J.L.Fye and M.F.Jarrold, Phys.Rev.Lett. **73**, 2063 (1994).
- [84] A.A.Shvartsburg, R.R. Hudgins, P. Dugourd and M.F.Jarrold, Chem.Soc.Rev. **30**, 36 (2001).
- [85] X.L.Zhu, X.C.Zeng and Y.A.Lei, J.Chem.Phys. **120**, 8985 (2004).
- [86] H.Cheng and L.Wang, Phys.Rev.Lett. **77**, 51 (1996); L.Wang, H.Wu and H.Cheng, Phys.Rev.B **55**, 12884 (1997).
- [87] D.P.Pappas, A.P.Popov, A.N.Anisimov, B.V.Reddy and S.N.Khanna, Phys.Rev.Lett. **76**, 4332 (1996).
- [88] K.Lee, J.Callaway and S.Dhar, Phys.Rev.B **30**, 1724 (1984); K.Lee, *et al.*, *ibid* **31**, 1796 (1985); M.Castro and D.R.Salahub, *ibid* **49**, 11842 (1994).

- [89] R.Whyman, in *Transition Metal Clusters*, edited by B.F.G.Johnson (John Wiley and sons, New York, 1980).
- [90] E.L.Muettert, *Science*. **196**, 839 (1977).
- [91] H.Conrad, G.Ertl, H.Knozinger, J.Kuppers and E.E.Latta, *Chem.Phys.Lett.* **42**, 115 (1976).
- [92] H.Haberlandt, in *Theoretical Aspects of Heterogeneous Catalysis*, edited by J.B.Moffat (Van Nostrand Reinhold, New York, 1990).
- [93] C.Massobrio, A.Pasquarello and A.D.Corso, *J.Chem.Phys.* **109**, 6626 (1998).
- [94] P.Jaque and A.Toro-labbe, *J.Chem.Phys.* **117**, 3208 (2002).
- [95] P.J.Dyson, *Coord.Chem.Rev.* **248**, 2443 (2004).
- [96] K.M.Neyman, G.N.Vayssilov and N.Rösch, *J.Oranomet.Chem.* **24**, 4384 (2004).
- [97] L.Triquero, U.Wahlgren, P.Boussard and P.Siegebahn, *Chem.Phys.Lett.* **237**, 550 (1995).
- [98] P.Jaque and A.Toro-Labbe, *J.Phys.Chem.B* **108**, 2568 (2004).
- [99] K.Jug, B.Zimmermann, P.Calaminici and A.M.Köster, *J.Chem.Phys.* **116**, 4497 (2002).
- [100] M.Kabir, A.Mookerjee and A.K.Bhattacharya, *Phys.Rev.A* **69**, 6987 (2004).
- [101] U.Lammers and G.Borstel, *Phys.Rev.B* **49**, 24 (1994).
- [102] D.Alamanova, V.G.Grigoryan and M.Springborg, *Phys.Rev.B* **73**, 115415 (2006).
- [103] E.F.Archibong and A.St-Amant, *J.Chem.Phys.* **109**, 962 (1998).
- [104] K.Raghavachari, *J.Chem.Phys.* **84**, 5672 (1986).
- [105] P.Wielgus, S.Pozzak, D.Majumdar, J.Saloni and J.Leszczynski, *J.Chem.Phys.* **128**, 144305 (2008).
- [106] I.Rata, A.A.Shvartsburg, M.Horoi, Th.Frauenheim, K.W.M.Siu and K.A.Jackson, *Phys.Rev.Lett.* **85**, 546 (2000).

- [107] K.A.Jackson, M.Horoi, I.Chaudhuri, T.Frauenheim and A.A.Shvartsburg, *Phys.Rev.Lett.* **93**, 013401 (2004).
- [108] K.A.Jackson, I.Chaudhuri, M.Yang and T.Frauenheim, *Phys.Rev.A* **71**, 033205 (2005).
- [109] B.X.Li, P.L.Cao and S.C.Zhan, *Phys.Lett.A* **316**, 252 (2003).
- [110] S.Yoo, X.C.Zeng, X.Zhu and J.Bai, *J.Am.Chem.Soc.* **125**,13316 (2003).
- [111] S.Yoo, J.J.Zhao, J.L.Wang and X.C.Zeng, *J.Am.Chem.Soc.* **126**, 13845 (2004).
- [112] S.Yoo and X.C.Zeng, *Angew.Chem.,Int.Ed.* **44**,1491 (2005).
- [113] J.Bai, *et.al*, *J.Phys.Chem A* **110**, 908 (2006).
- [114] A.Sieck, T.Frauenheim and K.A.jackson, *Phys.Status Soloidi B* **240**, 537 (2003).
- [115] S.Goedecker, W.Hellmann and T.Lenosky, *Phys.Rev.Lett.* **95**, 055501 (2005).
- [116] A.Tekin and B.Hartke, *Phys.Chem.Chem.Phys.* **6**, 503 (2004).
- [117] C.J.Phillips, *Phys.Rev.B* **47**, 14132 (1993).
- [118] J.D.Wales, *Phys.Rev.A* **49**, 2195 (1994).
- [119] U.Rothlisberger, W.Andreoni and P.Giannozzi, *J.Chem.Phys.* **96**, 1248 (1992).
- [120] X.G.Gong, Q.Q.Zeng and Y.Z.He, *J.Phys.:Condens.Matter* **7**, 577 (1995).
- [121] I.H.Lee, K.J.Chang and Y.H.Lee, *J.Phys.:Condens.Matter* **6**, 741 (1994).
- [122] J.Andzelm, N.Russo and D.R.Salahub, *J.Chem.Phys*, **87**, 6562 (1987).
- [123] E.M.Fernández, J.M.Soler, I.L.Garzón and L.C.Balbás, *Phys.Rev.B* **70**, 165403 (2004).
- [124] G.H.Guvelioglu, P.Ma, X.He, R.C.Forrey and H.Cheng, *Phys.Rev.Lett.* **94**, 026103 (2005).

- [125] S.Darby, T.V.M.Jones, R.L.Johnston and C.Roberts, *J.Chem.Phys.* **116**, 1536 (2002).
- [126] M.Kabir, A.Mookerjee and A.K.Bhattacharya, *Phys.Rev.A* **69**, 043203 (2004).
- [127] M.Yang, C.Köhler, T.Frauenheim, J.Jellinek and K.A.Jackson, *J.Chem.Phys.* **124**, 024308 (2006).
- [128] M.Kabir, A.Mookerjee, R.Datta, A.Banerjea and A.K.Bhattacharya, *Int.J.Mod.Phys.B* **17**, 10 (2003).

---

# Eidesstattliche Versicherung

---

Hiermit versichere ich an Eides statt, dass ich die vorliegende Arbeit selbständig und ohne Benutzung anderer als der angegebenen Hilfsmittel angefertigt habe. Die aus anderen Quellen oder indirekt übernommenen Daten und Konzepte sind unter Angabe der Quelle gekennzeichnet.

Die Arbeit wurde bisher weder im In- noch im Ausland in gleicher oder ähnlicher Form in einem Verfahren zur Erlangung eines akademischen Grades vorgelegt.

Ort, Datum

(Unterschrift)